Universitat Autònoma de Barcelona

Synthesis of Metal Oxide Nanoparticles for Superconducting Nanocomposites and Other Applications

Alba Garzón Manjón

Universitat Autònoma de Barcelona

PhD Thesis

Synthesis of Metal Oxide Nanoparticles for Superconducting Nanocomposites and Other Applications

Author: Alba Garzón Manjón

Supervisors:

Prof. Dr. Josep Ros Badosa

Dr. Susagna Ricart Miró

PhD program in Chemistry

Chemistry Department

Science Faculty

ICMAB

September, 2016

CSIC

Prof. Dr. Josep Ros Badosa form Universitat Autònoma de Barcelona (UAB) and **Dr. Susagna Ricart Miró** from Institut de Ciència dels Materials de Barcelona (ICMAB-CSIC)

Certify:

That the dissertation Synthesis of Metal Oxide Nanoparticles for Superconducting Nanocomposites and Other Applications submitted by Mrs. Alba Garzón Manjón to the Sciences Faculty in fulfillment of the requirements for the degree of Doctor of Philosophy in Chemistry Science program has been performed under their supervision.

Prof. Dr. Josep Ros Badosa **Dr. Susagna Ricart Miró**

Alba Garzón Manjón

Bellaterra, Barcelona. Wednesday, September 21, 2016

Als meus pares,

Sense el vostre esforç, dedicació,
paciència, il·lusió i confiança
no ho hagués aconseguit.
Gràcies per creure sempre en mi.
Us estimo.

ACKNOWLEDGEMENTS

Les paraules no podran arribar mai a expressar tot el que ha significat per a mi aquesta etapa tan bonica que ara es tanca per deixar pas a noves aventures; tot i així ho vaig a intentar:

Gràcies als directors d'aquesta tesis **Prof. Dr. Josep Ros** i **Dr. Susagna Ricart** per tota la formació, ajuda, atenció, constància i esforç dedicat durant aquests 6 anys i mig. M'heu fet créixer com a científica i com a persona. Ha sigut una de les millors etapes de la meva vida i sense vosaltres no hagués pogut arribar a la línia de meta. Se que no he sigut sempre fàcil i que a vegades us he posat dels nervis, però moltes gràcies també per la vostra paciència i sobretot per confiar en mi com ho heu fet. Us portaré sempre al cor.

Molt especialment voldria agrair i donar les gràcies al **Dr. Eduardo Solano**, per tot el que em va arribar a ensenyar, pels bons moments que vam passar a dintre i a fora del laboratori. Gracias por ayudarme tanto Edu, me enseñaste más de lo que te imaginas y me distes la oportunidad y la suerte de aprender de una gran persona. Cierro la etapa con una sonrisa pensando no solo en lo compartido químicamente sino también en la caja encima la mesa, en las canciones infinitas, en los problemas con el ordenador, en las sesiones de limpieza, en Mánjon despierta y en viva Mario Bros.

Katia G.Samper ens hem acompanyat des del principis de la carrera forjant una gran amistat que s'ha convertit en un dels pilars més importantíssim de la meva vida. No et pots ni imaginar el que m'has ajudat professionalment i personalment. Moltes gràcies bonica, per escoltar-me, per ajudar-me i per estar sempre, en els bons i en els dolents moments. Trobaré a faltar entrar al teu laboratori i que sense paraules sapiguem el que anem a dir, el que sentim. Se que sempre has estat, hi ets i hi seràs.

Aquest cop sí! M'agradaria donar-li les gràcies al **Dr. Leonardo Pérez** per introduir-me en el món de la recerca i per obrir-me les portes de l'inici d'un somni que començava a l'Abril del 2010.

A la **Rosa González**, per la gran confiança que ha depositat en mi fent créixer la nostra amistat, ara tant forta, durant tot el doctorat. Gràcies per ajudar-me amb les molècules, en la química i per recolzar-me sempre en les meves decisions. Porqué el idioma Klingon no lo entiende cualquiera, por esos cruasanes que dan energía, por ser tan buena conmigo, por quedarte a mi lado cuando más me hacía falta y por todos los buenos momentos vividos y que viviremos! Gracias, os quiero a los 4!

A **Jonathan de Tovar** por su gran ayuda, por ayudarme con los IR y la coordinación de las nanopartículas; por estar siempre apoyándome y dispuesto a escuchar. Ha sido una pasada estar a tu lado durante todo el doctorado!

Al **Dr. Pablo Castro** i a la **Dr. Judith Oró** tècnics del servei de microscòpia de la UAB i del ICMAB respectivament, per la seva ajuda durant tots aquests anys en la caracterització de les diferents nanopartícules que ens ha fet viure moments inoblidables i molt divertits.

Al personal dels diferents serveis de UAB i ICMAB: **SeRMN**, **Difracció de RX**, **SAQ** i **Microscòpia.** I als membres del grup de Recerca en Materials i Termodinàmica de la universitat de Girona pels estudis de TGA. A tots ells moltes gràcies!

A la secretaria del Departament de Química en especial a la **Neli Carmona, Elena Jiménez** i **Conxita Casado** per les seves hores dedicades als doctorands i pel seu gran treball i esforç. Sou genials, gràcies!

Al **Dr. Juli Real** per la seva amabilitat i la seva ajuda químicament i personalment! Trobaré molt a faltar les classes de laboratori compartint sempre bons moments i menjant deliciosos croissants de xocolata. Moltes gràcies per les nostres xerrades a sigut un gran plaer!!

Al **Dr. Pablo Cayado**, compañero de superconductores formando la segunda generación. Tal y como te prometí te daré los agradecimientos en catalán: Encara que a vegades m'hagis posat dels nervis i molt, ha sigut un plaer compartir aquesta experiència junts.

Al tot el grup **SUMAN** del ICMAB m'agradaria donar les gràcies també per tots els bons moments i tot l'esforç dedicat. A més, gràcies al projecte EUROTAPES he pogut arribar a créixer moltíssim científicament i ha sigut una gran sort poder compartir-ho amb tots ells.

A la **Roberta Ceravola**, muchísimas gracias por esas medidas sacando tiempo de donde no lo tenías! Sin ella, no hubiera podido acabar mi parte experimental!! Y también gracias por recibirme con esa genial sonrisa a pesar de todo el estrés.

M'agradaria donar les gràcies a tota la planta d'Inorgànica en especial al **Grup Bayón** (Merche, Joao, Dani, Jose, Miriam), al **Grup SelOxCat** (Marcos, Lluis, Bing, Elena) i al **Grup J.Suades & M. Capdevila** (Quim, Jordi B, Selene), han sigut uns grans companys de feina i amics. Les experiències conjuntament viscudes son tantes i tan genials que les paraules se'm queden curtes per escriure el que puc arribar a sentir. Moltes gràcies!

A tots els meus companys del **Grup Ros** (Chang Yong, Natalia, Jordi M, Silvia Frascati, Bea). Sembla que va ser ahir quan vaig començar assentada al costat de la porta, i ara deixo la meva última taula perquè noves generacions puguin tenir la sort que jo he tingut al treballar cada dia amb grans companys.

Als meus dos últims "esclavitos bonitos" **Gloria Garcia** i **Ferran Crugeira** acabant junts el seu TFG i la meva tesis doctoral treballant sempre a tope per obtenir bons resultats!

Al **Toni Aranda** per la seva gran col·laboració amb les cèl·lules i la seva ajuda que m'ha fet poder aprendre d'un nou i molt interesant camp.

A tot el **group of Prof. Dr. Sanjay Mathur** de Colònia (Köln). It was a big pleasure for me to have the opportunity to work with this nice and spectacular group. I could learn and enjoy a lot. All of us will be in my heart forever.

A una de les meves parelles preferides **Dr. Raquel Fiz** & **Dr. Sebastian Schneider**: Muchísimas gracias Raquel por toda tu ayuda prestada desde que llegue a Köln hasta ahora. Te has convertido en una persona muy importante para mí, en mi gran amiga a la que echo

de menos cada día.. I would like to say thank you to **Sebastian** to make me feel really COMFORTABLE!!! Both of you are the best, are part of my family!

Muy en especial me gustaría dar las gracias al **Dr. Jordi Garcia-Antón** por esta gran etapa que he podido compartir a su lado, por su gran ayuda y compañerismo. Siempre recordaré nuestras charlas en tu despacho y nuestros TEMs con una gran sonrisa. Gracias por ayudarme en todo y sobretodo en esos momentos difíciles que he pasado durante mi tesis doctoral.

A **Francisco Heras** y a **Loly Domingo** por su gran ayuda durante la redacción de la tesis, muchas gracias por esas grandes aportaciones y correcciones!

Javier Heras te has convertido en una de las personas más importante de mi vida y me has dado muchas fuerzas para creer en que podía hacerlo, en que soy capaz de conseguir lo que me proponga. Muchísimas gracias por tu dedicación y ayuda sobretodo durante la escritura de esta tesis con esas grandes aportaciones que tan y tan bien me han ido. Gracias por estar siempre a mi lado dándome lo mejor, dándomelo todo. Gracias por tu comprensión en los momentos más difíciles de este trabajo llevándome a la calma, escuchándome i desviviéndote por mi. Me has hecho crecer como científica y como persona y espero que ojalá pueda ayudarte de la misma manera en todas tus aspiraciones como tu lo has hecho conmigo. Lo he conseguido!! Te quiero, 4T!

Als meus pares **Alejandro Garzón** i **Antonia Mª Manjón,** a la meva germana **Gina Garzón** i a la meva iaia **Antonia Morante**, per estar incondicionalment al meu costat ajudant-me, desvivint-se i acompanyant-me en tots els meus projectes i aspiracions. Moltes gràcies per confiar i creure sempre en mi, sense vosaltres no ho hagués pogut aconseguir. Em sento la dona més afortunada del món per tenir la gran sort de formar part d'aquesta família Garzón-Manjón. Us estimo molt i espero que sempre continueu estan tan orgullosos. Gràcies per fer-me com soc, gràcies per ensenyar-me i instruir-me en aquesta vida amb aquests valors tan especials. Sempre al cor. Tot esforç sí que sempre té la seva recompensa, i aquest és el nostre, és aquesta tesis doctoral en química! Infinitament feliç amb vosaltres, sempre!!

CONTENTS

ABBREVIATIONS

^{1}H Nuclear Magnetic Resonance	^{1}H-NMR
acetylacetonate	acac
Benzyl alcohol	BnOH
Cerium(III) acetate	$Ce(OAc)_3$
Cerium(III) acetylacetonate	$Ce(acac)_3$
Chemical Solution Deposition	CSD
$CoFe_2O_4$	CFO
Critical Current	J_c
Critical Magnetic Field	H_c
Critical Temperature	T_c
Decanoic Acid	HDEC
Dynamic Light Scattering	DLS
Gas Chromatography-Mass Spectroscopy	GC-MS
High Temperature Superconductor	HTS
High Transmission Electronic Microscopy	HRTEM
Infrared Spectroscopy	IR
Iron(III) acetylacetonate	$Fe(acac)_3$
$LaAlO_3$	LAO
Microwave	MW
$MnFe_2O_4$	MFO
Nanoparticles	NPs
Octahedral	Oh
Spin Coating	SP
Superconductor	SC
Superconductor Quantum Interference Device	SQUID
Tetrahedral	Td
Thermogravimetric Analysis	TGA
Transmission Electronic Microscopy	TEM
Triethylene glycol	TREG
X-ray Diffraction	XRD

X-ray Photoelectron Spectroscopy	XPS
X-ray Power Diffraction	XRPD
$YBa_2Cu_3O_{7-d}$	YBCO
Zeta Potential	ZP

ABSTRACT

Thermal and microwave methodologies are used to synthesize different metal oxides nanoparticles such as magnetite (Fe_3O_4), cerium oxide (CeO_2). By modifying the precursors ($Fe(R_2diket)_3$ (R= Ph, ^tBu and CF_3), $Ce(acac)_3$ and $Ce(OAc)_3$), and following the same synthetic route, it is possible to control the size and shape of the nanocrystals obtained. The general route is carried out in triethylene glycol (TREG) or benzyl alcohol (BnOH) media, due to its high boiling point and, which acts also as a capping ligand of the nanoparticles, stabilizing them in polar solvents.

Nanoparticles have been characterized by several common physical laboratory techniques: High Resolution Transmission Electron Microscopy (HR TEM), infrared spectroscopy (IR), X-ray Powder Diffraction (XRPD), magnetometry via Superconducting Quantum Interference Device (SQUID), Nuclear Magnetic Resonance (RMN), Gas Chromatography-Mass Spectroscopy (GC-MS), X-ray Photoelectron Spectroscopy (XPS) and Thermogravimetric Analysis (TGA). With all these techniques, the final size, shape, composition, crystal structure, magnetic behaviour and capping ligand interaction have been studied, showing the high quality crystals generated. In addition, we demonstrate the high efficiency of all two one-pot methodologies that have been optimized to synthesize different families of nanoparticles.

The stable colloidal solutions obtained in ethanol have been used to generate ex-situ hybrid $YBa_2Cu_3O_{7-\delta}$ (YBCO) superconducting layers because the critical current can be increased when the nanoparticles are embedded.

Finally, a new application as an antioxidant behaviour in human cells is tested for the case of CeO_2 nanoparticles due to their specifically properties that make them really interested in this new field.

OBJECTIVES

The main objective of this PhD research work is the fabrication of different magnetic and non-magnetic metal oxide nanoparticles with control in size and stability in polar solvents to be used for applications in superconducting ceramic nanocomposites and as antioxidants in biomedicine.

To attain these final objectives, the first step will be the optimization of a synthetic thermal methodology using metallorganic precursors, high boiling point solvents. A comparison between two types of activation: Thermal and Microwave will be done. The final idea will be the development of a one-pot, easy, fast and economic synthetic route to generate nanocrystals with specific properties: size, shape and composition desired and high stability in polar media, such as water or alcohols, for their future applications.

For all these reasons, a deeply characterization study of the synthetized nanoparticles has to be performed to know their morphology (crystalline structure and capping ligand) in order to apply them in superconductivity and also as an antioxidant human cells material.

After the characterization process, the introduction of different metal oxide nanoparticles inside YBCO matrix is required. Furthermore, the final properties of these new nanocomposites thin films will be analysed to find the influence of the included magnetic and non-magnetic regions in the superconductor matrix.

On the other hand, CeO_2 nanoparticles will be also applied as antioxidants in human cells in order to analyse their ability to interact with reactive oxygen species.

When this research work will be concluded, a better understanding about the synthesis and the characterization of different metal oxide nanoparticles to apply them in superconductivity or in biological systems, improving the final properties, should have been achieved.

I GENERAL INTRODUCTION

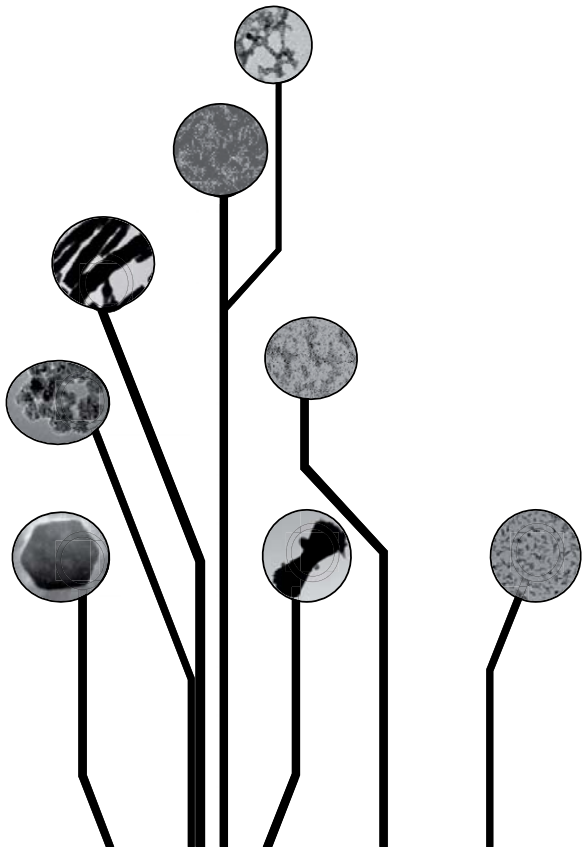

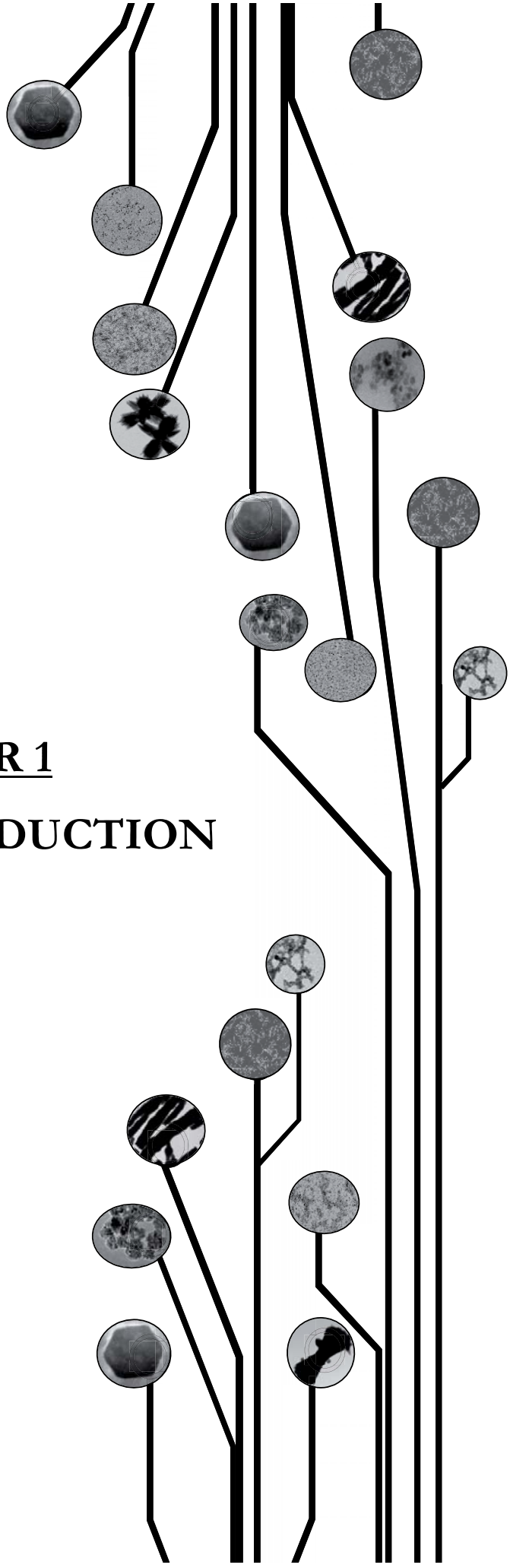

CHAPTER 1

GENERAL INTRODUCTION

CONTENTS

I General Introduction

Chapter 1: General Introduction

1. Nanoscience and Nanotechnology

"I would like to describe a field, in which little has been done, but in which an enormous amount can be done in principle. This field is not quiet the same as the others in that it will not tell us much of fundamental physics (in the sense of, 'What are the strange particles?') but it is more like solid-state physics in the sense that it might tell us much of great interest about the strange phenomena that occur in complex situations. Furthermore, a point that is most important is that it would have an enormous number of technical applications. What I want to talk about is the problem of manipulating and controlling thins on a small scale."

Richard Feynman, Caltech, 1959

"There's Plenty of Room at the Bottom"

Nowadays, nanoscience and nanotechnology have become decisive in the scientific development, achieving knowledge and progress to enhance the level of well-being in our society.

As starting point of this introduction the concept "nano" should be defined. The meaning of this prefix is one-billionth (10^{-9}) part that coming from Greek was used in order to describe something really small, as shown in figure 1.1. Therefore, nanoscale is comprehended, with at least one spatial dimension, between 1 and 100 nm.

Nanoscience [1] is the study of nanoscale materials employing the nanotechnology to characterize their specific physical, chemical and biological behaviours due to the influence of their small dimensions.

Nanotechnology[2] is the development of miniaturization techniques that starts at the macroscopic world, giving rise to the nanoworld. In addition, it is comprised the manipulation of functional systems at the atomic, molecular and supramolecular scale to achieve new materials, structures, components, and systems belonging to the nanoscale.

Both areas, nanoscience and nanotechnology, were emerged with Richard Feynman's conference growing together since 1959.

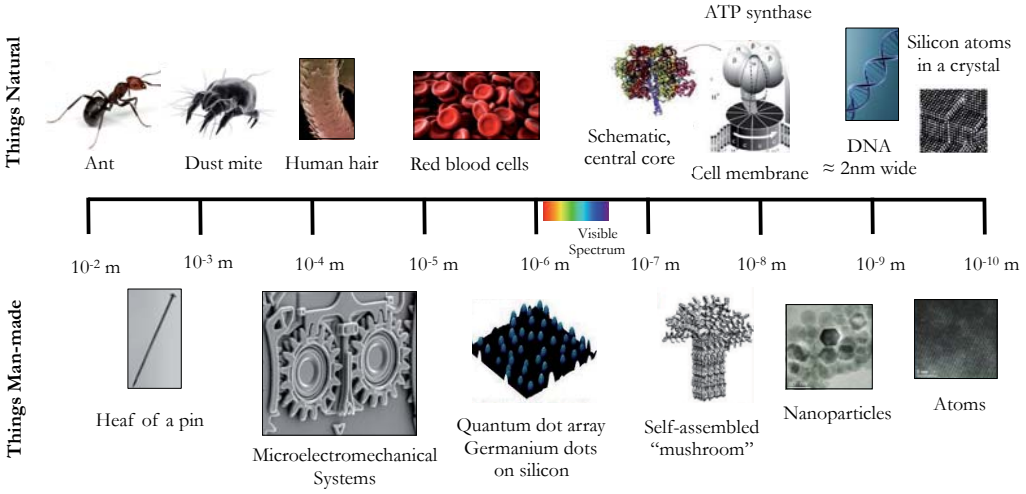

Figure 1.1: Size scale of nanoscience and nanotechnology

2. Nanostructured Material[3]

Nanomaterials are chemical substances or materials that are manufactured with at least one external dimension in the nanoscale. Nanostructured materials are developed to provide them with novel and unique properties, such as optical, electronic or mechanical, compared to the same material without nanoscale features.

2.1. Nanomaterials Classification

There are many different ways to classify nanomaterials depending, for example, on their morphology or composition (among others).

2.1.1. According to their morphology:

- **0D Nanomaterials** [4] : The main characteristic of zero-dimensional nanomaterials is that all three dimensions are compressed into nanoscale. They can

perform discrete nanomaterials such as nanoparticles, surface nanofeatured or bulk nanostructured materials as nanoparticle composites.

- **1D Nanomaterials**[5]: In this group are included nanorods and nanowires. This organization can be brought about by the use of templates such as carbon nanotubes, pores in alumina, steps on crystalline surface as well as polymer chains.

- **2D Nanomaterials**[6]: Thin films and interfaces, which have one of their three dimensions compressed into the nanoscale. They can be composed by metals, metallic oxides or carbon-based materials. These arrays have generally been prepared by simply evaporating dispersions of suitable functionalized, monodisperse nanocrystals on hydrophobic surfaces such as a carbon film. Sophisticated techniques have been developed to achieve a controlled deposition down to single atomic layers. Several matured vapour-phase techniques can be used to obtain controlled deposition of 2D nanomaterials such as pulsed laser deposition (PLD) or atomic layer deposition (ALD).

- **3D Nanomaterials**[7]: Three-dimensional arrays of nanomaterials can be obtained by the use of a layer-by-layer assembly technique. Multilayer deposition is achieved by the use of alternate layers of nanomaterials and linkers. Structures and devices are a clear example of these nanomaterials.

2.1.2. According to their composition:

- **Semiconductor Nanomaterials**[8]: In these materials, the electronic structure is constituted for the confinement of the electrons in nanometer-size foils or grains. Due to the quantization of electron energies, these systems are often called quantum structures or quantum dots (QDs) if the electrons are confined by potential barrier in the three spatial dimensions.

The quantization of electron energies in nanometer-size crystals produces changes in optical properties. This phenomenon exists also in larger crystals, where

it gives rise to the valence and conduction bands separated by the band gap. In bulk crystals, each electron band consists of a continuum of electron states. However, the energy spacing of electron states increases with decreasing QDs size, and therefore the energy spectrum of an electron band approaches a set of discrete lines in nanocrystals.

- **Metal Nanomaterials**[9]: Metallic nanocrystals have a wide range of applications in different fields. They are very interesting for their huge potential in nanotechnology. These materials are formed by a group of metal atoms with an oxidation state equal to zero. The intense interest in the metallic nanoparticles in different applications such as catalysis or biomedical derives from their unique chemical and electronic properties arising from the small volume to big surface area ratio and their separation in the electronic energy levels providing a specific band structure. This unique electronic structure allows the presence of plasmon excitations and quantum confinements.

- **Metal Oxides Nanomaterials**[10]: This group could be enclosed in semiconductor nanocrystals due to their characteristics but they have specific mechanical properties such as low elasticity, high plasticity, low hardness, etc. These nanocrystals are very important in many areas of chemistry, physics and materials science for the fabrication of microelectronic circuits, sensors, fuel cells. Magnetic nanoparticles such as magnetite or ferrite are also included in metal oxide nanoparticles. They have been widely used in the biotechnology, biomedical or catalysis. The main characteristic of magnetic nanoparticles is that with diameters smaller than some certain critical value usually show properties different from their bulk analogue. The magnetic moments in these particles are free to align with the field during the measuring time at room temperature. This phenomenon is called superparamagnetic behaviour and allows a promising future in applications of the magnetic nanoparticles in resonance imagining, tissue engineering and drug delivery among others.

2.2. Nanomaterials Properties

2.2.1. Surface-Volume Ratio[11]

The high surface-volume ratio is a meaningful characteristic of nanomaterials. The increased ratio of surface area to volume has an important role in the reactivity in the surfaces of particles. Nanomaterials have more surface area than bulk materials (figure 1.2) and for this reason, they present accessible sites for other chemicals to bind or react with them.

The large surface area to volume ratio of nanomaterials opens many capabilities for generating new materials and facilitating chemical processes. For example, they can be used as potent catalysts[12] or be applied in thin films[13] improving the properties of the bulk material.

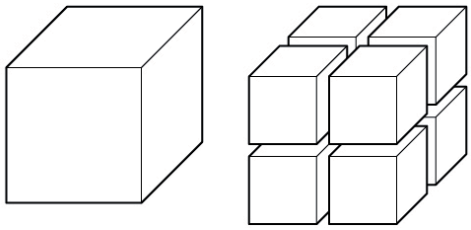

Figure 1.2: Surface-volume ratio

Conversely, the high surface-volume ratio in nanoparticles causes a bigger surface tension, which produce aggregation and coalescence[14]. In order to reduce this phenomenon, different methodologies are used to stabilise the nanomaterials such as the generation of coulombic repulsion between two individual particles (electrostatic methodology[15]), the addition of capping ligand to produce a steric hindrance and geometric constrains (steric methodology[16]) or the stabilisation systems with ionic liquid which is composed by cations and anions that electrostatically isolate the nanoparticles generating a shell of molecules producing steric stabilisation (ionic liquid methodology[17]).

2.2.2. Electronic and Optical[18]

Electronics, as the name implies, is a field of engineering that involves electrons transport and storage.

Nanocrystalline particles have behaviours between bulk solid and single molecule. Therefore, their physical properties gradually change from solid state to molecular properties with decreasing particle size producing different effects:

- Due to their small dimensions, the surface to volume ratio increases and for this reason, the surface properties are no longer negligible. An important property is that the surface atoms are highly unsaturated and their electronic contribution to the behaviour of the particles is totally different from that of the inner atoms.

- The second phenomenon, which occurs in metal and semiconductor nanoparticles, has a huge dependence of their electronic behaviours. As shown in the following figure 1.3, the nanoparticles electronic singularity is totally influenced by their size. Then, starting at the macroscopic material with overlapped orbitals represented by bands to the well-known discrete orbitals of a molecule, nanoparticles are between these two extremes. In metal nanoparticles, the quasi-continuous density of states in the valence and the conduction bands splits into discrete electronic levels; the layout between these levels and the band gap increasing by decreasing their particle size. In the case of semiconductors, the phenomenon is quite different because the band gap already exists in the bulk state. However, this band gap also increases when the particle size is decreased and the energy bands gradually convert into discrete molecular electronic levels. In semiconductors nanoparticles, the quantization effect that improves the optical gap is observed for clusters ranging from 1 to 10 nm. Metal particles consisting of 50 to 100 atoms with a diameter between 1 and 2 nm start to lose their metallic behaviour and tend to become semiconductors.

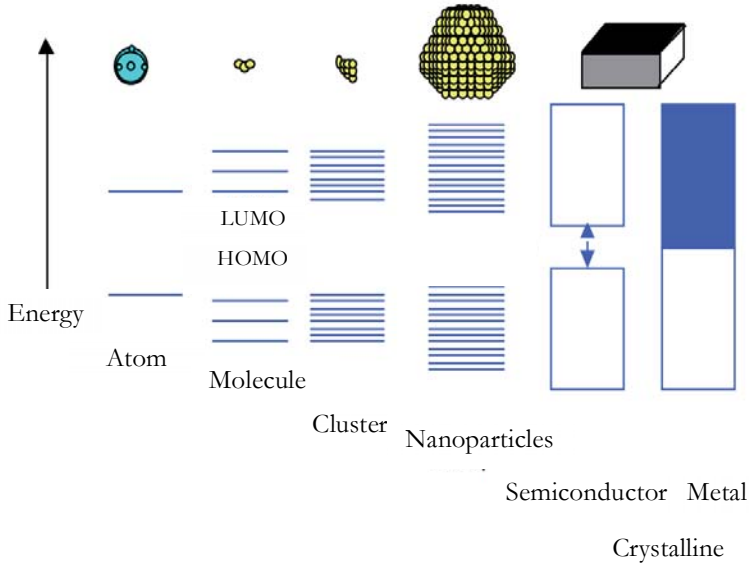

Figure 1.3: Size quantization effect

There are several kinds of nanoelectronic materials[19] composed usually by nanotubes or quantum dots, which allow higher electron mobility, high dielectric constant, and a symmetric electron/hole characteristic. The use of biological and complex organic molecules in circuits, nanowires electrical conduits, quantum dot relays, nanoresonators, single-electron transfer, single-photon optics, zeptomole level analytical capability, atomic level and better resolution, advanced solar cells and components, quantum computing and spintronics and nanoscale fields emitters the list goes on and the possibilities are endless.

On the other hand, optics is the study of the interactions of light with matter and other optical phenomena. Nano-optics can be defined as the study of optical phenomena and techniques near or beyond the diffraction limit. Optical nano effect[20] was uncovered in stained glass and nowadays quantum dots are the most advanced technology for electronic applications. Nano-optics is developing alongside nanotechnology and new instrumentation is designed to see them better as scanning electron microscope (SEM), transmission electron microscope (TEM), atomic force microscope (AFM).

One of the most important optic effects in clusters is the surface plasmon[21]. Since a large number of atoms of the metallic nanoparticles are actually on the

surface, the neighbouring electrons form a sort of an electron gas (cloud) since they are in continuous interaction among themselves. The surface plasmon is thus collective excitation of free electrons on the surface of the clusters. When the light is incident on nanoparticles, its electric field perturbs this electron cloud promoting electrons to a higher energetic level. This phenomenon creates surfaces charge separation usually called dipolar resonance. The dipolar oscillation of all electrons will have the same phase and when the frequency of the electromagnetic field resonates with the coherent electron motion that makes a high absorption in the optical spectrum. That plasmon oscillation phenomenon is responsible for the colour imparted. The frequency and width of the surface plasmon absorption depend on the size and shape of nanoparticles. Surface plasmon effect often occurs in metals like silver or gold in contact dielectrics such as air or silicon dioxide, but can also exist on interfaces other than flat surfaces, such as particles or rectangular strips, cylinders, and other structures.

2.2.3. Magnetism[22]

The main characteristic of magnetic nanoparticles is that they can be manipulated with a magnetic field gradient. In the present research work, magnetite nanoparticles have been synthetized and characterized.

Different kinds of materials can be classified according to their magnetic behaviours:

- **Non-magnetic**: Material that is not perturbed by magnetic field.

- **Diamagnetism**[23]: Diamagnetic material created an induced magnetic field in opposite direction to an externally applied magnetic field. That factor provokes repulsion between induced and applied fields. Usually composed of atoms, which have no net magnetic moments which means that all the orbitals shells are filled and all electron are paired.

- **Paramagnetism**[24]: Materials are attracted by an externally applied magnetic field, inducing an internal magnetic behaviour in the opposite direction. In this particular case, some of the atoms or ions in the material have a net magnetic moment due to unpaired electrons in partially filled orbitals.

- **Ferromagnetism** [25] : In this case, they can form permanent magnets exhibiting high magnetic permeability, characteristic saturation point, and magnetic hysteresis. Unlike paramagnetic behaviour, the atomic moments exhibit very strong interactions produced by electronic exchange and result in a parallel or antiparallel alignment of atomic moments.

- **Ferrimagnetism**[26]: A magnetic ordering is occurred as a result of the crystal structure. A ferrimagnetic material has populations of atoms with unequal and spontaneous opposing magnetic moments.

- **Antiferromagnetism** [27]: The magnetic moment of atoms is aligned in a regular pattern with neighboring spins pointing in opposite directions. The magnetic moments existing inside the material are distributed in other to achieve a net moment equal to zero.

- **Superparamagnetism**[28]: This kind of magnetism is specially found in small ferromagnetic or ferromagnetic nanoparticles. The magnetic material is totally magnetised under external magnetic field.

Magnetic material properties can be represented with a hysteresis loop (figure 1.4), which shows the variation of the magnetic density flux B with the external magnetic field H.

By applying a field ***H*** makes the magnetic induction to increase in the field

direction. If $\boldsymbol{H}$ is increased indefinitely the magnetization eventually reaches saturation $\boldsymbol{M_o}$ where all the magnetic dipoles are aligned in the direction of the applied magnetic field $\boldsymbol{H}$. The saturation magnetization $\boldsymbol{M_o}$ depends on the magnitude of the atomic magnetic moments m and the number of atoms per unit volume n, as shown in the following equation (Eq.1.1).

$$\mathbf{M_o} = \boldsymbol{n} \cdot \boldsymbol{m} \qquad \text{Eq.1.1}$$

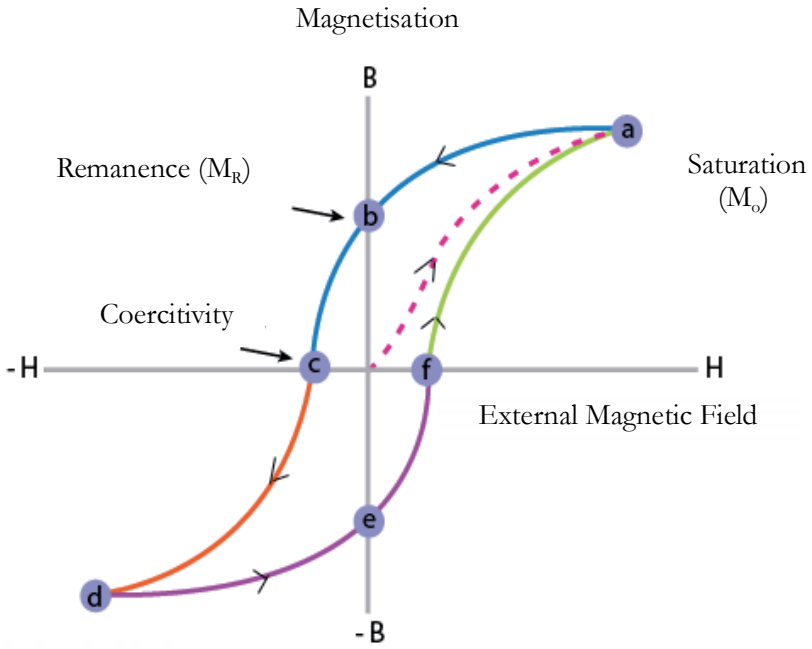

Figure 1.4: Hysteresis loop of a magnetic material

When the field is reduced to zero after the magnetic sample has been magnetized to saturation, the remaining magnetization is called the *remanent magnetization or remanence* $\boldsymbol{M_R}$. The *remanence* is used to describe the value of the persistent induction and magnetization after the application of the field to an arbitrary level. In other words, it becomes the upper limit of all remanent inductions or magnetizations.

The *coercivity* phenomenon appears when the magnetic field can be reduced to zero applying a reverse magnetic field of strength. As a value it depends on the condition of the sample, being affected by such factors as heat treatment or deformation.

Depending on the type of magnetic material, the hysteresis loop will present a particular shape (figure 1.5). **(a)** Diamagnetic materials show a typical negative hysteresis loop. **(b)** Paramagnetic materials subjected to magnetic fields other than very high fields the magnetization is proportional to the field. **(c)** Superparamagnetic materials, there is a quick response and saturation under magnetic field; the coercitivity and remanence are close to zero. **(d)** Ferromagnetic and ferrimagnetic materials (hard permanent magnet), which has a large coercitivity field, the loop forms an open cycle.

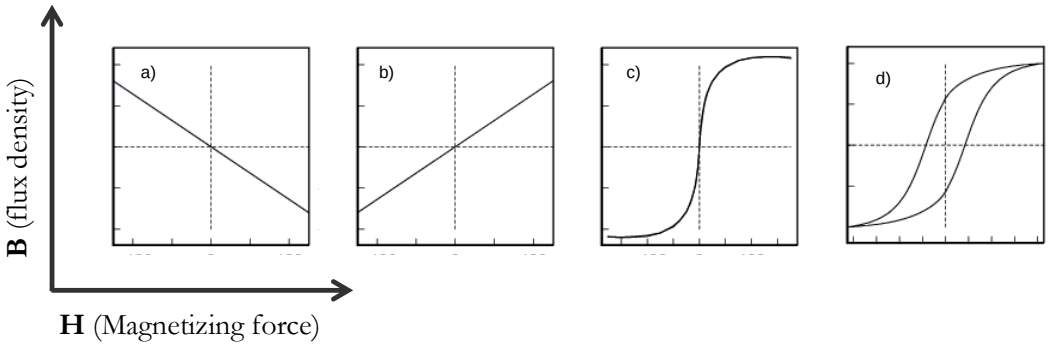

Figure 1.5: Hysteresis loops: a) diamagnetic, b) paramagnetic, c) superparamagnetic, d) ferromagnetic

2.3. Nanomaterials Applications

Functional materials synthesized on the nanoscale, represent evolutionary developments of existing technologies and are really attractive to apply them in many fields such as Hi-Tech Industry, medicine, chemistry or physics.

- **Medicine**[29]: The utilization of nanomaterials in medicine was developed in order to improve the well-being of our society. The application of nanomaterials, in the field of tumor drug delivery, are a huge advance due to this novel treatment modality can provide a safe and effective therapy using various nanomedicines in cancer treatment without apply aggressive and destructive treatments. An example of this new nanomedicine field is the application of nanomaterials to carry the antitumor reagent to the blood vessels in the tumor and possibly leak the tumor

tissue though the intercellular space between the endothelial cells[30]. The antitumor drug could reach the target region due to the nanoparticles and provide the drug inside the tumor to treat it and eliminate the cancerous cells. An other important application of nanomaterials, that will be deeply explained in section 4, is for antioxidant human cells applications due to their capacity to decrease the level of *reactive oxygen species* (ROS).

- **Hi-Tech Industry**[31]: One of the clearest examples of the Hi-Tech Industry is in the automotive companies. This community use nanotechnology and nanomaterials to improve the performance of new cars models. Some companies are using conductive carbon nanotube composite materials or others nanocomposites in fuel systems or in bumpers making some products 60% lighter, but twice as resistant to denting and scratching. Others examples of the variety of functions of nanomaterial products in the automotive industry are tires reinforced with nanoparticles for better abrasion resistance, structural plastic parts combining higher mechanical performance with reduced weight and anti-fog coatings for headlights and windshields. In addition, there are other applications of the nanomaterials in Hi-tech Industry is present mobile phone market[32], where the new smart phones are fabricated with nanomaterials to increase the effectiveness of electronic devices improving display screens, which involves to reduction of power consumption decreasing the weight and thickness of the screen, developing the density of memory chips and reducing the size of transistor used in integrated circuits.

- **Chemistry & Physics**[33]: Nanomaterials are really important pieces on the chemistry and physics fields due to they allow a huge and fast development of the forefront technology. New promising strategies are performed to improve and replace the old findings. Coated conductor development using nanocomposite film growth mechanisms have a huge interest for power applications and magnets[34]. The use of superconductor materials are widely applied in scientific facilities, magnetic resonance spectrometers or magnetic resonance imaging systems. A completely new frontier has been already investigated to produce high temperature superconductor

(HTS) nanocomposites structures where non-superconducting nanoparticles or nanorods can improve the properties of the current superconductors and for this reason, the current technology systems.

2.4. Characterization Methods

Characterization of nanomaterials, thanks to the improved availability of sophisticated physical and chemical techniques, allowed a huge development of nanoscience and nanotechnology. Characterization of nanomaterials includes the determination of materials composition, structure, size, shape and other properties.

This research work will develop and deeply study the synthesis and the characterization of different nanomaterials such as diverse oxide nanoparticles to generate nanostructured $YBa_2Cu_3O_{7-\delta}$ (YBCO) superconducting thin layer in order to improve the superconducting properties and to apply them as an antioxidant nanomaterials for human cells. For that reason, a full characterization is compulsory in order to know how is constituted, formed and stabilized the nanocomposite nanostructured superconducting system using different techniques such as X-Ray diffraction (XRD), Photoelectron Spectroscopy (XPS), electron microscopy such as Transmission Electron Microscope (TEM) or Scanning Electron Microscope (SEM), Infrared Spectroscopy (IR), Gas Chromatography-Mass Spectrometry (GS /MS), Dynamic Light Scattering (DLS), Thermogravimetric analysis and differential scanning calorimetry (DLS) and magnetometry such as Superconductor Quantum Interference Device (SQUID) or Field Cooling-Zero Field Cooling (FC – ZFC).

Due to the application of the different metal oxide nanoparticles synthetized during this thesis in superconductivity and in cell biology fields, an introduction of these two topics is also performed below.

3. Superconductivity

The superconductivity was discovered by Dutch physicist Heike Kamerlingh Onnes of Leiden University in 1911 when he cooled mercury with liquid helium (4K, -269ºC)[35].

Superconductivity is a physical phenomenon observed in metals and ceramic materials with favourable structural behaviours. These materials present a specific behaviour that allows to an applied electric current flow without resistance and to repulse magnetic flux completely when the temperature is below their critical temperature $\boldsymbol{T_c}$. This critical temperature is characteristic and a unique value to each material presenting an important dependence to the structure and chemical composition.

This superconductor property is due to *Cooper pairs* and consists on a couple of fermions that are attractively bound with equal but opposite momentum and spin. Cooper pairs theory establishes that superconductivity in conventional materials arises from interactions of the conduction electrons with the vibrations of the atoms. This interaction enables a small net attraction between pairs of electrons.

Furthermore, the *current density* ($\mathbf{J_c}$), and the magnetic field ($\mathbf{H_c}$) depend on the temperature ($\mathbf{T_c}$). However, Jc, Hc and Tc are independent parameters. If one of these three parameters, is exceeded; the superconductivity is broken obtaining a normal conductor material (figure 1.6).

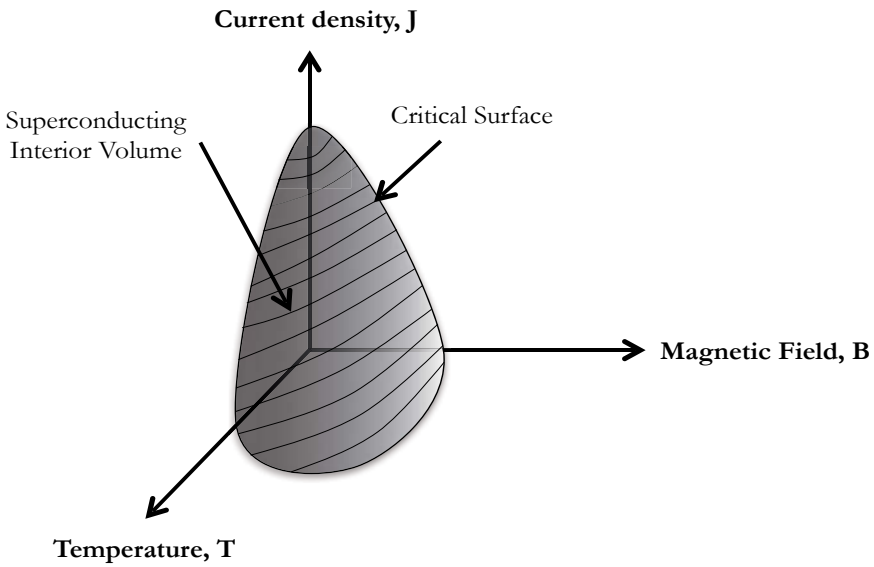

Figure 1.6: Superconductivity limits

3.1. Superconductors

In a superconductor below his critical temperature, no resistance is produced because electrons moving though the metal are no scattered due to there is not deviations from translational symmetry or vibrations of the lattice in the metal giving raise to a temperature independent contribution to the resistance.

The German physicists Walther Meissner and Robert Ochsenfeld discovered in 1933 the *Meissner effect*[36]. This effect is characteristic of superconducting materials and consists of the repulsion of a magnetic field from a superconductor (figure 1.7) becoming a perfect diamagnetism material.

A magnet moving by a conductor induces currents in the conductor but in a superconductor the induced currents exactly mirror the field that would have otherwise penetrated the superconducting material causing the magnet repulsion. The Meissner effect is so strong that a magnet can levitate over a superconductive material.

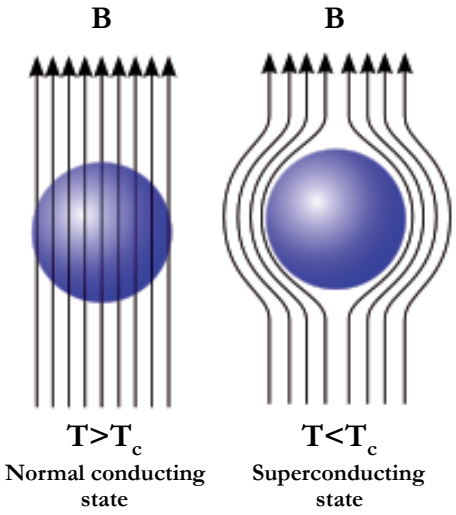

Figure 1.7: Meissner effect

In 1986, high temperature superconductors (HTS)[37], which have a critical temperature of 92K were discovered by Georg Bednorz and K. Alex Müller. The principal advantage to use HTS is that they can be cooled to superconductivity behaviour using liquid nitrogen (77 Kelvin). A clear example of this type of superconductors is the YBCO.

3.1.1. Types I and II superconductor

There are two kinds of superconductors: type I and type II[38]. The type I superconductors have a critical thermodynamic field B_c where the external magnetic field can not penetrate. In this Meissner state, the superconductor becomes a perfect diamagnetic material. When the magnetic field is higher than B_c, the superconductor becomes a normal conductor. On the other hand, in type II the Meissner state only occurs for lower magnetic fields than B_{c1}. When the magnetic field is higher than B_{c1}, this can penetrate inside the superconductor generating a quantized cylindrical flux lines called vortex[39].

Consequently, these superconductors have the ability to bring high currents in external applied magnetic fields. When the penetration of the external magnetic field increase, more vortexs are generated until reaches the B_{c2} where the superconductivity properties are lost (figure 1.8). In order to increase B_{c2}, new proposes to limit the movement of the vortex such as the embedding of nanoparticles inside of the superconductor are studied[40].

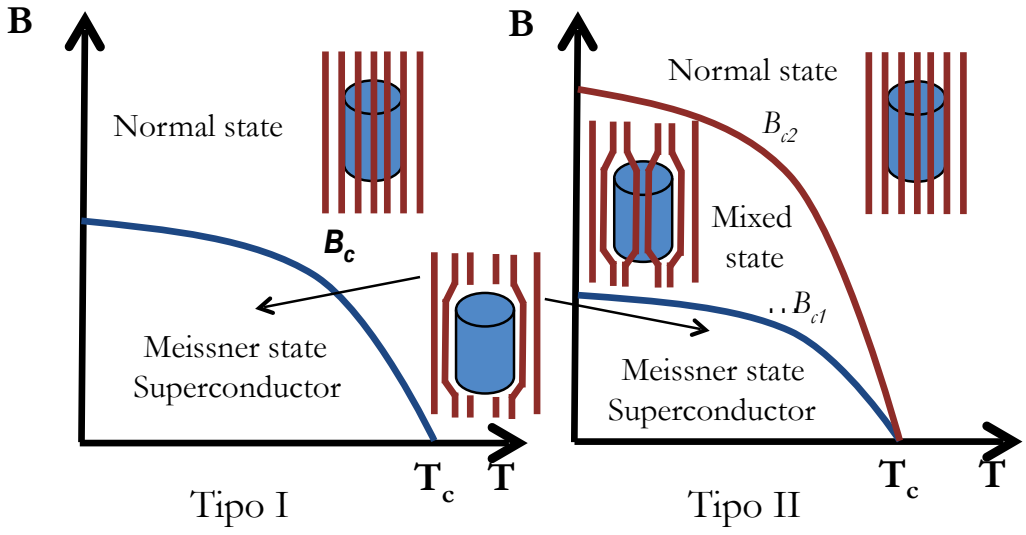

Figure 1.8: Magnetic phase diagram for type I and II superconductors

3.1.2. Vortex pinning[41]

Vortex pinning is an effect that appears in mixed state. The magnetic vortexs are anchored inside the superconducting structure and when an external magnetic field is applied, vortex pinning phenomenon avoids their movement. When the vortices can easily move in and out of the superconductor, pinning is very weak. When the vortexes are completely frozen in their position, though, pinning is very strong. Multiple factors determine the pinning force of vortices: the presence of impurities, the shape, size and distribution of the defects presents in the superconducting structure matrix. The superconductor natural defects such as precipitates, dislocations or anti-phase domains (region of a crystal where the atoms are configured in the opposite order to those in the perfect lattice system), can act as vortex pinning but if they are in high concentration the properties of the superconductor will be reduced. In order to control and reduce the effect of these natural structural defects, new strategies are developed focusing on the generation of artificial non superconducting nanoregions inside the superconductor structure to control and increase the properties in the mixed superconductor state. The introduction of self-assembled inclusions[42] into superconducting materials has been established as a very efficient route to improve their current-carrying capacity. In particular, such inclusions can be prepared in the form of almost spherical particles, nanorods or combination of both.

3.2. $YBa_2Cu_3O_{7-\delta}$ Superconductor

YBCO compound possess excellent current capabilities at high magnetic fields and thus, this HTS ($T_c \approx 92K$) is really interested to apply in different kinds of cryogenic technologies.

The YBCO structure[43] corresponds to a triple perovskite based on $BaCuO_3$ and $YCuO_2$ units, where CuO_2 planes and CuO_x layers oriented in c-direction, which are parallels to a-b direction, can produce the superconducting phenomenon due to the transport of carriers occurs in this specific planes generating the *Cooper pairs*. This phenomenon appears because CuO_x layers are forming chains, which have the

property to be charge reservoirs giving carriers to CuO_2. Concretely, the current only flows in CuO_2 planes producing the conductivity to be confined in a-b planes, which is achieved with an epitaxial YBCO conformation as shows in following figure 1.9.

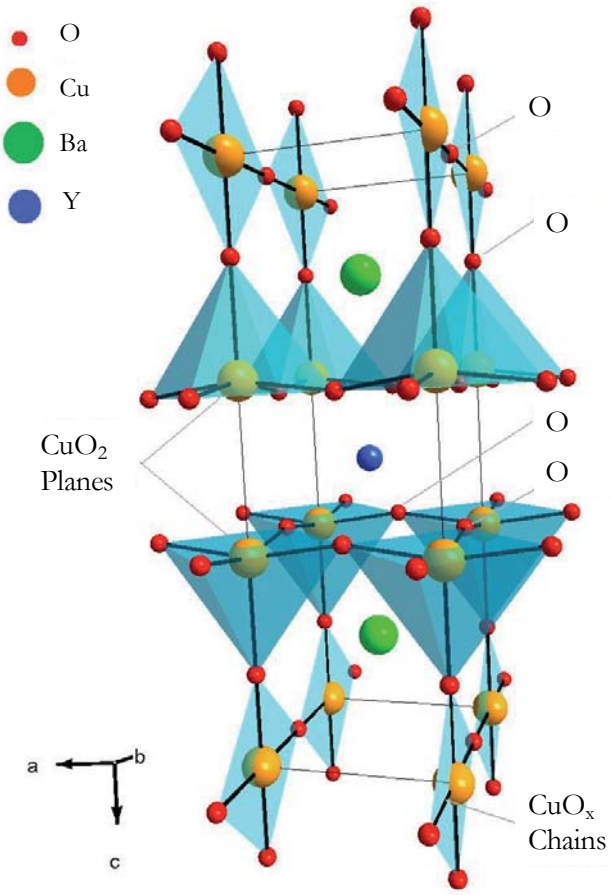

Figure 1.9: $YBa_2Cu_3O_{7-\delta}$ Structure

In CuO_x chains oxygen vacancies are produced and thus, the structure can be affected. When the chains are full of oxygen the structure corresponds to orthorhombic Pmmm ($a \neq b \neq c$; a = 0.3886 nm, b = 0.3821 nm, c = 1.1687 nm) as was shown in figure 4.1. Moreover, when there is no oxygen in the chain tetragonal P4/mmm structured is formed ($a \neq c$; a = b = 0.3870 nm; c = 1.1801 nm). This specific property, defines the stoichiometry of the oxygen in the final YBCO, which is represented by δ and goes from 0 to 1 values (0 = no oxygen ; 1 = full of oxygen).

Furthermore, the values of δ are really important in order to obtain a superconductor material due to only the orthorhombic structure can produce the superconductivity phenomenon instead of tetragonal structure where isolating material is formed. For this reason, it is crucial to control the quantity of oxygen during the formation of YBCO compound performing an oxygenation process.

3.3. Superconductor Applications

The ability of superconductors to conduct electricity with zero resistance can be really useful in a huge rang of different applications:

- **Transportation**[44]: Superconductors are implemented a new generation of transport technologies including marine propulsion systems, magnetically levitated trains, railway tractions transformers, etc.

- **Medicine**[45]: Progress in HTS guarantee more compact and less costly in magnetic resonance image (MRI) systems with a higher imaging quality. Furthermore, MRS has a great benefit because they are non-invasive diagnostic techniques.

- **Industry**[46]: Powerful magnets for applications in different industrial processing will be able to reduce the percentage of electricity losses. More examples of the superconductor application in industry field are for example s sensors and transducers, magnetic shielding, motors, fusion, transformers and inductors, transmission, generators, etc.

- **Electronics**[47]: Superconducting analogue devices have demonstrated to get higher sensitivities, speed, and frequency limits and lower power dissipation than competing semiconductor devices. The use of superconductor devices in different techniques such as millimetre wave detection or digital radio, have advantages and may be expected to continue to be developed over the coming decades.

• **Communications**[48]: Superconductor filters have come into widespread use in mobiles communications systems. They enhance signal-to-noise ratios, enabling reliable service and with fewer mobile towers. Superconductor chips offer dramatic performance improvements in many commercial and military applications.

• **Scientific Research** [49] : Today superconductor materials, are improving scientific research facilities. They are searching for new techniques pushing the frontiers of human knowledge.

For all these applications and more, the study and improvement in superconductivity field are in full swing and has become a state of the art.

4. Antioxidant Nanomaterials for Human Cells

The unique chemical and biological properties of nanomaterials, as was explained in this chapter, make them also useful in many products for humans[50], including some in industry, agriculture, business, medicine, clothing, cosmetics, and food. Furthermore, the tiny size of these new materials allows their utilization directly in human bodies due to their capacity to pass more easily through cell membranes and other biological barriers[51]. Thanks to their specific properties, including high surface-to-volume ratios, nanomaterials are reactive or catalytic, and thus can be potentially useful for the safe development of nanotechnology and the safe use of commercial nanomaterials.

The mechanisms underlying the toxicity of nanomaterials have recently been studied intensively. An important mechanism of nanotoxicity is the capture of reactive oxygen species (ROS), resulting in the subsequent elimination of oxidative stress in tissues[52].

In the mitochondria of cells, during the synthesis of ATP, the formation of superoxide anion radicals, and subsequently other oxygen-containing radicals are also performed. Thus, ROS are byproducts of cellular oxidative metabolism, which also include superoxide anion radicals, hydroxyl radicals, singlet oxygen, and hydrogen peroxide (H_2O_2)[53]. Overproduction of ROS can induce oxidative stress,

resulting in cells failing to maintain normal physiological redox-regulated functions [54]. The damage in cell function and development includes oxidative modification of proteins to generate protein radicals [55], initiation of lipid peroxidation[56], DNA-strand breaks, modification to nucleic acids[57], modulation of gene expression through activation of redox-sensitive transcription factors[58], and modulation of inflammatory responses through signal transduction[59], leading to cell death and genotoxic effects[60]. It has been demonstrated that ROS and oxidative stress are associated with many age-related degenerative diseases [61], including amyotrophic lateral sclerosis, arthritis, cardiovascular disease, inflammation, Alzheimer's disease, Parkinson's disease, diabetes, and cancer. For this reason, the reduction of ROS induced by nanomaterials, directly or indirectly, plays a vital role in human cells to avoid the antioxidant process.

The level of ROS reduction by engineered nanomaterials is dependent on the chemical nature of the nanoparticles[62]. Compared to their bulk-size counterparts, engineered nanomaterials possess a high surface reactivity, demonstrating their ability to react with hydrogen peroxide, which is becoming a new strategy to guarantee a longer life of biological systems as an antioxidant behaviour.

5. Bibliography

1) Nanoscience and nanotechnologies: opportunities and uncertainties. Royal Society and Royal Academy of Engineering. July 2004.

2) Nanotechnology Information Center: Properties, Applications, Research and Safety Guidelines. American Elements. Retrieved 13 May 2011.

3) Ozin, G. A., & Cademartiri, L. (2009). Nanochemistry: What is next? *Small*, *5*(11), 1240–1244. doi:10.1002/smll.200900113.

4) Pang, S., Zhou, Z., & Wang, Q. (2013). Smart 0D nanomaterials assembled by green luminescent terbium hybrids for the detection of tryptophan. *Journal of Nanoparticle Research*, *15*(3). doi:10.1007/s11051-013-1495-7.

5) Han, J. T., Choi, S., Jang, J. I., Seol, S. K., Woo, J. S., Jeong, H. J., & Lee, G.Woong. (2015). Rearrangement of 1D Conducting Nanomaterials towards Highly Electrically Conducting Nanocomposite Fibres for Electronic Textiles. *Scientific Reports*, *5*, 9300. doi:10.1038/srep09300.

6) Luo, B., Liu, G., & Wang, L. (2016). Recent Advances in 2D Materials for Photocatalysis. *Nanoscale,* 8, 6904-6920. Doi: 10.1039/ C6NR00546B.

7) Liu, P., Hao, Q., Xia, X., Lu, L., Lei, W., & Wang, X. (2015). 3D hierarchical mesoporous flowerlike cobalt oxide nanomaterials: Controllable synthesis and electrochemical properties. *Journal of Physical Chemistry C*, *119*(16), 8537–8546. doi:10.1021/acs.jpcc.5b01315.

8) O'Brian, P., & Pickett, N.L., (2001). Nanocrystalline Semiconductors: Synthesis, Properties, and Perspectives. *Chemistry of Material,* 13, 3843-3858. Doi:10.1021/cm000843p.

9) Kelly, K. L., Coronado, E., Zhao, L. L., & Schatz, G. C. (2003). The Optical Properties of Metal Nanoparticles: The Influence of Size, Shape, and Dielectric Environment. *The Journal of Physical Chemistry B*, *107*(3), 668–677. doi:10.1021/jp026731y.

10) Franke, M. E., Koplin, T. J., & Simon, U. (2006). Metal and metal oxide nanoparticles in chemiresistors: Does the nanoscale matter? *Small*, *2*(1), 36–50. doi:10.1002/smll.200500261.

11) Issa, B., Obaidat, I. M., Albiss, B. A., & Haik, Y. (2013). Magnetic nanoparticles: Surface effects and properties related to biomedicine applications. *International Journal of Molecular Sciences*, *14*(11), 21266–21305. doi:10.3390/ijms141121266.

12) Gawande, M. B., Goswami, A., Felpin, F.-X., Asefa, T., Huang, X., Silva, R., & Varma, R. S. (2016). Cu and Cu-Based Nanoparticles: Synthesis and Applications in Catalysis. *Chemical Reviews*, *116*(6), 3722–3811. doi:10.1021/acs.chemrev.5b00482.

13) Hu, L., Hecht, D. S., & Grüner, G. (2010). Carbon Nanotube Thin Films: Fabrication, Properties, and Applications. *Chemical Reviews*, *110*(10), 5790–5844. doi:10.1021/cr9002962.

14) Ingham, B., Lim, T. H., Dotzler, C. J., Henning, A., Toney, M. F., & Tilley, R. D. (2011). How Nanoparticles Coalesce: An in Situ Study of Au Nanoparticle Aggregation and Grain Growth. *Chemistry of Materials*, *23*(14), 3312–3317. doi:10.1021/cm200354d.

15) Pramod, P., Joseph, S. T. S., & Thomas, K. G. (2007). Preferential End Functionalization of Au Nanorods through Electrostatic Interactions. *Journal of the American Chemical Society*, *129*(21), 6712–6713. doi:10.1021/ja071536o.

16) Chong, J. Y. T., Mulet, X., Keddie, D. J., Waddington, L., Mudie, S. T., Boyd, B. J., & Drummond, C. J. (2015). Novel Steric Stabilizers for Lyotropic Liquid Crystalline Nanoparticles: PEGylated-Phytanyl Copolymers. *Langmuir*, *31*(9), 2615–2629. doi:10.1021/la501471z.

17) Gkermpoura, S., Obiols-Rabasa, M., Iatridi, Z., & Tsitsilianis, C. (2015). Thermo-Resistant Soft Glassy Suspensions of Polymeric Micellar Nanoparticles in Ionic Liquid. *ACS Applied Materials & Interfaces*, *7*(23), 12411–12421. doi:10.1021/am507587s.

18) Shi, G., & Kioupakis, E. (2015). Electronic and Optical Properties of Nanoporous Silicon for Solar-Cell Applications. *ACS Photonics*, *2*(2), 208–215. doi:10.1021/ph5002999.

19) Lee, W. S., Choi, J., Park, I., & Lee, J. (2012). Room-Temperature Compressive Transfer Printing of Nanowires for Nanoelectronic Devices. *Langmuir*, *28*(51), 17851–17858. doi:10.1021/la3036133.

20) Pazos-Perez, N., Garcia de Abajo, F. J., Fery, A., & Alvarez-Puebla, R. A. (2012). From Nano to Micro: Synthesis and Optical Properties of Homogeneous Spheroidal Gold Particles and Their Superlattices. *Langmuir*, *28*(24), 8909–8914. doi:10.1021/la3002898.

21) Chou, Y.H., Chou, B.T., Chiang, C.-K., Lai, Y.Y., Yang, C.T., Li, H., & Lu, T.C. (2015). Ultrastrong Mode Confinement in ZnO Surface Plasmon Nanolasers. *ACS Nano*, *9*(4), 3978–3983. doi:10.1021/acsnano.5b01643.

22) Salafranca, J., Gazquez, J., Pérez, N., Labarta, A., Pantelides, S. T., Pennycook, S. J., & Varela, M. (2012). Surfactant Organic Molecules Restore Magnetism in Metal-Oxide Nanoparticle Surfaces. *Nano Letters*, *12*(5), 2499–2503. doi:10.1021/nl300665z.

23) Sklute, E. C., Eguchi, M., Henderson, C. N., Angelone, M. S., Yennawar, H. P., & Mallouk, T. E. (2011). Orientation of Diamagnetic Layered Transition Metal Oxide Particles in 1-Tesla Magnetic Fields. *Journal of the American Chemical Society*, *133*(6), 1824–1831. doi:10.1021/ja107090n.

24) Zanzoni, S., Pedroni, M., D'Onofrio, M., Speghini, A., & Assfalg, M. (2016). Paramagnetic Nanoparticles Leave Their Mark on Nuclear Spins of Transiently Adsorbed Proteins. *Journal of the American Chemical Society*, *138*(1), 72–75. doi:10.1021/jacs.5b11582.

25) Townsend, J., Burtovyy, R., Galabura, Y., & Luzinov, I. (2014). Flexible Chains of Ferromagnetic Nanoparticles. *ACS Nano*, *8*(7), 6970–6978. doi:10.1021/nn501787v.

26) Lee, N., Choi, Y., Lee, Y., Park, M., Moon, W. K., Choi, S. H., & Hyeon, T. (2012). Water-Dispersible Ferrimagnetic Iron Oxide Nanocubes with Extremely High r2 Relaxivity for Highly Sensitive in Vivo MRI of Tumors. *Nano Letters*, *12*(6), 3127–3131. doi:10.1021/nl3010308.

27) Van Roosbroeck, R., Van Roy, W., Stakenborg, T., Trekker, J., D'Hollander, A., Dresselaers, T., … Lagae, L. (2014). Synthetic Antiferromagnetic Nanoparticles as Potential Contrast Agents in MRI. *ACS Nano*, *8*(3), 2269–2278. doi:10.1021/nn406158h.

28 Kralj, S., & Makovec, D. (2015). Magnetic Assembly of Superparamagnetic Iron Oxide Nanoparticle Clusters into Nanochains and Nanobundles. *ACS Nano*, *9*(10), 9700–9707. doi:10.1021/acsnano.5b02328.

29) Abadeer, N. S., & Murphy, C. J. (2016). Recent Progress in Cancer Thermal Therapy Using Gold Nanoparticles. *The Journal of Physical Chemistry C*, *120*(9), 4691–4716. doi:10.1021/acs.jpcc.5b11232.

30) Wang, Z., Tiruppathi, C., Minshall, R. D., & Malik, A. B. (2009). Size and Dynamics of Caveolae Studied Using Nanoparticles in Living Endothelial Cells. *ACS Nano*, *3*(12), 4110–4116. doi:10.1021/nn9012274.

31) Kim, Y., Yoon, C., Ham, S., Park, J., Kim, S., Kwon, O., & Tsai, P.-J. (2015). Emissions of Nanoparticles and Gaseous Material from 3D Printer Operation. *Environmental Science & Technology*, *49*(20), 12044–12053. doi:10.1021/acs.est.5b02805.

32) Espinoza, V. S., Erbis, S., Pourzahedi, L., Eckelman, M. J., & Isaacs, J. A. (2014). Material Flow Analysis of Carbon Nanotube Lithium-Ion Batteries Used in Portable Computers. *ACS Sustainable Chemistry & Engineering*, *2*(7), 1642–1648. doi:10.1021/sc500111y.

33) Wen, A. M., Infusino, M., De Luca, A., Kernan, D. L., Czapar, A. E., Strangi, G., & Steinmetz, N. F. (2015). Interface of Physics and Biology: Engineering Virus-Based Nanoparticles for Biophotonics. *Bioconjugate Chemistry*, *26*(1), 51–62. doi:10.1021/bc500524f.

34) Xu, J., Yang, X., Wang, H., Chen, X., Luan, C., Xu, Z., … Lee, C.-S. (2011). Arrays of ZnO/ZnxCd1–xSe Nanocables: Band Gap Engineering and Photovoltaic Applications. *Nano Letters*, *11*(10), 4138–4143. doi:10.1021/nl201934k.

35) King, R. B. (1999). Chemical Structure and Superconductivity. *Journal of Chemical Information and Computer Sciences*, *39*(2), 180–191. doi:10.1021/ci980050b.

36) Zolotavin, P., & Guyot-Sionnest, P. (2010). Meissner Effect in Colloidal Pb Nanoparticles. *ACS Nano*, *4*(10), 5599–5608. doi: 10.1021/ nn102009g.

37) Llordés, A., Zalamova, K., Ricart, S., Palau, A., Pomar, A., Puig, T., & Obradors, X. (2010). Evolution of Metal-Trifluoroacetate Precursors in the Thermal Decomposition toward High-Performance $YBa_2Cu_3O_{7-\delta}$ Superconducting Films. *Chemistry of Materials*, *22*(5), 1686–1694. doi:10.1021/cm903080k.

38) Rosenstein, B., & Li, D. (2010). Ginzburg-Landau theory of type II superconductors in magnetic field. *Reviews of Modern Physics*, *82*(1), 109–168. doi:10.1103/RevModPhys.82.109.

39) Browning, V. M., Skelton, E. F., Qadri, S. B., Osofsky, M. S., Hu, J. Z., Finger, L. W., & Meyers, K. R. (1999). Magnetotransport and Structural Studies of the High Temperature Superconductor $YBa_2Cu_3O_{7-\delta}$. In *Spectroscopy of Superconducting Materials* (Vol. 730, pp. 5–78). American Chemical Society. doi:doi:10.1021/bk-1999-0730.ch005.

40) Cayado, P., De Keukeleere, K., Garzón, A., Perez-Mirabet, L., Meledin, A, De Roo, J., Valles, F., Mundet, B., Rijckaert, H., Pollefeyt, G., Coll, M., Ricart, S., Palau, A., Gázquez, J., Ros, J., Van Tendelco, GObradors, X. (2015). Epitaxial $YBa_2Cu_3O_{7-x}$ nanocomposite thin films from colloidal solutions. *Superconductor Science and Technology*, *28*(12), 124007. doi:10.1088/0953-2048/28/12/124007.

41) Obradors, X., Puig, T., Palau, a, Pomar, a, Sandiumenge, F., Mele, P., & Matsumoto, K. (2011). Nanostructured superconductors with efficient vortex pinning. *Physics*, *5*, 1–35. doi:10.1016/B978-0-12-374396-1.00112-4.

42) Koshelev, A. E., Sadovskyy, I. A., Phillips, C. L., & Glatz, A. (2015). Optimization of vortex pinning by nanoparticles using simulations of time-dependent Ginzburg-Landau model, *c*, 1–6. doi:10.1103/ PhysRevB.9 3.060508.

43) Hot superconductors , 20 years on, *5*(6), 2006. doi:10.1038/nmat1651.

44) Werfel, F. N., Floegel-Delor, U., Rothfeld, R., Riedel, T., Goebel, B., Wippich, D., & Schirrmeister, P. (2011). Superconductor bearings, flywheels and transportation. *Superconductor Science and Technology*, *25*(1), 014007. doi:10.1088/0953-2048/25/1/014007.

45) Yu, G., Li, Y., Motoyama, E. M., Zhao, X., Barii, N., Cho, Y., & Greven, M. (2010). Magnetic resonance in the model high-temperature superconductor HgBa $_2$CuO$_{4+d}$?? *Physical Review B - Condensed Matter and Materials Physics*, *81*(6). doi:10.1103/PhysRevB.81.064518.

46) Bubendorfer, A. J., Joubert, J., Kemmitt, T., Campbell, L. J., & Long, N. J. (2004). High temperature superconductor films and devices for the microwave communication industry. *Current Applied Physics*, *4*(2-4), 284–287. doi:10.1016/j.cap.2003.11.029.

47) Likharev, K. K. (2012). Superconductor digital electronics. *Physica C: Superconductivity and Its Applications*, *482*, 6–18. doi:10.1016/j.physc.2012.05.016.

48) Chang, W., Albrecht, S. M., Jespersen, T. S., Kuemmeth, F., Krogstrup, P., Nygård, J., & Marcus, C. M. (2015). Hard gap in epitaxial semiconductor-superconductor nanowires. *Nature Nanotechnology*, *10*(3), 232–6. doi:10.1038/nnano.2014.306.

49) Van Driessche, I., Feys, J., Hopkins, S. C., Lommens, P., Granados, X., Glowacki, B. A, &Bäcker, M. (2012). Chemical solution deposition using ink-jet printing for YBCO coated conductors. *Superconductor Science and Technology*, *25*(6), 065017. doi:10.1088/0953-2048/25/6/065017.

50) Fu, P. P., Xia, Q., Hwang, H.-M., Ray, P. C., & Yu, H. (2014). Mechanisms of nanotoxicity: generation of reactive oxygen species. *Journal of Food and Drug Analysis*, *22*(1), 64–75. doi:10.1016/j.jfda.2014.01.005.

51) Gonzalez, L., Lison, D., & Kirsch-Volders, M. (2008). Genotoxicity of engineered nanomaterials: A critical review. *Nanotoxicology*, *2*(December), 252–273. doi:10.1080/17435390802464986.

52) Karakoti, A., Singh, S., Dowding, J. M., Seal, S., & Self, W. T. (2010). Redox-Active Radical Scavenging Nanomaterials. *Chemical Society Reviews*. 39(3), 4422–4432.

53) Yin, J. J., Liu, J., Ehrenshaft, M., Roberts, J. E., Fu, P. P., Mason, R. P., & Zhao, B. (2012). Phototoxicity of nano titanium dioxides in HaCaT keratinocytes-Generation of reactive oxygen species and cell damage. *Toxicology and Applied Pharmacology*, *263*(1), 81–88. doi:10.1016/j.taap.2012.06.001.

54) Meng, H., Xia, T., George, S., & Nel, A. E. (2009). A Predictive Toxicological Paradigm for the Safety Assessment of Nanomaterials. *ACS Nano*, *3*(7), 1620–1627. doi:10.1021/nn9005973.

55) Stadtman, E. R., & Berlett, B. S. (1997). Reactive Oxygen-Mediated Protein Oxidation in Aging and Disease. *Chemical Research in Toxicology*, *10*(5), 485–494. doi:10.1021/tx960133r.

56) Butterfield, D. A., & Kanski, J. (2001). Brain protein oxidation in age-related neurodegenerative disorders that are associated with aggregated proteins. *Mechanisms of Ageing and Development*, *122*(9), 945–962. doi:10.1016/S0047-6374(01)00249-4.

57) Evans, M. D., Dizdaroglu, M., & Cooke, M. S. (2004). *Oxidative DNA damage and disease: Induction, repair and significance. Mutation Research - Reviews in Mutation Research* (Vol. 567). doi:10.1016/j.mrrev.2003.11.001.

58) Shi, H., Hudson, L. G., & Liu, K. J. (2004). Oxidative stress and apoptosis in metal ion-induced carcinogenesis. *Free Radical Biology and Medicine*, *37*(5), 582–593. doi:10.1016/j.freeradbiomed.2004.03.012.

59) Bodamyali, T., Stevens, C., Blake, D., & Winyard, P. (2000). Reactive oxygen/nitrogen species and acute inflammation: a physiological process. *In: Winyard PG, Blake DR, Evans CH, Editors.* , 11–29. doi:10.1007/978-3-0348-8482-2_2.

60) Fu, P. P., Xia, Q., Sun, X., & Yu, H. (2012). Phototoxicity and environmental transformation of polycyclic aromatic hydrocarbons (PAHs)-light-induced reactive oxygen species, lipid peroxidation, and DNA damage. *Journal of Environmental Science and Health. Part C, Environmental Carcinogenesis & Ecotoxicology Reviews*, *30*(1), 1–41. doi:10.1080/10590501.2012.653887.

61) Sohal, R. S., Mockett, R. J., & Orr, W. C. (2002). Mechanisms of aging: An appraisal of the oxidative stress hypothesis. *Free Radical Biology and Medicine*, *33*(5), 575–586. doi:10.1016/S0891-5849(02)00886-9.

62) Akhtar, M. J., Ahamed, M., Kumar, S., Siddiqui, H., Patil, G., Ashquin, M., & Ahmad, I. (2010). Nanotoxicity of pure silica mediated through oxidant generation rather than glutathione depletion in human lung epithelial cells. *Toxicology*, *276*(2), 95–102. doi:10.1016/j.tox.2010.07.010.

II METAL OXIDE NANOPARTICLES

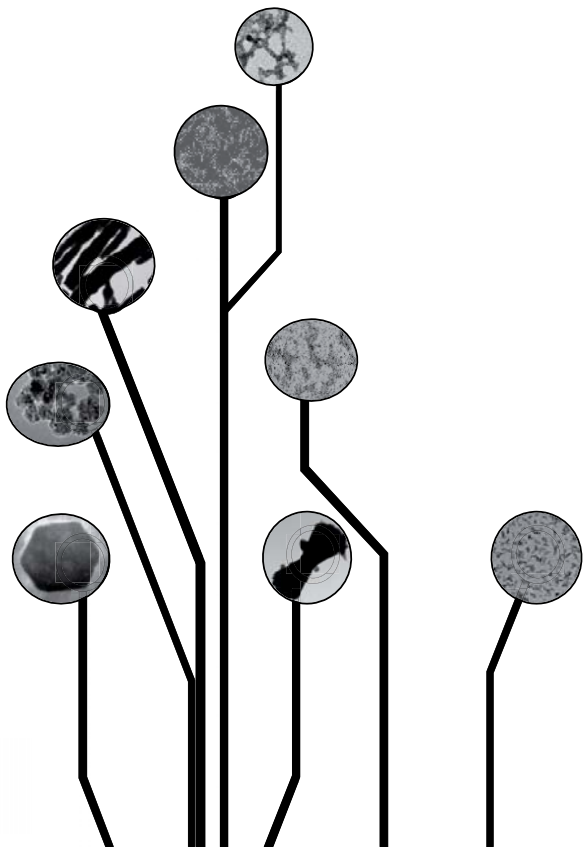

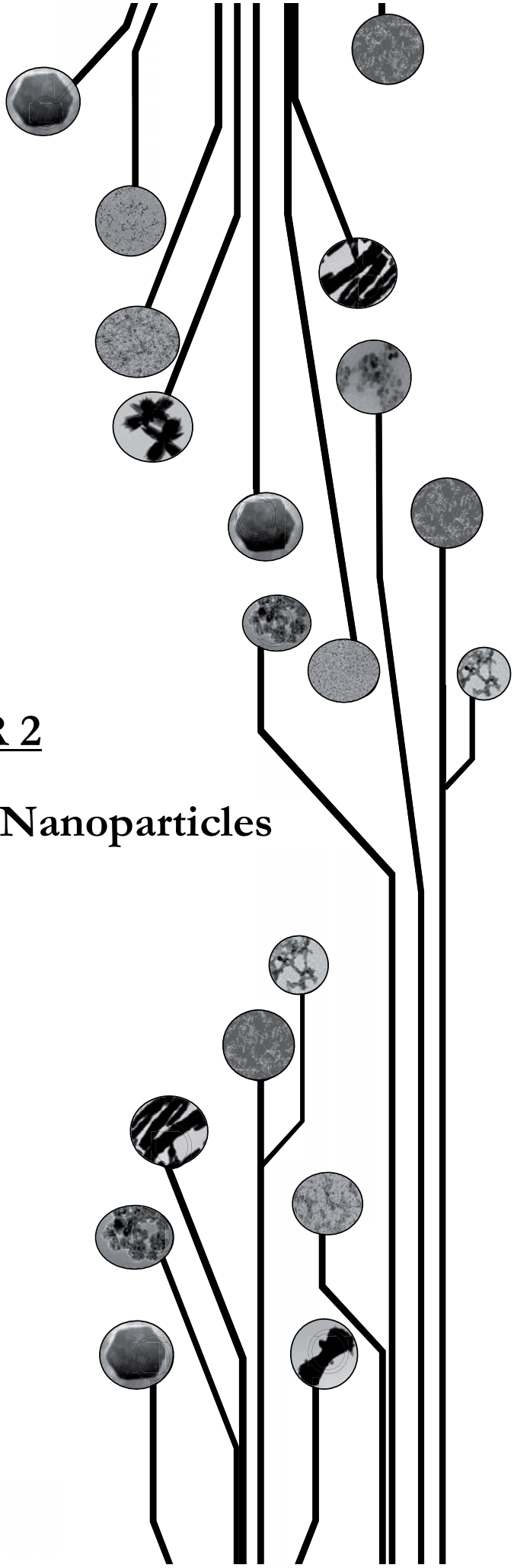

CHAPTER 2

Magnetic Iron Oxide Nanoparticles

Chapter 2 is based on the published article:

Induced shape controllability by tailored precursor design in thermal and microwave assisted synthesis of Fe_3O_4 nanoparticles[i]

The synthesis of magnetite nanostructures (Fe_3O_4) by thermal and microwave process was optimized to control the shape and the size of nanoparticles. The methodology is based on a easy modification of the α-terminal position belonging to the iron(III) tris(2,4-pentanedionate) precursor using triethylene glycol as a high boiling point solvent. Different shapes were obtained changing α-terminal group from the initial $–CH_3$ to –Ph; $–^tBu$; and $–CF_3$ respectively. The new precursor morphologies produce characteristic shapes of the obtained nanoparticles such as round, cuboctahedron, flower-like Fe_3O_4 and bow-like FeF_2 nanostructures. Furthermore, triethylene glycol allows producing polar dispersible nanoparticles with a high stabilization and well dispersed without aggregations. The two implemented process, thermal and microwave, produce similar structures, except for the precursor containing the aromatic group (–Ph), through which cuboctahedron (thermal) and elongated polycrystalline microwires (microwave) were achieved. The effect of α-terminal group demonstrated their influence on the final shape, structure and composition of the nanocrystals synthesized. The obtained nanoparticles were studied and characterized by high-resolution transmission electron microscopy, X-ray powder diffraction, and thermogravimetric analysis. Final results demonstrated a strong relation between the precursor design and the final morphology of nanoparticles, which could be explained by different precursor–particle interactions during nucleation and crystal growth. The composition of nanostructures was the expected Fe_3O_4 unlike fluorinated precursor where FeF_2 was obtained as the principal reaction product.

[i]Garzón-Manjón, A., Solano, E., de la Mata, M., Guzmán, R., Arbiol, J., Puig, T., Obradors, X., Yáñez, R., Ricart, S., Ros, J. (2015). Induced shape controllability by tailored precursor design in thermal and microwave-assisted synthesis of Fe_3O_4 nanoparticles. *Journal of Nanoparticle Research*, *17*, 291. doi:10.1007/s11051-015-3070-x.

CONTENTS

II Metal Oxide Nanoparticles

Chapter 2: Magnetic Iron Oxide Nanoparticles

1. Introduction: State of the art

Over the last decade, broad efforts have been made to generate different nanomaterials through easy and reproducible methodologies[1]. For a broad range of application the main objective has been the synthesis of monodispersed and well-formed nanoparticles as a stable colloidal solution in different solvents[2].

Magnetic nanoparticles are a class of nanoparticle which can be easily tracked, manipulated and targeted using external magnetic field (figure 2.1). When a magnetic field is applied to the nanoparticles, a magnetic dipole is induced. As soon as the external magnetic field is removed, the magnetic dipole disappears and nanoparticles return to their native nonmagnetic state. These phenomena provide them a huge research interest from a wide range of disciplines including magnetic fluids[3], catalysis[4], biotechnology/biomedicine[5], magnetic resonance imaging[6], data storage[7] and environmental remediation[8].

Figure 2.1: Magnetic solution nanoparticles under permanent magnet

They are mainly composed of magnetic elements such as iron, nickel, cobalt and their respective oxides. Among various magnetic particles, iron oxides have received immense attention owing to their strong magnetic responsiveness.

Table 2.1. shows a summarized of different type of iron oxide particles along with their structural and magnetic properties. These nanoparticles possess different physicochemical properties originating from the oxidation state of iron[9].

The most widely used are iron-based nanoparticles Fe_3O_4 and Fe_2O_3. These type of inorganic nanoparticles can form large aggregates, which may alter their magnetic properties.

Composition	Type	Structure / magnetic properties	Name
Fe_2O_3	α-Fe_2O_3	In the α -Fe_2O_3 structure, all Fe^{3+} ions have an octahedral coordination	Hematite
	γ-Fe_2O_3	γ -Fe_2O_3 have a cation-deficient AB2O4 spinel, the metal atoms A and	Maghemite
		B occur in tetrahedral and octahedral environments, respectively	
Fe_3O_4		Cubic inverse spinel Fe3O4. Ferrimagnetic at temperatures below 858 K.	Magnetite
FeO		Cubic Fe^{2+} oxide. Anti-ferromagnetic (TC=185 K) in the bulk state.	Wustite
$Fe_2O_3.H_2O$	α-FeOOH	Anti-ferromagnetic in the bulk state (TC=393 K)	Goethite
	β-FeOOH	Paramagnetic at 300 K	Akagenite
	γ-FeOOH	Paramagnetic at 300 K	Lipidocrokite
	δ-FeOOH	Ferrimagnetic	Ferroxyhite

Table 2.1: Types of iron magnetic nanoparticles

Many synthetic routes have been developed to achieve proper control of particle size, polydispersity, shape and crystallinity of magnetic iron oxide including co-precipitation, microemulsion, thermal decomposition, solvothermal, microwave assisted, chemical vapour deposition, combustion synthesis, among others in order to obtain a stables colloidal solutions without aggregates.

2. Synthetic Methodologies of Magnetic Iron Oxide Nanoparticles

The different synthetic methods have special interest due to they can be scaled up and size distribution can be varied by the reaction conditions such as concentration of precursors, type of base and salt, pH and ionic strength of the precipitating medium:

2.1. Co-precipitation Method[10]

This method is a facile and convenient process to synthesized metal oxides nanoparticles. One of the most commonly way to produce iron oxide nanocrystals is by the addition of base to Fe^{2+}/Fe^{3+} salt solution at room or elevated temperature[11]. Adequate election of a base like NH_4OH instead of NaOH resulted in better crystallinity, smaller size and higher saturation magnetization of magnetite nanocrystals[12].

Furthermore, the size, shape and composition can also be controlled by the variation of different salts such as chlorides, nitrates or sulphates, Fe^{2+}/Fe^{3+} ratio, the temperature of the reaction, the pH value and the ionic strength of media. For example, the precipitation at low temperature (below 60ºC) usually produce Fe_2O_3, while at higher reaction temperature such as 80ºC favour the formation of Fe_3O_4

The major drawback of co-precipitation method is the insufficient size control distribution and sometimes the uncontrolled shape, but still this process is one of the favourite route to produce magnetic oxide nanoparticles due to requires low-reaction temperature and short reaction time than others methods such as thermal decomposition or hydrothermal.

2.2. Microemulsion Method[13]:

Microemulsion method is a versatile synthetic methodology, which enables control of particle properties such as size, geometry, morphology and homogeneity. Microemulsions are isotropic, macroscopically homogeneous and thermodynamically stable solutions containing at least three components; a polar phase (usually water), a nonpolar phase (usually oil) and a surfactant.

In this process, the aqueous phase is dispersed as microdroplets surrounded by a monolayer on surfactant molecules in the continuous non-aqueous phase. If a water-soluble metal salt is added in the aqueous phase of the microemulsion, it will reside within the aqueous droplets surrounded by oil. If two identical microemulsions are produced with a reactant *A* dissolved in the aqueous cores of one microemulsion and a reactant *B* in the aqueous cores of other microemulsion, upon mixing, these microdroplets continuously collide, coalesce and break again and form precipitate *AB*, which will be contained entirely within the aqueous cores of the microemulsions as shown in figure 2.2.

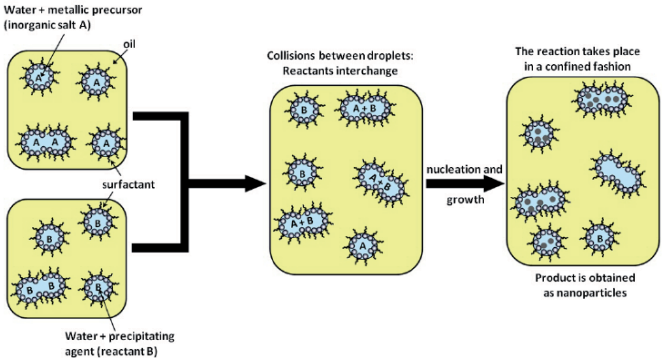

Figure 2.2: Microemulsion scheme

One of the most characterized surfactant system used in the synthesis of magnetic iron oxide nanoparticles is sodium dioctylfosuccinate (Aerosol OT or AOT)[14]. The size and the polydispersity of the nanoparticles are influenced by factors such as the type of solvent and surfactant or co-surfactant, the addition of electrolyte, the concentration of reagent and the molar ratio.

Although many types of magnetic iron oxide nanoparticles have been fabricated using this method, the relatively wider range of particle size and shape, the lower yield and the use of amount solvents make the microemulsion process difficult to scale up as compared to other methods such as thermal decomposition and co-precipitation.

2.3. Solvothermal Reaction Methods[15]:

These reactions are performed in reactors or autoclaves where high pressure and temperature values are the typical conditions. Solvothermal method, also called hydrothermal if the solvent is water, are based on the ability of the reaction mixture to hydrolyse and dehydrate metal salts and the poor solubility of the resulting nanoparticles to generate supersaturation. The main characteristics of this method, are the advantages of low reaction temperature, low cost and low reaction time.

Ferrites can be synthesised by two different approaches using solvothermal conditions, first being hydrolysis and oxidation and the secondly, with the neutralization of mixed metal hydroxides[16].

This method offers a relatively simple route to make metal oxide nanoparticles of specific size and morphology. Furthermore, hydrothermal process could be easily scale-up, although the mechanism of particle formation is not yet determined.

The main drawback is the slow reaction kinetics and for this reason, microwave heating is an alternative to increase the crystallization of the final nanoparticles. Furthermore, microwave irradiation has others significant advantages of higher reaction rates and product yields in shorter time[17].

2.4. Chemical Vapour Deposition

In the chemical vapour deposition (CVD) process, a carrier gas stream containing precursors is continuously delivered to a reaction chamber maintained under a vacuum and high temperature (more than 900ºC)[18] . The CVD reaction is performed in the heated reaction chamber and the products combine to form clusters of nanoparticles. Growth and agglomeration of the nanocrystals are mitigated by the rapid expansion of the two phase gas stream at the outlet of the reaction chamber. A clear example of the utilization of this method is the synthesis of iron oxide by the reaction of ferric chloride ($FeCl_3$) with water at 1000ºC[19].

CVD has some inconvenient such as the relatively low yield, the existence of complex phase and the difficulty in separating iron oxide nanoparticles from their impurities.

2.5. Thermal Decomposition

On of the most common method for the synthesis of metal oxide nanoparticles is the thermal decomposition of organometallic precursors in the presence of organic surfactants[20], which are used to protect sterically the nanoparticles. None the less, the synthesis process can produce agglomerates and can have a large size distribution. For this reason, surfactants are used to limit the growth of the nanoparticles and

increase their stabilization in this methodology.

There are different organometallic precursors to produce these kind of nanoparticles, including metal acetylacetonates ($M(acac)_n$), (M = Fe, Mn, Co, Ni, Cr), metal cupferronates (M_xCup_x) (M = metal ion; Cup = *N*-nitrosophenylhydroxylamine, $C_6H_5N(NO)O^-$) or carbonyls. Moreover, alkyl ammines, polyols or different alcohols are use as surfactants and/or solvents.

The size and morphology of magnetic oxide nanoparticles depends on different factors including the concentration of the organometallic precursors, surfactants, solvents, reaction temperature and time.

The thermal decomposition of organometallic precursors with metal in the zero-valent state initially leads to a formation of metal nanoparticles, which can be oxidized to obtain a high-quality monodispersed metal oxide nanocrystals[21]. Moreover, in case of organometallic precursors with a cationic metal centres such as $Fe(acac)_3$, the decomposition in absence of reducing agent leads directly to metal oxide nanoparticles[22] formation.

Fe_3O_4 nanoparticles with sizes adjustable over a wide size range (3-50 nm) could be synthesized by decomposition method. This method is also successfully used for synthesis of other magnetic nanocrystals such as Cr_2O_3, MnO, Co_3O_4 and NiO.

One of the typical thermal decomposition synthesis is the *polyol route*, which is based on the synthesis of different types of nanoparticles in high-boiling point multivalent alcohols such as ethylene glycol (EG), diethylene glycol (DEG), triethylene glycol (TREG) and so on up to polyethylene glycol (PEG), which contain more than 2000 ethylene groups.

This method was reporter in 1989 by Fievet, Lagier and Figlarz[23] describing the synthesis of Co, Ni, Cu and Pt nanoparticles[24]. Afterwards, the route was applied to further metals, intermetallics and alloys such as Rh, Au, FeNi, FeCoNi, among others.

The high reproducibility, controllability and the chelating properties of the polyols provide great advantages in order to control shape, size and agglomeration behaviours of the nanoparticles. Furthermore, other important point to use this process is that polyol route allows a high adaptability and flexibility to synthetize nanomaterials due to the sheer multitude of available polyols.

One of the main advantages of the polyols is their high solubility with a high

boiling point solvent, which allow to perform reactions at high temperature up to 320ºC without high pressure and autoclaves. These temperatures assure the high crystallinity of nanoparticles from the liquid phase without the need of any thermal post-sintering of Fe, Co, Ni, Cu, Ru, Rh, oxide powders.

The solubility of compounds is equivalent of water and for this reason, polyol route allows using simple, low-cost precursors as halides, nitrates, sulphates or acetylacetonates. Moreover, after the reaction, the final nanoparticles have a high insolubility in this media, which is a clear advantage to obtain them.

Furthermore, polyol route is a promising technique to obtain well-defined shapes and size nanoparticles in a controlled synthesis. In this way, nucleation and growth steps can be completely separated and finally, an uniform nanoparticles are obtained.

In this chapter the synthesis of magnetite by polyol route is performed in order to obtain a high controllability of the size, shape and morphology of the obtained Fe_3O_4 nanoparticles.

3. Magnetic Oxide Nanoparticles Applications

Magnetic oxide nanoparticles are of great interest for a wide range of disciplines such as magnetic fluids, catalysis, biomedicine, magnetic energy storage, information storage. The application of these nanoparticles also highly depends on their stability and for this reason, this research work is based on the synthesis of magnetic iron oxide nanoparticles, specifically Fe_3O_4, in order to obtain stable dispersions for their future applications.

3.1. Fe_3O_4 Nanoparticles Applications

The main advantage to use magnetite nanoparticles is due to their chemical stability, biocompatibility, low toxicity, small size and high surface area that provide them better physical and chemical characteristics [25] . Furthermore, their superparamagnetic property and easy manipulation under the influence of an external magnetic field allows the nanoparticles to be reused or recycled. The synthesis of Fe_3O_4 nanoparticles in a large quantity, is faster and reproducible. In addition, the ease surface modification permits to apply them in wide range of application[26]:

- **Biomedicine applications; drug-delivery:** The use of Fe_3O_4 nanoparticles in the development of delivery drugs systems, where iron oxide could be manipulated by an external field due to it superparamagnetic behaviour, make magnetite really interested in target tissues[27] and in the increasing stability against degradation by enzymes[28]. These nanoparticles are relatively biocompatible and can also be used as contrast agents in magnetic resonance imaging. Furthermore, Fe_3O_4 has also been studied in other different drug-delivery applications such as controlled magnetic transportation of anticancer drugs[29] as well as generation of hyperthermia.

- **Magnetic resonance tomography (MRT)[30]:** This technique permits non-invasive visualization of cross-sectional images of human body where magnetic nanoparticles are powerful contrasting agents due to their magnetic behaviour. Consequently, magnetite has thus far only been useful in distinguishing between healthy and malignant liver cells. This limitation can be overcome through functionalization of nanoparticles with various ligands, which allows for organ-specific transport, to make possible MRT imaging of various bodily organs.

- **Metal removal[31]:** Magnetite nanoparticles are used for the removal of heavy metals and metalloids from water, mainly copper, chromium, mercury, arsenic and lead. The functionalization of the nanoparticles is necessary in order to employ them as an effective sorbent material for these toxic soft salts.

- **Electronic devices[32]:** The application of magnetite nanoparticles in modern information technologies is due to their availability of ultra-high density magnetic data storage devices. One of the most prominently use is for *magnetic hard disc drives* (HDD), where the ever decreasing physical size of a magnetic bit in these HDD systems, gives rise to the fact that as long as the grain size is kept constant the number of individual magnetic grains within a magnetic bit is decreasing with increasing storage density.

4. Fe_3O_4 Nanoparticles Structure

4.1. Crystal Structure[33]

Magnetite is a common magnetic iron oxide that posses a cubic inverse spinel structure space group *Fd3m*, a = 8,396 *Å,* where the oxygen anions O^{2-} form a *face-centered cubic* (fcc) closed packing with Fe^{2+} and Fe^{3+} cations located in interstitial sites. There are two different kinds of cation sites in the magnetite crystal: tetrahedral and octahedral. Tetrahedrally coordinated A sites occupied by Fe_A, typically assigned with a charge state 3+, and octahedrally coordinated B sites occupied by Fe_B, typically assigned with charge state 2+ and 3+ in equal numbers: $(B^{III})^{tet}(A^{II}B^{III})^{oct}O_4$.

The bulk crystallographic structure of magnetite can be represented as a stack of (100) layers containing either iron atoms in tetrahedral sites (A) or oxygen and iron ions in octahedral sites (B) as shown in figure 2.3. In octahedral sites, only half of them are occupied and Fe ions form close-packed rows along the [011] direction. In successive B planes, these rows are arranged perpendicular to each other.

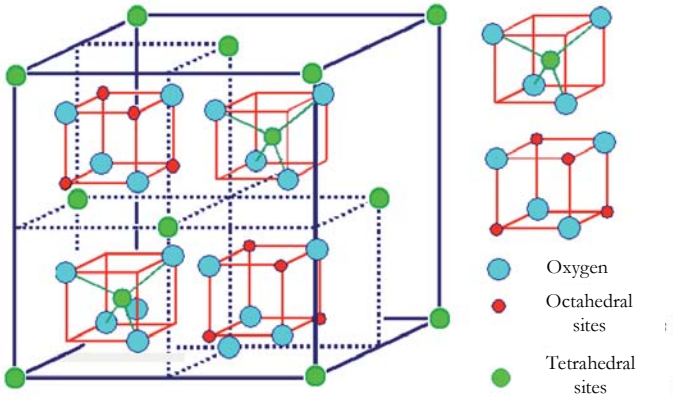

Figure 2.3: Side view of the inverse spinel Fe_3O_4 structure

4.2. Magnetic Structure[34]

Magnetite structure presents a different orientation of the magnetic spin. The T_c of magnetite is observed at 850K (577ºC) and below this temperature, cations situated in octahedral sites (occupied by ferrous and ferric species), which are antiparallel with

cations situated in tetrahedral sites (ferric species), are antiferro-magnetic due to Fe^{3+} ions on octahedral and tetrahedral sites are aligned antiparallel and cancel each other. For this reason, the global net magnetic moment of the unit cell comes from Fe^{2+} ions providing at room temperature a ferrimagnetic material. (figure 2.4).

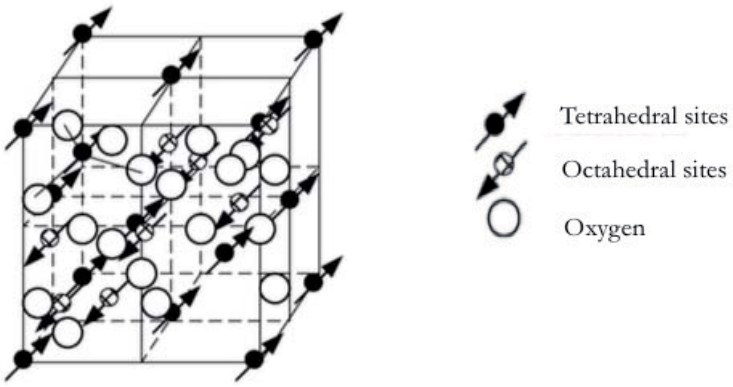

Figure 2.4: Magnetic Fe_3O_4 spinel cell

As temperature increase to T_c, thermal fluctuations destroy the ferromagnetic alignment of magnetic moments on tetrahedral sites and therefore, ferrimagnetic strength is diminished. When T_c is attained, net magnetization becomes zero and superparamagnetic behaviour is observed.

5. Nanoparticles Synthesis

The employment of iron (III) acetylacetonate as a precursor leads to the formation of spherical nanoparticles[35]. However, in this research work, the modification of the 1,5 terminal groups (α-position) of the acetylacetonate was performed in order to produce changes on the morphology of the synthetized nanoparticles, without further utilization of additives or templates, influence on the thermodynamics and kinetics of the crystal growth.

The effect of four different substituents on the α-terminal position of the iron diketone precursors on the morphology of the final nanoparticles was evaluated. These four substituents modify the iron precursor by adding steric hindrance with -Ph or -^{t}Bu groups or modifying polarity with –CF_3 group giving a variety of final

shapes, which further depend on the heating technique utilized: Thermal or microwave process. Thus, with the aim to understand the impact of these variables (ligand design and heating procedure), an exhaustive analyse of chemical precursors, synthetic nanoparticles process and characterization of the obtained nanoparticles are performed in this research work.

5.1. Chemical Precursors

$Fe(R_2diket)_3$ where R is a phenyl, ^{t}butyl or trifluoromethyl were used to synthesized magnetite nanoparticles.

The synthesis of different precursors (figure 2.5) was carried out mixing solutions of disubsitued propanedione (R_2diket with R = -Ph, -^{t}Bu and -CF_3) in tetrahydrofuran with sodium acetate (15 mmol) and iron (III) chloride (5 mmol) in Milli-Q water. The reaction was performed heating up to 70ºC under magnetic stirring. After 30 min, the mixture was filtered to obtain a dark precipitate. Then, the solid was thoroughly washed with Milli-Q water and ethanol, dried in vacuum and analysed via infrared spectroscopy as shown in figure 2.6.

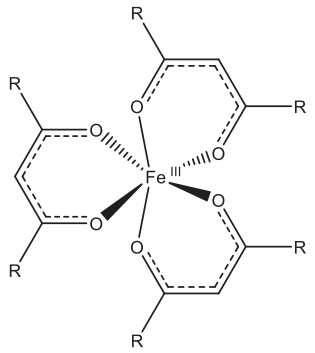

Figure 2.5: $Fe(R_2diket)_3$, R = -Ph, ^{t}Bu and CF_3

These compounds have the property to decompose thermally releasing the metallic centre to produce the nanoparticles. During their decomposition CO_2 and the corresponding acetone[36] are generated as by-products.

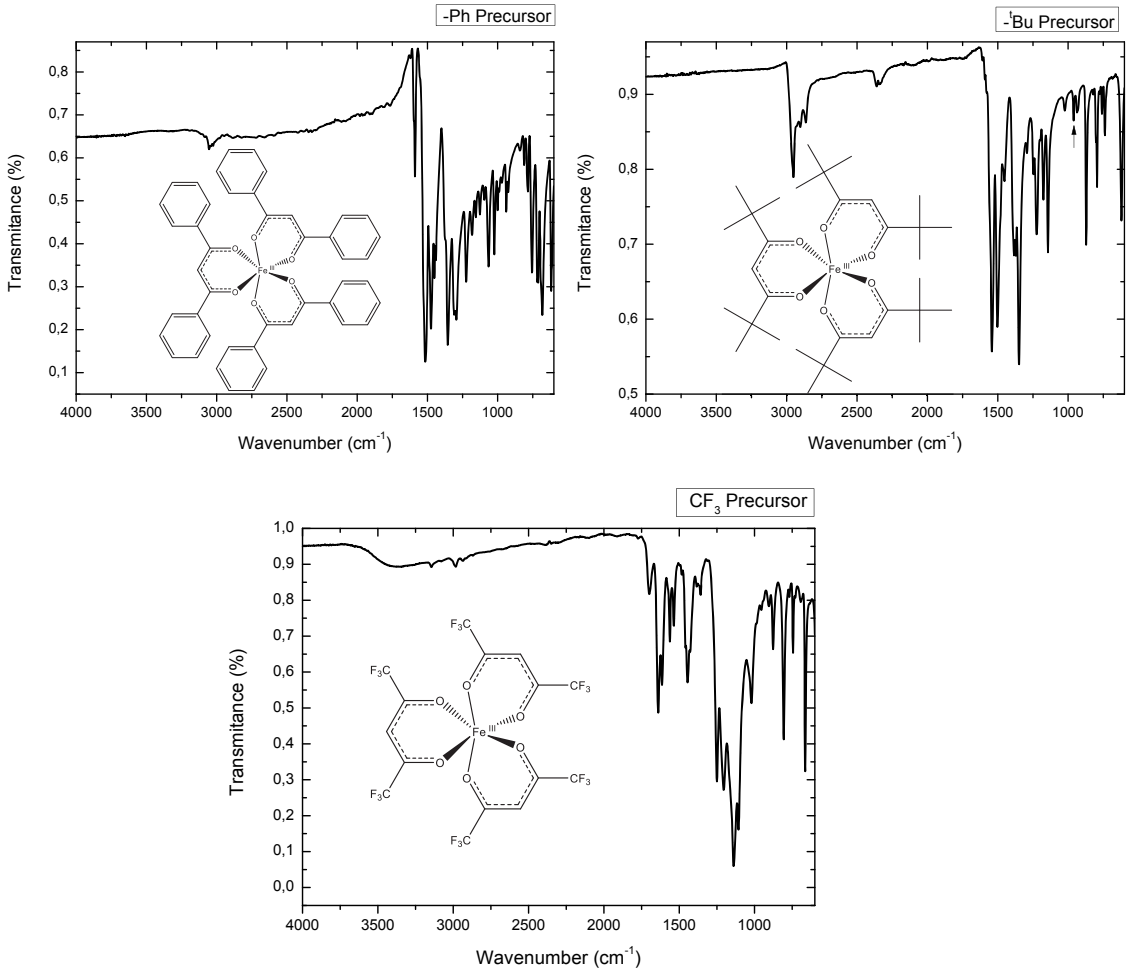

Figure 2.6: Infrared spectroscopy of the three different precursors to synthetize the nanoparticles

Bands at 1350 at 1500 cm^{-1} correspond to stretching vibrations of C-C=C-O and C=C-C=O from the diketonate part. In the case of −Ph precursor, this presents the aromatic ring characteristic band at 1580 cm^{-1}produced by the C-C stretch and the stretching vibration band that corresponds to carbon sp^2 at 3050 cm^{-1}. The band at 870 cm^{-1} is characteristic of the C-^{t}Bu link symmetric stretching vibration. Finally, the presence of the $–CF_3$ precursor was proved by the ensemble of bands between 1300 - 1100 cm^{-1} and 770 – 692 cm^{-1} produced by the C-F bond.

The releasing of the metal precursor during the nanoparticles synthesis is a significant consideration for morphology and composition controllability. LaMer curve[37] (figure 2.7) shows that the free precursor is concentrated in the solvent until a critical point where the nucleation is generated. After that, the growth of the nanoparticles occurs up to the solubility of them is reached.

The nanoparticles growth is related to many important factors to take into account. From a kinetic point of view, the precursor decomposition affects to the growth pathway. When the precursor decomposition is a slow process, the liberation of a few nucleus to the reaction media occurs, allowing growth and incorporate new atoms to the structure until the solubility stop it. Conversely, if is an immediately decomposition pathway, a lot of nucleus are delivered to the reaction media at a first stage and the nanoparticle size is limited by the precursor concentration.

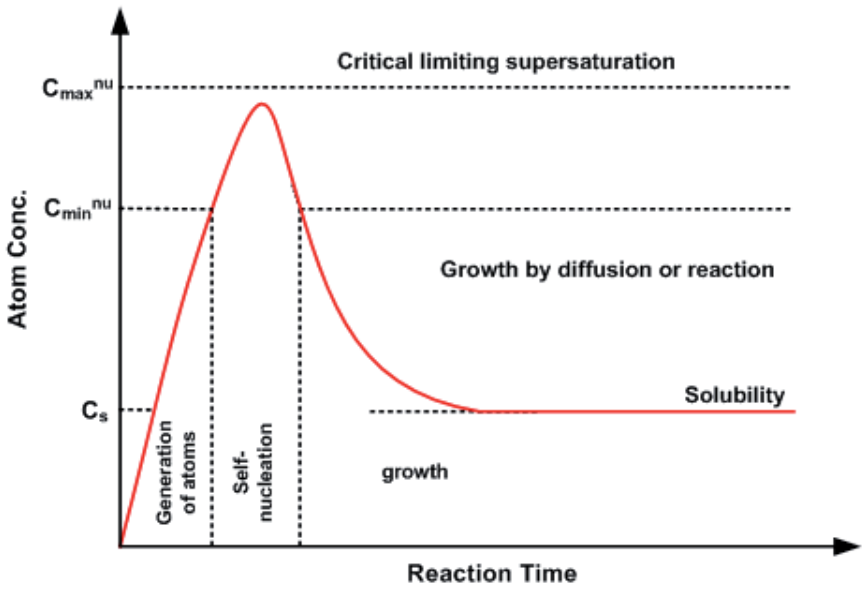

Figure 2.7: LaMer curve

In order to optimise the nanoparticles growth a temperature ramp condition needs to be studied.

5.2. Synthetic Nanoparticles Process

The synthetic methodology was based on a previously described polyol route and was carried out via thermal and microwave procedures (figure 2.8):

- **Thermal process**: $Fe(R_2diket)_3$ (1 mmol) was suspended in triethylene glycol (25 mL) using an ultrasonic bath. The mixture was poured into a round-bottomed flask equipped with a reflux condenser, a magnetic stirrer, a thermograph, and a heater. The reaction was heated 1ºC/min to 280ºC. The reaction mixture becomes to a black solution between 115ºC and 170ºC depending on the precursor decomposition temperature. After 2,5 h of dwell time, the mixture was cooled to room temperature (ambient rate). Nanocrystals were separated and washed thoroughly by repeated centrifugation and dispersion in a mixture of ethylacetate and ethanol (4:1). Finally, a stable dispersion was yielded by redispersion in ethanol.

- **Microwave process**: $Fe(R_2diket)_3$ (1 mmol) was suspended in triethylene glycol (25 mL) and transferred to a microwave vial. After ultasonication, the mixture was heated under magnetic stirring by microwave radiation (300W) to 220ºC. The final temperature was achieving in 10 min with the maximum temperature ramp of 20ºC/min. After heating, the temperature was maintained for 10 min and the solution was cooled inside the microwave by external air flow. The Fe_3O_4 nanocrystals were separated by centrifugation and thoroughly washed with ethylacetate and ethanol (4:1). Redispersion in ethanol yielded a stable dispersion.

Figure 2.8: ***(left)*** *Thermal process* ***(right)*** *Microwave process*

The nanoparticles disperse easily in polar solvents (water, alcohols) and remains highly stables for several months at room temperature for concentrations up to 260 mM of final free Fe_3O_4.

The main difference between thermal and microwave methodologies is the heating process. While thermal is a continuous heating, microwave is a radiation heating system. These two different methodologies can produce differences in the size or shape of the final synthetized nanoparticles as will be discussed at the following section. Figure 2.9 shows graphically the reaction condition during the synthesis using thermal or microwave process.

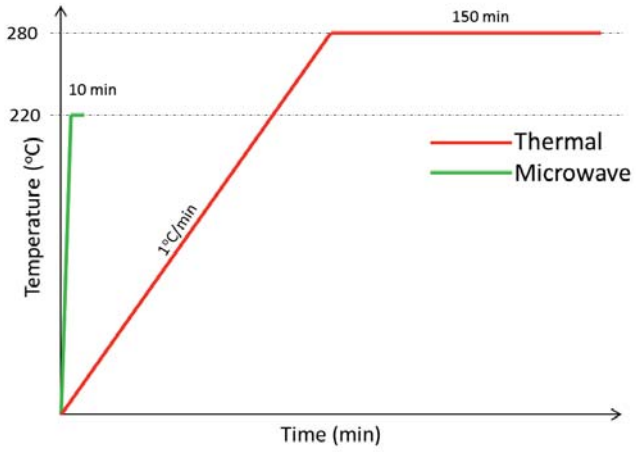

Figure 2.9: Reaction conditions of thermal and microwave process

5.3. Solvent and Capping Ligand

Solvent and capping ligand of the nanoparticles are decisive during the synthetic process. The capping ligand has to be compatible with the future nanoparticles and the solvent has to be easily removable from them.

Triethylene glycol has the capacity to act as a solvent an as a capping ligand providing nanoparticles high stabilization in polar solvent for several months.

Respecting to control the size of the nanoparticles through the ratio metal/capping ligand/solvent, for these process triethylene glycol is unbelievably in excess respect to the metal precursors and for this reason, it is an important factor to take in consideration to control the size of the nanoparticles.

Finally, there is an other important role, in this particular approach, of the solvent in the synthesis of Fe_3O_4 nanoparticles; triethylene glycol can also act as a reducing agent allowing the reduction of part of the initial iron(III) in the performed precursor.

5.4. Nanoparticles Stabilization

The triethylene glycol, that acts as a capping ligand, allows the high stabilization of the nanoparticles in polar solvents. This phenomenon is due to the formation of a colloidal dispersion producing interactions between the capping ligand and the solvent. These interactions maintain the nanoparticles suspended into the liquid avoiding the aggregation and the final precipitation. The principal interaction of triethylene glycol with the solvent is due to hydrogen formation

The most commonly used solvents, where the nanoparticles are dispersed and stabilized, are ethanol or methanol. The future application of them in superconductor tapes generation requires the nanoparticles stabilization in absolute methanol, which is the solvent used in the standard YBCO precursor solution for the *Chemical Solution Deposition* (CSD) approach to *High Temperature Superconductors* (HTSC) layers.

6. Characterization

The characterization of the nanoparticles was a crucial point in order to know their composition, size, shape, stability, structure and capping ligand. The techniques used to characterize magnetite are microscopy such as Transmission Electron Microscopy (TEM) or Scanning Electron Microscopy (SEM), X-Ray Diffraction (XRD), Infrared Spectroscopy (IR), Thermal Gravimetric Analysis (TGA) and magnetometry.

6.1. Microscopy

Electron microscopy has revolutionized our understanding of materials by completing the processing structure properties links down to atomistic levels[38]. The huge abilities of electron microscopy to provide the structure, phase and

crystallographic information allow us to overcome the limited image resolution in light microscopes, which is imposed by the wavelength of visible light.

6.1.1. Transmission Electron Microscopy

The BF-TEM images shown in figure 2.10 the influence of the precursor design ($Fe(R_2diket)_3$) to the final synthetized nanoparticles:

- **$Fe(acac)_3$ ($R = CH_3$)**: Microwave and thermal synthetic routes gave round-shaped nanoparticles with an average diameter of 7 nm, but a definite size distribution in case of microwave heating.

- **$Fe(Ph_2diket)_3$ ($R = Ph$)**: When the precursor was synthetized with a -Ph group, the nanoparticles obtained using thermal process are 14 ± 3 nm cuboctahedron-shaped (hexagonal for 2D view), whereas microwave synthesis gave spherical particles with a diameter of 3.5 ± 0.4 nm. These nanoparticles arranged to large elongated micrometric aggregates with a length between 700 and 1700 nm and a width between 170 and 400 nm.

- **$Fe(^tBu_2diket)_3$ ($R = {}^tBu$)**: This specific precursor, gave similar aggregates among 45 ± 5 nm and nanoparticles of 8 ± 2 nm either using thermal or microwave process.

- **$Fe((CF_3)_2diket)_3$ ($R = CF_3$)**: In this final case, $-CF_3$ terminal diketones presented bow-like structures growing from a central point with a final size of around 1300 ± 200 nm.

In order to understand the relation between the chemical nature of the enforced precursor and the different morphology of the synthetized nanoparticles, HRTEM studies were performed except for the $–CH_3$ precursor, whose studies were previously carried out by our group[39].

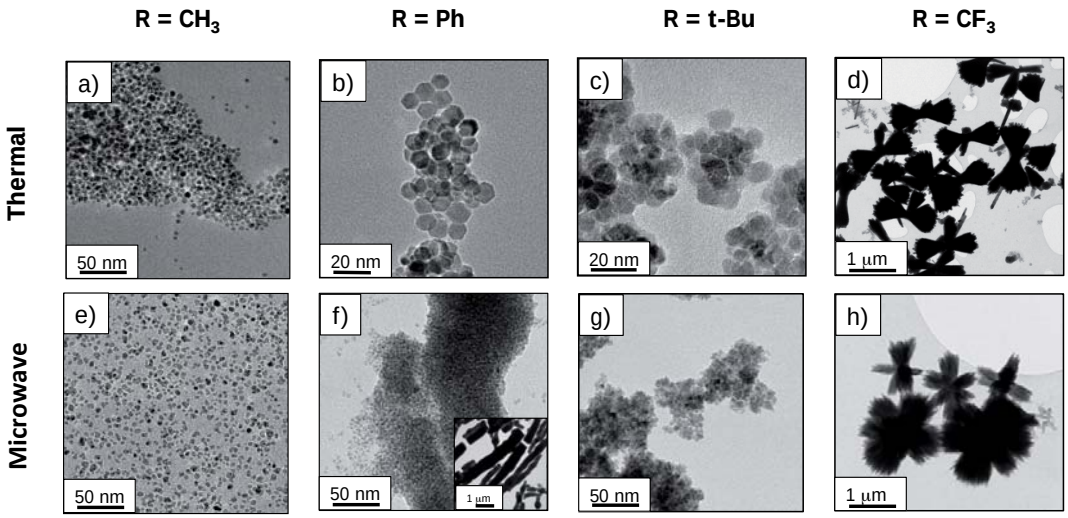

Figure 2.10: BF TEM images showing size and shape of the nanoparticles obtained by thermal and microwave process

i HRTEM of Nanoparticles by $Fe(Ph_2diket)_3$

HRTEM analysis of nanoparticles synthesized by $Fe(Ph_2diket)_3$ precursor exposed differences between thermal and microwave reaction process. First of all, microscopic studies of nanoparticles using thermal synthesis produce the nanoparticles showed in figure 2.11 (right). Mainly, the nanocrystals presented cuboctahedron faceted structures with 4:3 ratio between the (111):(100) planes. This result was confirmed by 3D supercell simulation shown in figure 2.11 (left), which associates the HRTEM image with the theoretical proposed cuboctahedron model.

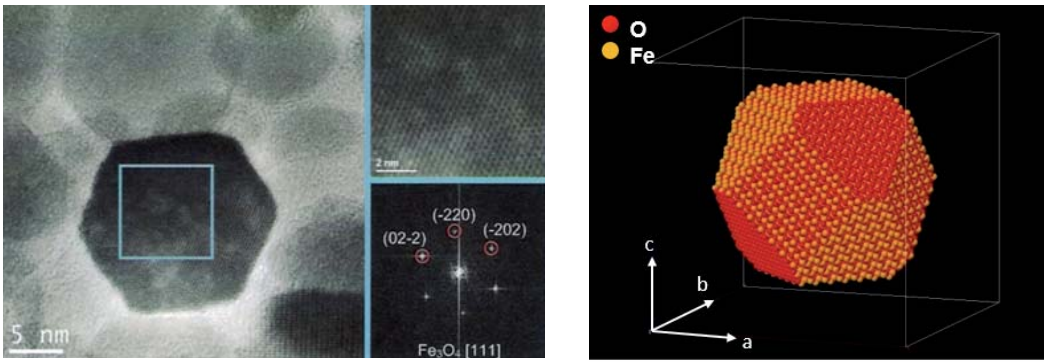

Figure 2.11: ***(right)*** *HRTEM image of facetated nanoparticles with electron diffraction pattern* ***(left)*** *Simulation of the cuboctahedron*

On the other hand, SEM images of microwave synthesized nanorods using the same precursor presented the formation of anisotropic structures as shown in figure 2.12.

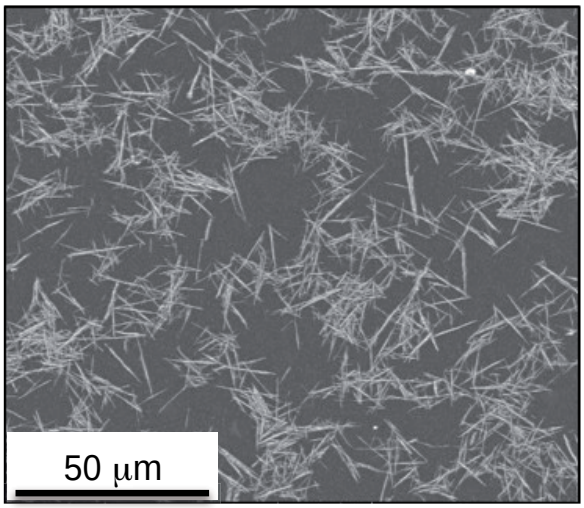

Figure 2.12: SEM image of nanorods formed using the –Ph precursor by MW process

These nanorods were organized by spherical nanoparticles with a diameter of 3.5 ± 0.4 nm. The polycrystalline material nature could be acquired by the reflection rings in the *Fast Fourier Transform* (FFT) (figure 2.13). In addition, the structural analyses of some grains confirmed the inverse spinel structure of Fe_3O_4.

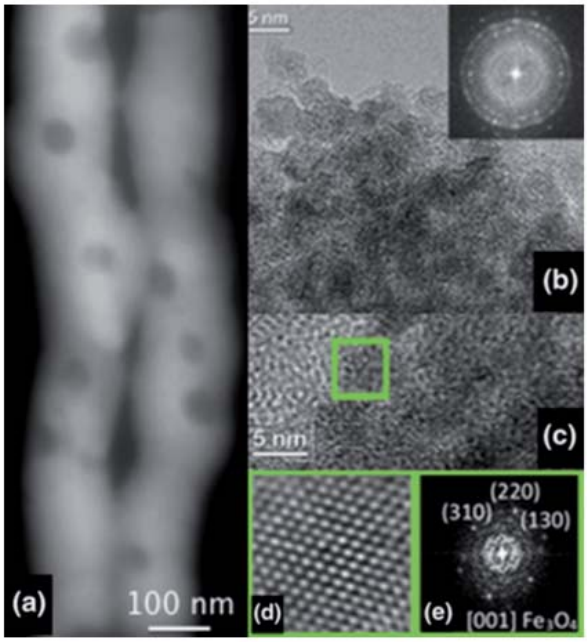

Figure 2.13: TEM of a Polycrystalline microrod ***(a)*** *Structural defects of a single nanorod observed in dark-field view* ***(b-d)*** *Polycrystalline constitution of one nanorod* ***(e)*** *Electron diffraction pattern with the crystallographic planes for a Fe_3O_4 material*

Furthermore, *Electron Energy Loss Spectroscopy* (EELS) analyses confirmed a homogenous element distribution as well as the expected stoichiometric ratio for Fe_3O_4 synthetized by thermal and microwave process (figure 2.14).

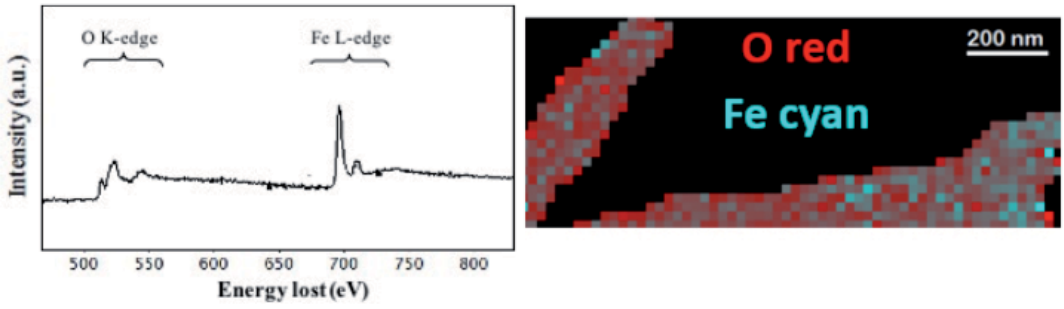

a) Thermal b) Micowave

Figure 2.14: ***(left)*** *EELS spectrum of nanoparticles synthetized by thermal process, where only iron and oxygen are detected* ***(right)*** *Element mapping of the nanoparticles synthesized by microwave process. There are different colours for the iron (cyan) and oxygen (red)*

ii HRTEM of Nanoparticles by Fe(^{t}Bu$_2$diket)$_3$

Thermal and microwave process produce, in both routes, nanoparticles with flower-like shape as shown in figure 2.15, where HRTEM and electron diffraction patterns confirmed the spinel structure of Fe_3O_4. Similar structures of magnetite nanocrystals were reported with a thermal procedure in non-polar media using trioctylamine (TOA) as a capping ligand and solvent[40]. The geometrical similitude between the TOA and the –^{t}Bu seems to relate the steric hindrance with this denominated flower-like shape structure.

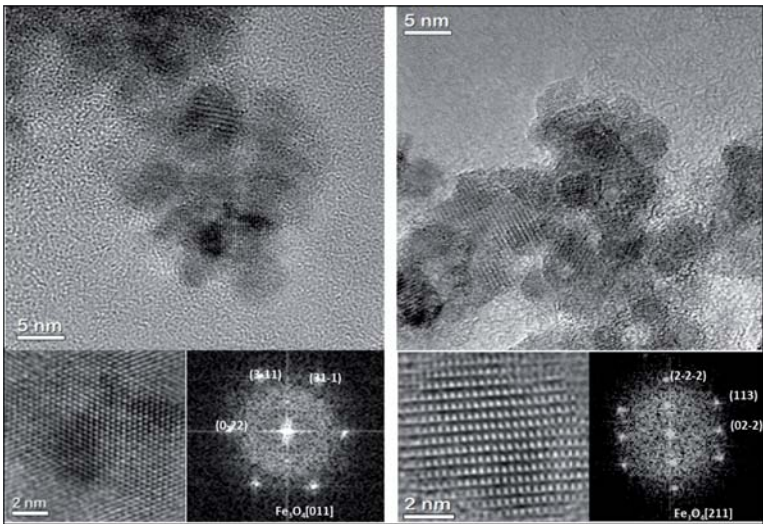

Figure 2.15: ***(left)*** *Nanoparticles obtained from the decomposition of –^{t}Bu precursor by thermal process* ***(right)*** *Nanoparticles obtained from the decomposition of –^{t}Bu precursor by microwave process*

iii HRTEM of Nanoparticles by Fe((CF$_3$)$_2$diket)$_3$

Bow-like nanoparticles were obtained by the decomposition of –CF_3 precursor. The nanoparticles were composed of different porous branches interconnected at their central part (figure 2.16 (I)).

The structure corresponds to a polycrystalline material composed of small nanocrystals. Every branch was formed by three different large porous crystals going from the center towards the tips in different orientations. HRTEM micrographs show how the atomic crystal planes diverge from the center of the structure in three

different preferential directions (figure 2.16 (II)). FFT shows the three differently oriented diffraction patterns for each crystal (green, blue and red color identification). Applying a *Bragg filter* to those frequencies corresponding to one of the differently oriented crystal, it is possible to distinguish the crystal growth orientation for each part of the structure. The [110] direction is identified as the main growth direction although every branch is oriented randomly.

(I)

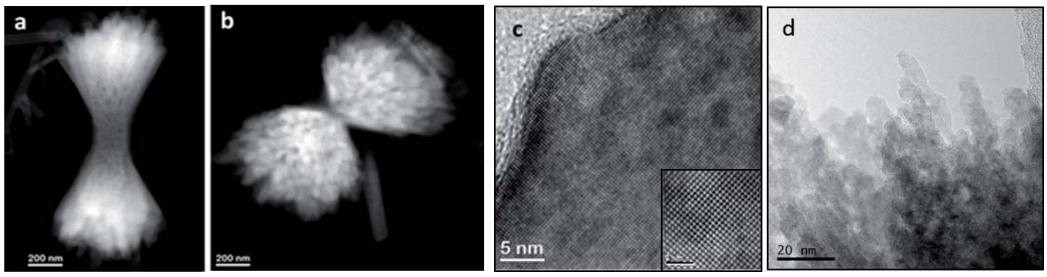

(II)

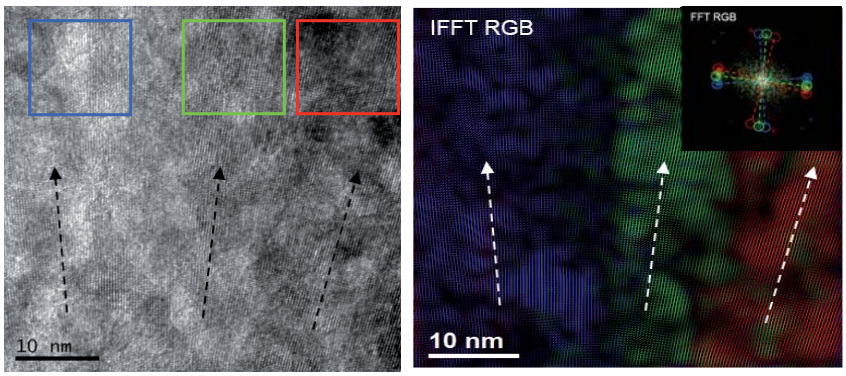

Figure 2.16: ***(I)*** *HRTEM image of nanoparticles synthetized by thermal (a) and microwave (b) process. (c) zoom view of the structure (d) crystalline branches* ***(II)*** *A colored FFT analysis to analyse the three growth directions of bow-shaped structures*

EELS measurements as shown in figure 2.17 allowed obtaining the composition of the structure that corresponds mix between FeF_2 and Fe_3O_4. This mix composition was totally different from the results obtained for the other precursors. A deeply study of composition was carried out varying the dwell time during the reaction as is presented in next X-Ray diffraction section.

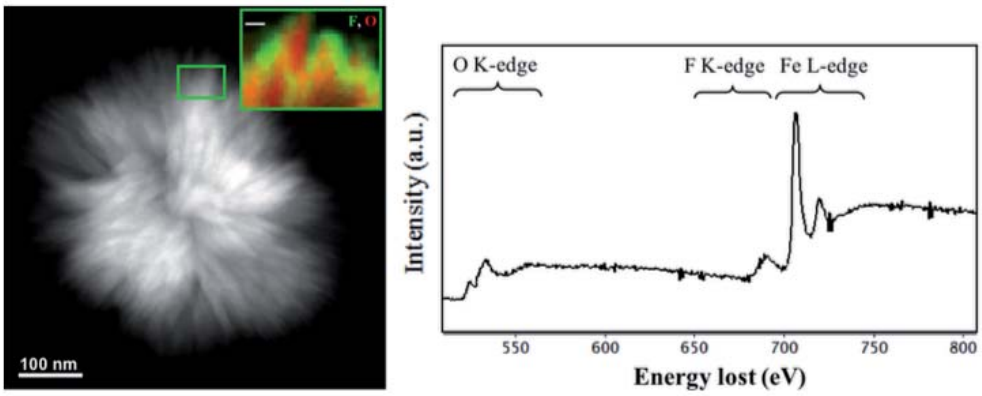

Figure 2.17: EELS spectrum of nanoparticles using the –CF_3 precursor, where iron, flour, and oxygen are detected

6.2. Thermal Gravimetric Analysis

Thermogravimetric analysis (TGA) is based on the changes in physical and chemical properties of material, when the temperature is increasing, measuring the difference in the weight and providing information about the composition and the purity of the sample.

The decomposition temperature for the three different precursors was determined in order to know the influence of the precursor design on the structure and morphology of the obtained nanoparticles.

The raised results demonstrated the shape dependence with respect to the modified diketone employed as coordinating ligand of the iron(III) precursor.

The decomposition temperature analysis for $Fe(Ph_2diket)_3$, $Fe(^tBu_2diket)_3$, and $Fe((CF_3)_2diket)_3$ is shown in figure 2.18, where the mass loss in function of the temperature was performed. This loss was attributed to the chemical decomposition of the precursor in gas phase generating volatile fragments.

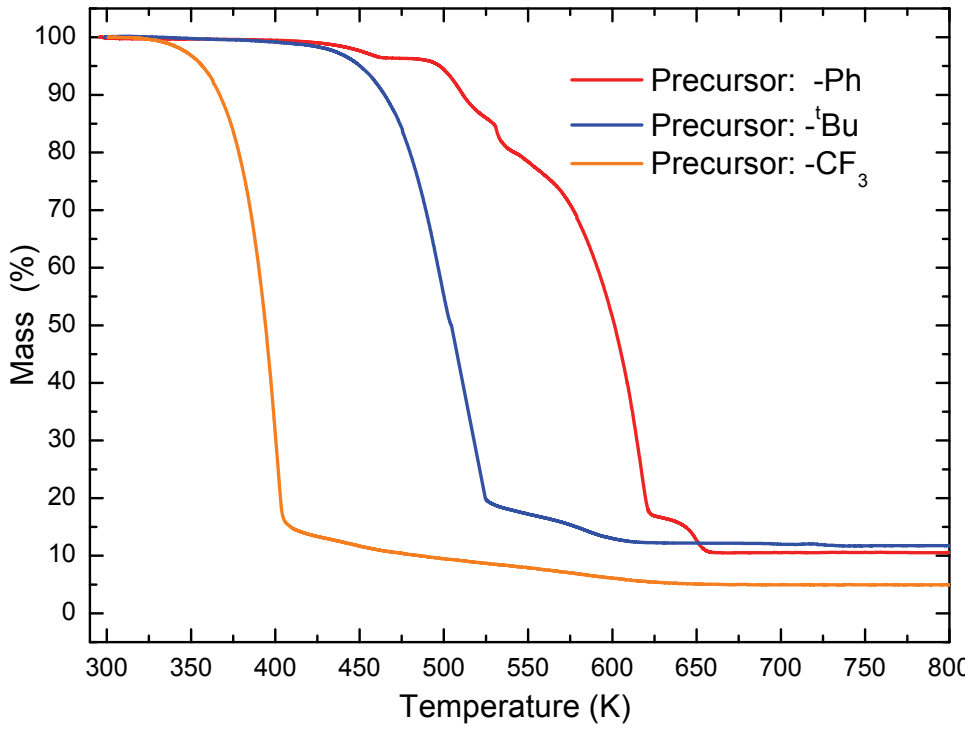

Figure 2.18:: TGA analysis of the three different precursors

6.3. X-Ray Diffraction

X-Ray powder diffraction (XRD) patterns from the synthetized nanoparticles using the three different precursors (-Ph, -^{t}Bu and -CF_3) whether through thermal or microwave process, demonstrated that the nanoparticles obtained using $Fe(Ph_2diket)_3$ or $Fe(^tBu_2diket)_3$ precursors were of pure cubic Fe_3O_4 phase independently of the applied synthetic route (figure 2.19 (I)). In case of $Fe((CF_3)_2diket)_3$, a mix crystalline composition between FeF_2 and Fe_3O_4 were obtained for the thermal procedure figure 2.19 (II a), while microwave produced pure FeF_2 (figure 2.19 (II b)) as confirmed by EELS measurements.

(I)

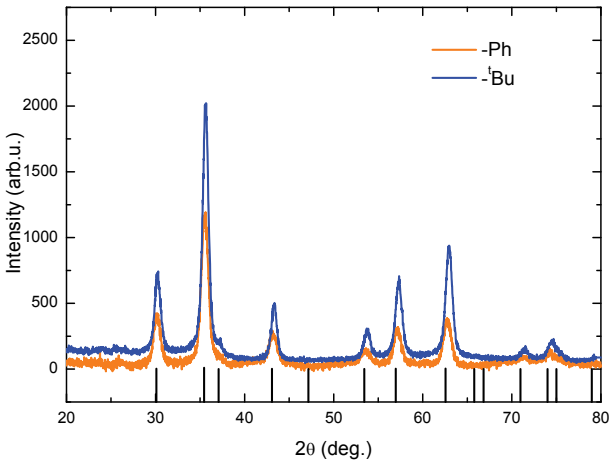

(II)

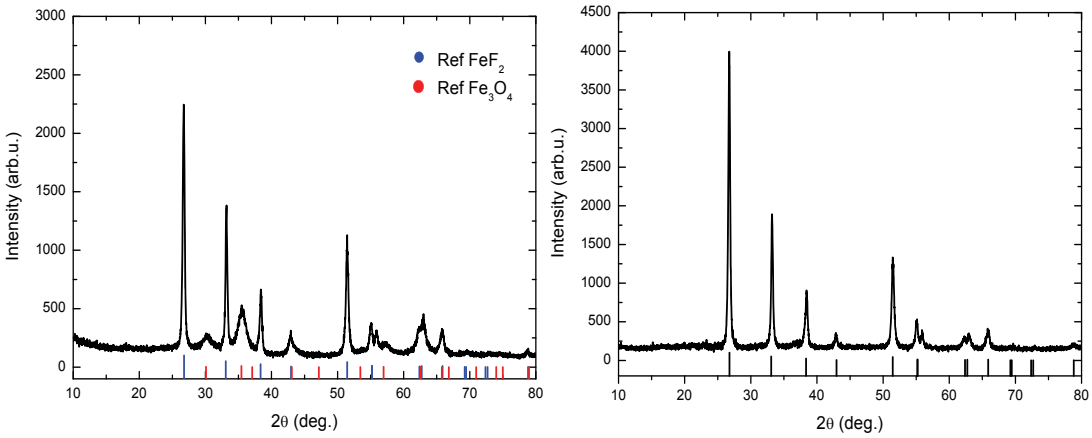

(a) –CF_3 Thermal **(b) –CF_3 Microwave**

Figure 2.19: ***(I)*** *XRDP measurement for the different nanoparticles obtained with –Ph and -^{t}Bu precursors: Fe_3O_4 phase* ***(II)*** ***(a)*** *XRDP measurement for nanoparticles obtained with –CF_3 precursor from thermal process*

XRD pattern technique not allows distinguishing magnetite from maghemite. However, recently published studies of iron oxide synthesis using $Fe(acac)_3$ as a precursor demonstrate a 45/55 ratio of maghemite/magnetite for microwave and thermal synthesis[41].

On the other hand, FeF_2 phase evolution was investigated using this technique in order to understand the final composition of the nanoparticles obtained. For this

reason, the reaction was performed changing the dwell time during the nanoparticles synthesis from 2h 30 min to 10h applying the same final temperature (280ºC).

The XRDP shows a increase of FeF_2/Fe_3O_4 ratio when the dwell time is longer, after 10h at 280ºC (figure 2.20). This phenomenon can be explained due to the hypothetic difference between thermodynamic and kinetic compounds. A possible explanation is that the initially formed magnetite can act as crystallization seeds for iron fluoride, which is thermodynamically favoured using the applied reactions parameters.

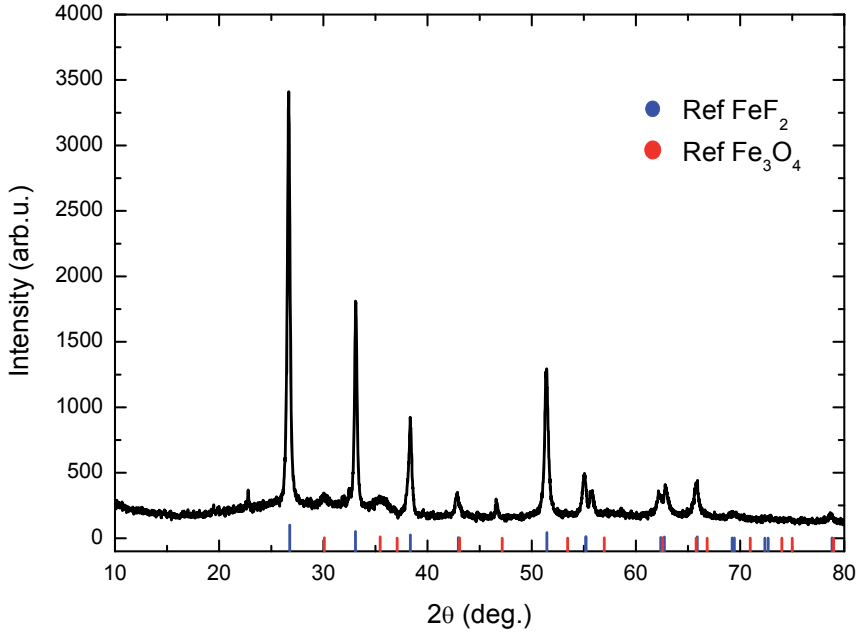

Figure 2.20: XRDP measurement for nanoparticles obtained with –CF_3 precursor from thermal process after 10h of dwell. Note the relation between FeF_2 and Fe_3O_4 is less than when the dwell is 2.5 hours

6.3.1. FeF_2 Structure

Iron(II) fluoride posses a body centered tetragonal structure (rutile) with a space group $P4_2/mnm$ as shown in figure 2.21. The lattice parameters are $a = b =$ 4,697 *Å* and c = 3,309 *Å*. The iron (II) cations are inserted into octahedral sites, but they form a distorted octahedron, with two fluorine atoms ≈ 2.03 *Å* apart from their

first neighbour Fe^{2+} atoms, while the remaining F^- atoms are at a distance of ≈ 2.15 *Å* from the Fe^{2+} atoms. This Jahn-Teller distortion is correlated to changes in the spin polarization along the Fe-F bond. Furthermore, the unit cell contains two layers of fluoride ions, with three ions in each layer. The fluorine anions have a coordination number of 3 resulting in a trigonal planar coordination.

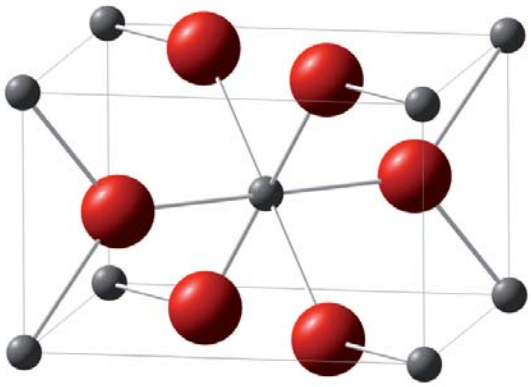

Figure 2.21: Rutile FeF_2 structure

6.4. Infrared Spectroscopy

Infrared spectroscopy (IRS) represents a fingerprint of a sample with absorptions peaks, which corresponds to the vibrational frequencies. For that reason, it is possible to analyse the chemical composition of the organic compounds stabilizing the nanoparticles.

Nanoparticles synthetized by the three different precursors presented similar spectra due to the triethylene glycol bands, where the high boiling point solvent acts also as a capping ligand (figure 2.22).

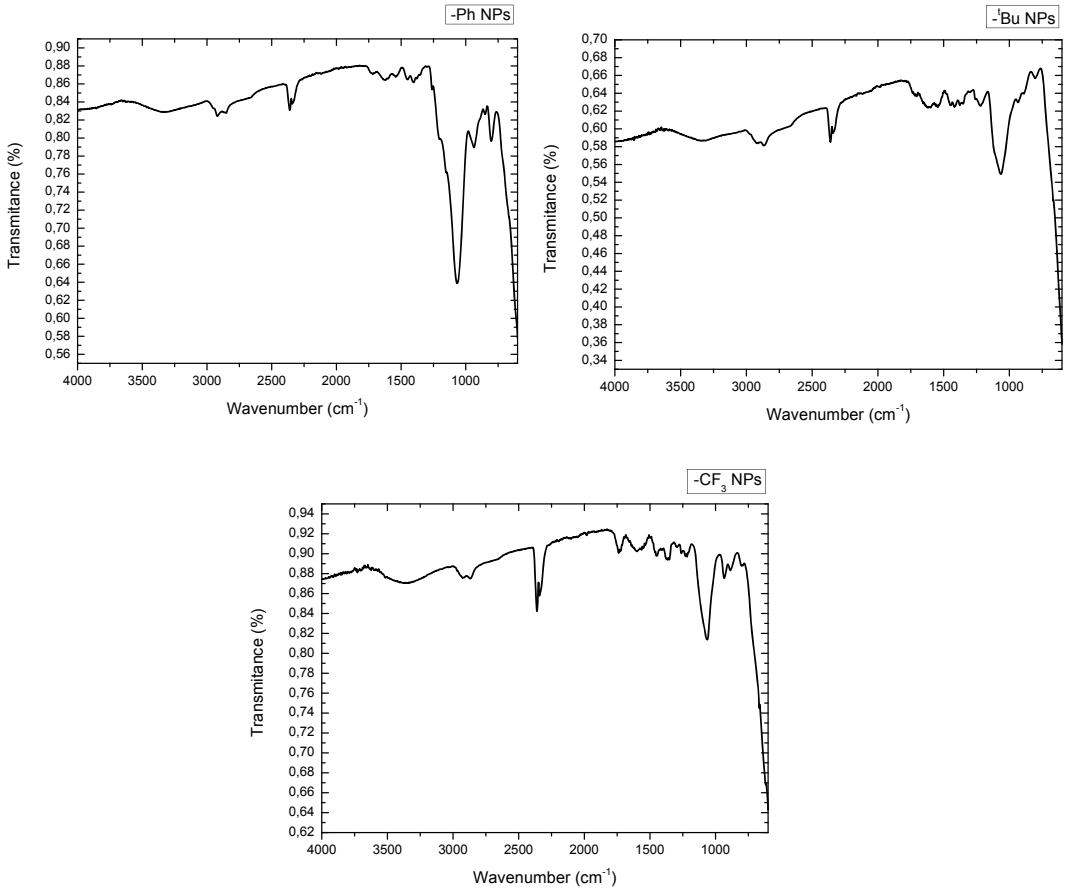

Figure 2.22: Infrared spectroscopy of nanoparticles synthetized by the three different precursors

The peaks that correspond to triethylene glycol are at 3400 cm^{-1} signal due to O-H stretching vibration from the solvent and absorbed water molecules. From 2900 to 2800 cm^{-1} the asymmetric and symmetric stretching vibrations of methylene (CH_2) are observed, and the absorption bands at 1147, 1116 and 1062 cm^{-1} correspond to the presence of C-O-C stretching vibrations.

6.5. Magnetometry

Magnetometry analysis was performed though *Superconductor Quantum Interference Device* (SQUID) to analyse the magnetism of magnetite nanoparticles synthetized in this research work. The SQUID provide a hysteresis loop as explained in previous magnetism related section, where magnetism nanoparticles behaviour was classified

in diamagnetic, paramagnetic, ferromagnetic, ferrimagnetic, antiferromagnetic and superparamagnetic, depends on the shape of the curve.

The magnetic behaviour of the obtained nanoparticles was performed in order to obtain the *magnetization saturation* (M_s) and *coercive field* ($\mu_0 H_0$).

In SQUID measurements, the quantity of triethylene glycol needs to be taken into account to correct the mass of magnetic material due to its property of acting as a capping ligand. The quantity of organic ligand was analysed by *thermal gravimetric analysis* (TGA), and it comprises around 10-20% of total weight as shown in figure 2.23.

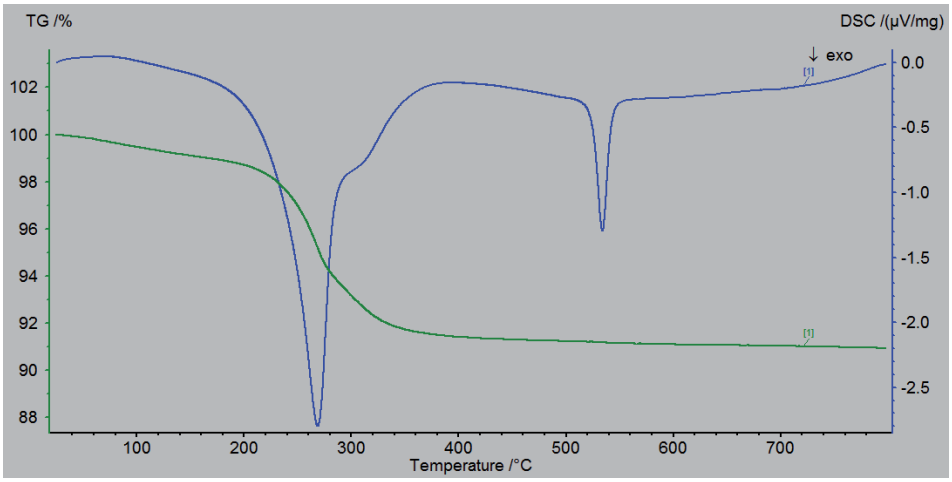

Figure 2.23: TGA of the obtainde nanoparticles using the different precursors and process

Consequently, once the hysteresis loops have been corrected, the M_s per mass unit could be calculated by the following equation 2.2:

$$\boldsymbol{M(H) = M_s + \chi_d H} \qquad \text{Eq. 2.2}$$

- $\boldsymbol{\chi_d}$ is the high-field differential susceptibility accounting for the superficial spin disorder.

Figure 2.24 shows the obtained hysteresis loop, for thermal and microwave process, and table 2.2 the extracted data:

(I)

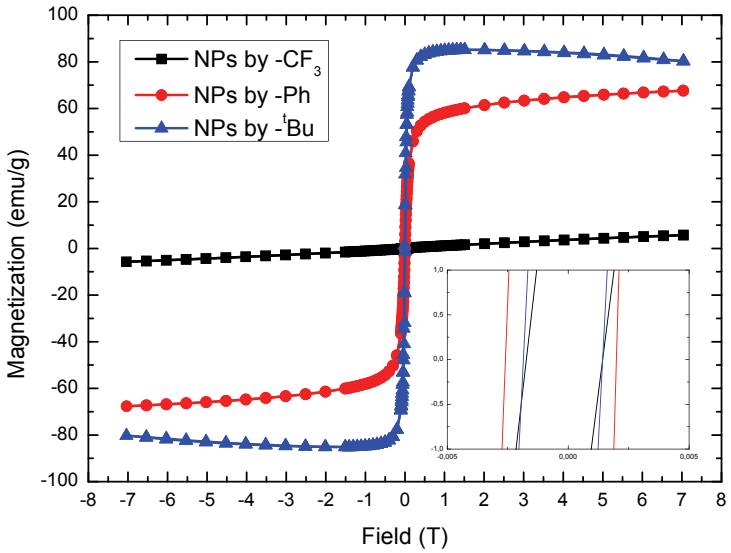

(II)

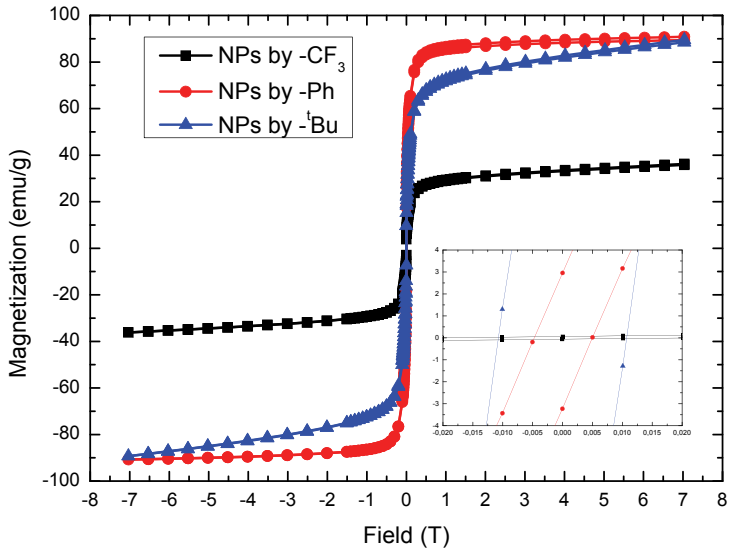

Figure 2.24: ***(I)*** *SQUID magnetometry results for thermal synthesis* ***(II)*** *SQUID magnetometry results for tmicrowave synthesis*

	Thermal process		Microwave process	
	$\mathbf{M_s}$	$\mathbf{\mu_0 H_0}$	$\mathbf{M_s}$	$\mathbf{\mu_0 H_0}$
Nanoparticles	(emu/g)	(Oe)	(emu/g)	(Oe)
NPs by $Fe(Ph_2diket)_3$	89.0	18	62.1	96
NPs by $Fe(^tBu_2diket)_3$	82.3	31	88.0	214
NPs by $Fe((CF_3)_2diket)_3$	33.9	31	0	0

Table 2.2: Magnetization values and coercive field for thermal and microwave nanoparticles synthesis

Hysteresis loop shows the expected superparamagnetic behaviour for all the nanoparticles obtained by thermal process using –Ph and –^{t}Bu precursor.

Concerning $Fe((CF_3)_2diket)_3$ precursor in thermal process, due to the mixture of Fe_3O_4 and FeF_2, a notable decrease in the magnetization saturation value occurs. This effect can be justified by the antiferromagnetic character of FeF_2.

The reproducible differences in the high Ms values for the $Fe(Ph_2diket)_3$ and $Fe(^tBu_2diket)_3$ precursors can be attributed to differences in the particle shape and internal crystalline order.

Furthermore, in the case of $Fe(^tBu_2diket)_3$ precursor and for a high magnetic fields, a diamagnetic behaviour was detected and attributed to the presence of the remaining triethylene glycol in the nanoparticles after the chemical washing procedure. Then, the $\mathbf{M_s}$ value was recalculated after subtracting the diamagnetic contribution to the global measure.

Concerning the coercive field values, nanoparticles obtained by microwave process presented a higher coercivity. The main reason for this effect is derived from the experimental conditions, because microwave needs lower temperatures and shorter time than thermal synthesis. In conclusion, the final nanoparticles would present a higher internal disorder, which is related to the larger coercive field.

The fluorinated nanoparticles produced by microwave process has in the hysteresis loops an antiferromagnetic behaviour only due to the FeF_2 compound without the presence of Fe_3O_4 as confirmed by XRD technique. The mechanism behind the formation of pure FeF_2 can be attributed to the difference in the synthetic mechanism influenced by microwave radiation through the non-thermal effects[42].

Concerning the nanoparticles synthetized by –Ph and -^{t}Bu precursors, there were no evidence of a different composition with the two methodologies performed (thermal or microwave process always form magnetite nanoparticles using this two different precursors).

7. Nanoparticles Control Shape

The driving force of the formation of different morphologies seems to be related to the physicochemical properties of the initial precursors. The decomposition temperature, basicity, solubility and size of the complexes will be able to affect on supersaturation, pH value, nucleation and crystal growth during the reaction. Furthermore, in microwave synthesis, the electric dipole moment of the precursor can have further impact.

7.1. Nanoparticles Control Shape: $Fe(Ph_2diket)_3$

The obtained faceted nanoparticles using thermal process could be related to the presence of aromatic groups forming part of the $Fe(Ph_2diket)_3$. Previous investigations demonstrate similar results where intermolecular interactions of the initial precursors have strong influence on the particle morphologies[43]. In this –Ph precursor case, the intermolecular interactions of the aromatic precursor by π-stacking allows the formation of facetated nanoparticles. This effect can be explained by ligands interactions between undissociated complexes and ligands coordinated on the surface of the nucleation seeds. These interactions can affect their Nernst and zeta potential and further both the interparticle interactions as well as the diffusion of precursors to the growing facets. In conclusion, nanocrystal facetated shape is governed by π-stacking interaction between different phenyl groups, which influence the energetics of crystal planes[44]. Distinctions in their intrinsic energy can induce for precursor interface interactions, in this case anisotropic, which strongly affect the diffusion of molecules.

On other hand, for the case of using microwave process, nanorods composed by spherical nanoparticles are obtained due to microwave assisted heating leads to a

faster consumption of the –Ph precursor generating burst nucleation and for this reason, the formation of more crystallization nuclei at the early stages of the reaction. As a result, all the crystallographic planes grow with the same kinetics (isotropic growth) and the round-shape particles from supra-aggregates with rod-like shapes to minimize their surface energy.

7.2. Nanoparticles Control Shape: Fe(^{t}Bu$_2$diket)$_3$

In the –^{t}Bu precursor case the decomposition temperature range is close to 440K (167ºC). The resulting nanoparticles have spherical morphology in flower-like aggregates. The obtained results can be produced for the steric hindrance due to the presence of bulky ligands[45].

7.3. Nanoparticles Control Shape: Fe((CF$_3$)$_2$diket)$_3$

The FeF_2 nanoparticles synthetized by –CF_3 precursor have a higher purity in case of the microwave process. In thermal route, the slower heating rates resulted in less precursor consumption, a prolonged nucleation phase (modest supersaturation), and longer reaction time. Due to the supersaturation is lower in thermal than in microwave synthesis, the difference in thermodynamics is negligible and the kinetically favoured Fe_3O_4 formation prevails the growth of the thermodynamically favoured FeF_2. In case of microwave heating, the fast achievement of the final temperature increase results in a higher degree of supersaturation and a higher relevance of thermodynamics[46].

8. External Fluoride Synthesis

The synthesis of FeF_2 nanocrystals was carried out using different external fluorides as precursors in order to understand better the formation of FeF_2 instead of Fe_3O_4 nanoparticles.

8.1. Chemical Precursor

Two different external fluoride precursor were used to carry out the synthesis of FeF_2 nanoparticles. The new synthesis (figure 2.25) was performed mixing iron(III) acetylacetonate with and ionic or covalent (C-F link) external fluoride such as sodium fluoride and tetrabutylammonium tetrafluoroborate (TBATFB).

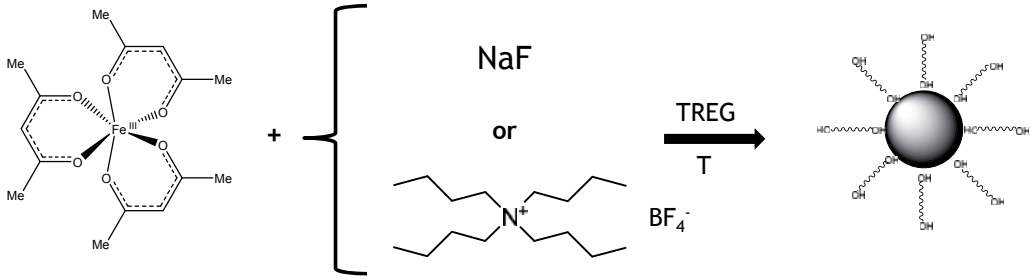

Figure 2.25: Scheme of nanoparticles synthesis using the two different external fluoride precursors

Furthermore, the final concentration of the external fluoride was the same than in the $Fe((CF_3)_2diket)_3$ precursor in order to reproduce the obtained results.

8.2. Synthetic FeF_2 Nanoparticles Process

The nanoparticles were performed using the same conditions in thermal and in microwave process than the previously synthesis using –Ph, -^{t}Bu and -CF_3 precursors: $Fe(acac)_3$ (1 mmol) and external fluoride (6 mmol) were suspended in triethylene glycol (25 mL) using an ultrasonic bath. Then, thermal or microwave methodologies were applied to synthetize nanoparticles where the solvent acts also as a capping ligand. Finally, nanocrystals were separated and washed thoroughly by repeated centrifugation and redispersed in ethanol to obtain a stable dispersion.

8.3. FeF_2 Nanoparticles Characterization

The nanoparticles synthetized, employing $Fe(acac)_3$ mixed with an external fluoride precursor, were characterized in order to know the morphology and the composition of the nanocrystals. The techniques used to characterize these specific

nanoparticles are TEM to obtain the shape and size of the nanoparticles and XRD pattern, which allow to give the final composition (Fe_3O_4 and / or FeF_2).

TEM analysis of nanoparticles performed by $Fe(acac)_3$ and an ionic external fluoride precursor produced spherical nanoparticles with a diameter of 5.7 ± 0.8 nm.

Conversely, the use of a covalent C-F link generates bow-like nanoparticles with a final size of around 1300 ± 200 nm such as the synthetized nanocrystals using only $–CF_3$ precursor (figure 2.26).

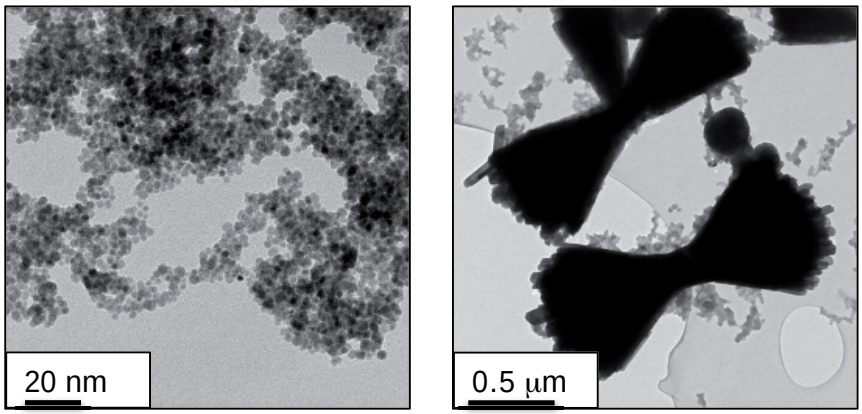

Figure 2.26: ***(left)*** *TEM from nanoparticles using ionic external fluoride* ***(right)*** *TEM from nanoparticles using covalent C-F link*

XRD patterns from spherical nanoparticles whether through thermal or microwave process, demonstrated that the structure corresponds to Fe_3O_4 pure phase while, nanocrystals obtained using iron(III) acetylacetonate with TBATFB as a precursor and also for both methodologies the structure coincide with FeF_2 without the presence of Fe_3O_4 compound as shown in figure 2.27.

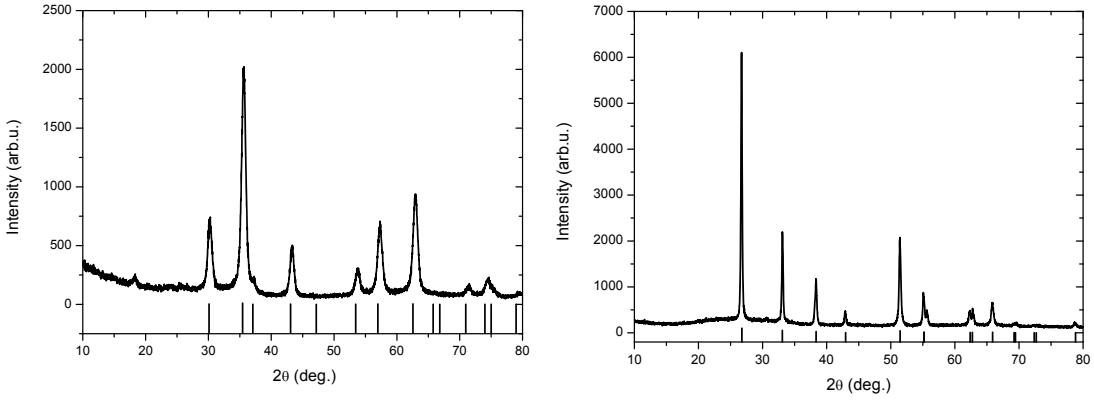

Figure 2.27: ***(left)*** *XRD from Fe_3O_4 nanoparticles using ionic external fluoride* ***(right)*** *XRD from FeF_2 nanoparticles using covalent C-F link*

The use of complexes with covalent link between carbon and fluoride produce that the free metal ions generated during the reaction, are supply for fluoride anions via a slow thermal decomposition process of the different precursors. The concentration of monomer is also changed slowly as a result of the slow release of F^- anions. Therefore, the growth of nanocrystals can be well controlled in the early stage of growth process for a relatively long period, which leads to the formation of monodisperse FeF_2 nanocrystals.

Initially, all the ions are coordinated by oxygen atoms but during the reaction process, F^- anions released from the precursors will replace the oxygen atoms to form fluoride compounds[47].

9. Conclusions

Cuboctahedron, flower-like, and bow-like shaped nanoparticles were produced via thermal and microwave heating using tailor iron precursor with different terminal α group on the $Fe(R_2diket)_3$ (R = -Ph, -^{t}Bu or -CF_3). For the case of bow-like nanoparticles, they could also be synthetized using $Fe(acac)_3$ mixed with a precursor containing C-F covalent link.

Shape, structure, and composition of the obtained nanoparticles were extensively studied through TEM, XRD, IRS, magnetometry, and TGA techniques. Besides the expected spinel structure upon using –Ph and –^{t}Bu precursors, fluorinated precursors leads to the formation of FeF_2 nanocrystals due to the presence of fluoride anion in the reaction media.

The relationship of the chemical nature of the precursor and the final shape of the obtained nanoparticles has been analysed, studied and observing a clear influence of the intermolecular interactions: π-stacking for the aromatic precursor forming facetated nanoparticles (thermal process) and organized tubes composed of smaller spherical nanoparticles (microwave process); steric hindrance for the –^{t}Bu precursor with flower-like shape; and finally the fluorinated precursors allowed to form FeF_2 nanostructures growing on Fe_3O_4 nucleus.

As a summary, control shape leads to the possibility to change the morphology of the synthetized nanoparticles by modifying the precursor in a glycol medium without adding any co-reactant, resulting in a highly stable colloidal dispersion of shaped nanoparticles in polar media such as water, chloroform and alcohols[48].

10. Bibliography

1) Hao, R., Xing, R., Xu, Z., Hou, Y., Gao, S., & Sun, S. (2010). Synthesis, functionalization, and biomedical applications of multifunctional magnetic nanoparticles. *Advanced Materials (Deerfield Beach, Fla.)*, *22*(25), 2729–42. doi: 10.1002/adma.201000260.

2) Niederberger, M., & Garnweitner, G. (2006). Organic reaction pathways in the nonaqueous synthesis of metal oxide nanoparticles. *Chemistry - A European Journal*, *12*, 7282–7302. doi: 10.1002/ chem.200600313.

3) Tang, J., Pu, S., Dong, S., & Luo, L. (2014). Magnetic field sensing based on magnetic-fluid-clad multimode-singlemode-multimode fiber structures. *Sensors (Switzerland)*, *14*(10), 19086–19094. doi:10.3390/s141019086.

4) Dalpozzo, R. (2015). Magnetic nanoparticle supports for asymmetric catalysts. *Green Chemistry*, *17*, 3671–3686. doi:10.1039/c5gc00386e.

5) Li, X., Wei, J., Aifantis, K. E., Fan, Y., Feng, Q., Cui, F.-Z., & Watari, F. (2016). Current investigations into magnetic nanoparticles for biomedical applications. *Journal of Biomedical Materials Research. Part A*, 1285–1296. doi:10.1002/jbm.a.35654.

6) Busquets, M. A., Estelrich, J., & Sánchez-Martín, M. J. (2015). Nanoparticles in magnetic resonance imaging: from simple to dual contrast agents. *International Journal of Nanomedicine*, *140*(10), 1727–1741. doi:10.2147/IJN.S7650.

7) Singamaneni, S., Bliznyuk, V. N., Binek, C., & Tsymbal, E. Y. (2011). Magnetic nanoparticles: recent advances in synthesis, self-assembly and applications. *Journal of Materials Chemistry*, *21*(42), 16819–16845. doi:10.1039/c1jm11845e.

8) Kong, J., Coolahan, K., & Mugweru, A. (2013). Manganese based magnetic nanoparticles for heavy metal detection and environmental remediation. *Analytical Methods*, *5*(19), 5128–5133. doi:10.1039/c3ay40359a.

9) Kaur, R., Hasan, A., Alam, S., Saini, M., & Raza, S.K. (2014). Synthesis and surface engineering of magnetic nanoparticles for environmental cleanup and pesticide residue analysis: A review. *Journal of Separation Science*, *37*(14), 1805–1825. doi:10.1002/jssc.201400256.

10) Khalil, M. I. (2015). Co-precipitation in aqueous solution synthesis of magnetite nanoparticles using iron (III) salts as precursors. *Arabian Journal of Chemistry*, *8*(2), 279–284. doi:10.1016/j.arabjc.2015.02.008.

11) Faraji, M., Yamini, Y., &Babelan, Z. (2011).Magnetic Nanoparticles: Synthesis, Stabilization, Functionalization, Characterization and Applications. *Journal of the Iranian Chemical Society,*, *3*(4), 155–160.

12) Nyiro-Kosa, I., Recnik, A., & Posfai, M. (2012). Novel methods for the synthesis of magnetite nanoparticles with special morphologies and textured assemblages. *Journal of Nanoparticle Research*, *14*(10). doi:10.1007/s11051-012-1150-8

13) Hasany, S. F., Ahmed, I., J, R., & Rehman, a. (2012). Systematic Review of the Preparation Techniques of Iron Oxide Magnetic Nanoparticles. *Nanoscience and Nanotechnology*, *2*(6), 148–158. doi: 10.5923/ j.nn. 20120206.01.

14) Okoli, C., Sanchez-Dominguez, M., Boutonnet, M., Järås, S., Civera, C., Solans, C., & Kuttuva, G. R. (2012). Comparison and Functionalization Study of Microemulsion-Prepared Magnetic Iron Oxide Nanoparticles. *Langmuir*, *28*(22), 8479–8485. doi:10.1021/la300599q.

15) Ozel, F., & Kockar, H. (2015). Growth and characterizations of magnetic nanoparticles under hydrothermal conditions: Reaction time and temperature. *Journal of Magnetism and Magnetic Materials*, *373*, 213–216. doi: 10.1016/j.jmmm.2014.02.072.

16) Ge, S., Shi, X., Sun, K., Li, C., Uher, C., Baker, J. R., & Orr, B. G. (2009). Facile Hydrothermal Synthesis of Iron Oxide Nanoparticles with Tunable Magnetic Properties. *The Journal of Physical Chemistry C*, *113*(31), 13593–13599. doi:10.1021/jp902953t.

17) Hu, H., Yang, H., Huang, P., Cui, D., Peng, Y., Zhang, J., … Shi, D. (2010). Unique role of ionic liquid in microwave-assisted synthesis of monodisperse magnetite nanoparticles. *Chemical Communications (Cambridge, England)*, *46*(22), 3866–8. doi:10.1039/b927321b.

18) Fei, H., Peng, Z., Li, L., Yang, Y., Lu, W., Samuel, E. L. G., & Tour, J. M. (2014). Preparation of carbon-coated iron oxide nanoparticles dispersed on graphene sheets and applications as advanced anode materials for lithium-ion batteries. *Nano Research*, *7*(4), 1–9. doi:10.1007/s12274-014-0416-0.

19) Martinez, A., Garcia-Lobato, M.A., & Peey, D . (2009). Study of the Poperties of Iron Oxide Nanostructures. *Research in Nanotechnology Developments*, 17, 183-194.

20) Pérez-Mirabet, L., Solano, E., Martínez-Julián, F., Guzmán, R., Arbiol, J., Puig, T., Obradors, X., Ricart, S., Yáñez, R., & Ros, J. (2013). One-pot synthesis of stable colloidal solutions of MFe2O4 nanoparticles using oleylamine as solvent and stabilizer. *Materials Research Bulletin*, *48*(3), 966–972. doi:10.1016/ j.materresbull.2012.11.086.

21) Wu, W., Wu, Z., Yu, T., Jiang, C., & Kim, W.-S. (2015). Recent progress on magnetic iron oxide nanoparticles: synthesis, surface functional strategies and biomedical applications. *Science and Technology of Advanced Materials*, *16*(2), 023501. doi:10.1088/1468-6996/16/2/023501.

22) Patsula, V., Kosinová, L., Lovrić, M., Ferhatovic Hamzić, L., Rabyk, M., Konefal, R., & Horák, D. (2016). Superparamagnetic Fe3O4 Nanoparticles: Synthesis by Thermal Decomposition of Iron(III) Glucuronate and Application in Magnetic Resonance Imaging. *ACS Applied Materials & Interfaces*, *8*(11), 7238–7247. doi:10.1021/ acsami.5b12720.

23) Viau, G., Fievet-Vincent, F., & Fievet, F. (1996). Monodisperse iron-based particles: precipitation in liquid polyols. *Journal of Materials Chemistry*, *6*(6), 1047. doi: 10.1039/jm9960601047.

24) Deschamps, A., Lagier, J., Fievet, F., & Aeiyachb, S. (1992). New Chemical One-step Process for Preparing Fine Metallic Particles embedded in a Polymer Matrix, *2*(1 I), 1213–1214.

25) Beyki Shemirani, F., M. H. (2015). Dual application of facilely synthesized Fe3O4 nanoparticles: Fast reduction of nitro compound and preparation of magnetic polyphenylthiourea nanocomposite for efficient adsorption of lead ions. *RSC Advances*, *5*. doi: 10.1039/c4ra12549e.

26) Hasany, S. F., Rehman, a., Jose, R., & Ahmed, I. (2012). Iron oxide magnetic nanoparticles: A short review, (February 2016), 298–321. doi:10.1063/1.4769153.

27) Plank, C., Schillinger, U., & Scherer, F. (2005) The magnetofection method: using magnetic force to enhance gene delivery. *Biolical Chemistry* . 2005;384(5): 737–747. doi: 10.1515/BC.2003.082.

28) Dorniani, D., Hussein, M. Z. Bin, Kura, A. U., Fakurazi, S., Shaari, A. H., & Ahmad, Z. (2012). Preparation of Fe_3O_4 magnetic nanoparticles coated with gallic acid for drug delivery. *International Journal of Nanomedicine*, *7*, 5745–56. doi:10.2147/IJN.S35746.

29) Basel, M. T., Balivada, S., Wang, H., Shrestha, T. B., Seo, G. M., Pyle, M., & Troyer, D. L. (2012). Cell-delivered magnetic nanoparticles caused hyperthermia-mediated increased survival in a murine pancreatic cancer model. *International Journal of Nanomedicine*, *7*, 297–306. doi:10.2147/IJN.S28344.

30) Busquets, M. A., Estelrich, J., & Sánchez-Martín, M. J. (2015). Nanoparticles in magnetic resonance imaging: from simple to dual contrast agents. *International Journal of Nanomedicine*, *140*(10), 1727–1741. doi:10.2147/IJN.S76501.

31) Zargoosh, K., Abedini, H., Abdolmaleki, A., & Molavian, M. R. (2013). Effective Removal of Heavy Metal Ions from Industrial Wastes Using Thiosalicylhydrazide-Modified Magnetic Nanoparticles. *Industrial & Engineering Chemistry Research*, *52*(42), 14944–14954. doi:10.1021/ie401971w.

32) Spirou, S. V, Tsialios, P., & Loudos, G. (2015). Shielding of Sensitive Electronic Devices in Magnetic Nanoparticle Hyperthermia Using Arrays of Coils. *Journal of Physics: Conference Series*, *637*, 012042. doi:10.1088/1742-6596/637/1/012042.

33) Giusta, A., Princivalle, F., & Carbonin, S. (1987). Crystal structure and cation distribution in some natural magnetites. *Mineralogy and Petrology*, *37*, 315–321. doi: 10.1007/BF01161823.

34) Roca, A. G., Morales, M. D. P., O'Grady, K., & Serna, C. J. (2006). Structural and magnetic properties of uniform magnetite nanoparticles prepared by high temperature decomposition of organic precursors. *Nanotechnology*, *17*, 2783–2788. doi: 10.1088/0957-4484/ 17/11/010.

35) Solano, E., Yáñez, R., Ricart, S., & Ros, J. (2015). Journal of Magnetism and Magnetic Materials New approach towards the polyol route to fabricate MFe_2O_4 magnetic nanoparticles : The use of MCl_2 and Fe $(acac)_3$ as chemical precursors. *Journal of Magnetism and Magnetic Materials*, *382*, 1–6. doi: 10.1016/j.jmmm.2015.02.002.

36) Hoene, J. Von, Charles, R. G., & Hickam, W. M. (1958). Thermal Decomposition of Metal Acetylacetonates: Mass Spectrometer Studies. *The Journal of Physical Chemistry*, *62*(9), 1098–1101. doi: 10.1021/j150567a019.

37) Vreeland, E. C., Watt, J., Schober, G. B., Hance, B. G., Austin, M. J., Price, A. D., Huber, D. L. (2015). Enhanced Nanoparticle Size Control by Extending LaMer's Mechanism. *Chemistry of Materials*, *27*(17), 6059–6066. doi: 10.1021/ acs.chemmater.5b02510.

38) Bullock, G. R. (1984). The current status of fixation for electron microscopy: a review. *Journal of Microscopy*, *133*(January), 1–15. doi: 10.1111/j.1365-2818.1984.tb00458.x.

39) Solano, E., Perez-Mirabet, L., Martinez-Julian, F., Guzman, R., Arbiol, J., Puig, T., Obradors, X., Yáñez, R., Pomar, A., Ricart, S., Ros, J. (2012). Facile and efficient one-pot solvothermal and microwave-assisted synthesis of stable colloidal solutions of MFe_2O_4 spinel magnetic nanoparticles. *Journal of Nanoparticle Research*, *14*(8). doi: 10.1007/s11051-012-1034-y.

40) Zhang, L., Dou, Y.-H., & Gu, H.-C. (2006). Sterically induced shape control of magnetite nanoparticles. *Journal of Crystal Growth*, *296*(2), 221–226. doi: 10.1016/j.jcrysgro.2006.08.010.

41) Solano, E., Frontera, C., Puig, T., Obradors, X., Ricart, S., & Ros, J. (2014). Neutron and X-ray diffraction study of ferrite nanocrystals obtained by microwave-assisted growth. A structural comparison with the thermal synthetic route. *Journal of Applied Crystallography*, *47*(1), 414–420. doi: 10.1107/S1600576713032895.

42) Zhang, Y., Sun, X., Si, R., You, L., & Yan, C. (2005). Single-Crystalline and Monodisperse LaF_3 Triangular Nanoplates from a Single- Source Precursor. *Mercury*, *34*(0002), 5–7.

43) Feng, W., Sun, L. D., & Yan, C. H. (2011). Role of surface ligands in the nanoparticle assemblies: A case study of regularly shaped colloidal crystals composed of sodium rare earth fluoride. *Langmuir*, *27*(7), 3343–3347. doi: 10.1021/la104743p.

44) Hofmeister, H. (2009). Shape variations and anisotropic growth of multiply twinned nanoparticles. *Zeitschrift Fur Kristallographie*, *224*(11), 528–538. doi:10.1524/zkri.2009.1034.

45) Zhang, L., Dou, Y. H., & Gu, H. C. (2006). Sterically induced shape control of magnetite nanoparticles. *Journal of Crystal Growth*, *296*(2), 221–226. doi:10.1016/j.jcrysgro.2006.08.010.

46) Feng, W., Sun, L. D., Zhang, Y. W., & Yan, C. H. (2010). Synthesis and assembly of rare earth nanostructures directed by the principle of coordination chemistry in solution-based process. *Coordination Chemistry Reviews*, *254*(9-10), 1038–1053. doi: 10.1016/j.ccr.2010.02.007.

47) Jayarathna, L., Bandara, A., Ng, W. J., & Weerasooriya, R. (2015). Fluoride adsorption on $\gamma - Fe_2O_3$ nanoparticles. *Journal of Environmental Health Science and Engineering*, *13*(1), 54. doi: 10.1186/ s40201-015-0210-2.

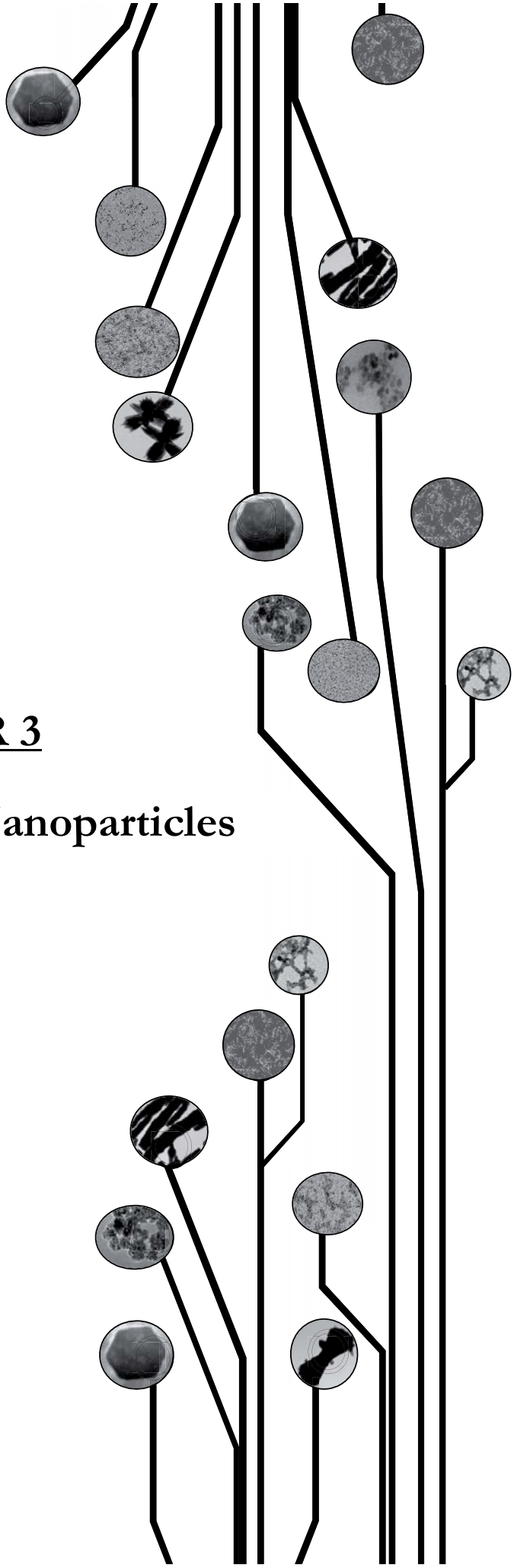

CHAPTER 3

Cerium(IV) Oxide Nanoparticles

Chapter 3 is based on the in progress article:

Fast and one-pot methodology for the synthesis of CeO_2 nanoparticles with a labile capping ligands stable in polar solvents:

The use of $Ce(acac)_3$ and $Ce(OAc)_3$ as precursors to produce CeO_2 nanoparticles with high stability, generating an excellent dispersion in polar solvents (water, alcohols), make our synthetic methodology really useful due to its is also fast, easy, economic and one-pot process. The two investigated synthetic routes, thermal and microwave, produce spherical or cubic nanoparticles depending on the precursor. The nanocrystals are performed with high boiling point solvents benzyl alcohol (BnOH) and triethylene glycol (TREG), which produces a high crystalline nanoparticles confirmed by X-Ray Powder Diffraction (XRPD). Furthermore, a deeply characterization is performed in order to propose a synthetic mechanism and to investigate the surface of the different nanoparticles by different techniques such as proton nuclear magnetic resonance (^{1}HNMR), infrared spectroscopy (IR) and gas chromatography-mass spectroscopy (GC-MS). Finally, X-ray photoelectron spectroscopy (XPS) technique is used in order to study the composition of these nanocrystals.

The final objective is to perform nanoparticles well characterized with concentrations up to 90 mM and stables during long periods of time for superconductivity or antioxidant human cells applications.

CONTENTS

II Metal Oxide Nanoparticles

Chapter 3: Cerium(IV) Oxide Nanoparticles

1. Introduction: State of the art

Nanocrystalline cerium(IV) oxide has been called as "industrial vitamin" and a "treasury" of new materials[1] because their unique atomic structure compared with other material provides special properties in luminesces, magnetisms and electronics thanks to their 4f electronic configuration.

This specific feature makes cerium(IV) oxide really important to achieve new applications, that are not possible with transition or main group metals, in engineering, biological and technology[2] fields such as solid-oxide fuel cells[3], catalytic materials[4], solar cells[5], potential pharmacological agents[6] and three-way catalyst[7] for automobile exhaust-gas treatments, oxidative coupling of methane and water-gas shift reaction.

Numerous techniques such as hydrothermal [8], solvothermal [9], aqueous precipitation [10], reversed micelles [11], thermal decomposition [12] and flame spray [13] methods are used to synthesize cerium(IV) oxide nanoparticles in order to obtain the desired nanomaterial, with a specific characteristics. They can determine the solubility, size, nature of capping ligand, charge, structural arrangement and morphology of nanoparticles, thus affecting their properties. However, for biological applications, biocompatible CeO_2 nanomaterials has been systematically synthesized in pure water [14] or with the protection of polyethylene glycol [15] or glucose[16], among others.

This chapter provides a study of cerium(IV) oxide nanoparticles in different aspects such as synthetic methodologies, nanoparticles structure, reaction mechanisms and a full characterization. The final interest will be to study its use in two fields, superconductivity for the design of nanocomposites layers and biomedical for the fabrication of antioxidant nanomaterials.

1.1. CeO_2 Nanoparticles Applications

Recently, nanostructured cerium(IV) oxide nanoparticles has emerged as a riveting and advantageous material in different fields such as bioanalysis [17], biomedicine[18], drug delivery[19], bioscaffolding[20] and superconductivity[21]:

- **Bioanalysis:** The stable physical and chemical structure makes cerium oxide nanoparticles suitable use in biological assays to eliminate the shortcomings of organic fluorophores, radioactive labelling or natural enzymes, which are photobleachable, toxic, and expensive and easily degradable, respectively. These multi-enzyme-like properties have been successfully used for biological detection and analysis.

- **Drug delivery devices and bioscaffold:** Cerium(IV) oxide nanoparticles show high potential application in biotechnology as drug delivery systems and bioscaffolds. This nanomaterial could be used as nanocarrier or scaffold and also act as a therapeutic agent. A clear example of this application is that cerium oxide nanoparticles could increase the production of collagen by human mesenchymal stem cells cultured on porous bioactive scaffolds, which can bind to bone and act as a temporary guide and stimulus for bone growth in three dimensions.

- **Catalysis:** An other important use of cerium(IV) oxide is as catalyst for a widely variety of reactions[22], including the oxidation of different compounds such as CO and in the synthesis of benzaldehyde from benzyalcohol, which is a typically product used in perfumery and pharmaceutical industrial[23]. Furthermore, selective oxidation and reductions under efficient catalyst is an industrially important reaction as it avoids large amounts of highly toxic heavy metals wastes, generating from traditional production process[24].

- **Biomedicine:** Different investigations have encouraged researchers to pursue cerium(IV) oxide nanoparticles as a therapeutic agent to treat a number of diseases, including cancer, due to their diverse abilities of this nanomaterial. Various

studies show cerium(IV) oxide to be toxic to cancer cells, inhibit invasion and sensitize cancer cells to radiation therapy. These kind of nanoparticles display minimal toxicity to normal tissues and can provide extra protection. Moreover, an other interested application is on the reduction of unwanted reactive oxygen species in biological systems, which are the responsible of the deterioration of human cells producing inflammation, degenerative disorders, aging, etc.

- **Superconductivity:** Cerium(IV) oxide nanoparticles are good candidate in the preparation of epitaxial nanocomposites films based on the use of $YBa_2Cu_3O_{7-\delta}$ colloidal solution containing different crystalline performed oxide nanoparticles to improve the high temperature superconductor properties due to the critical current can be increased when the nanoparticles are embedded.

The unique physical and chemical properties of this compound and the achieved significant advances of it clearly demonstrate that cerium(IV) oxide is an optimum and versatile material, that makes it attractive for widespread applications in scientific investigations and in industrial process.

2. CeO_2 Nanoparticles Structure

Cerium(IV) oxide nanoparticles can be synthesized with a high control of morphology and size. A structural description is necessary in order to develop the following results, which are essential for the investigation of their properties and characteristics.

Unlike the other lanthanide series, which only exhibit a trivalent state, cerium atom can exist in either +3 (fully reduced) or +4 (fully oxidized) state due to the partially filled subshells of electrons, 4f and 5d, with several excited substates predicted[25]. Ce(IV) state crystallizes in the fluorite

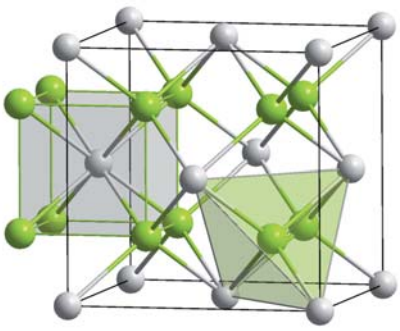

Figure 3.1: Cerium(iv) oxide structure

structure[26] (Fm3m) in which every cerium atom (grey) is surrounded by eight oxygen anions and every oxygen atoms occupies a tetrahedral position (green) as shown in figure 3.1.

However, a significant concentration of intrinsic defects is usually present, with a portion of cerium present in the Ce(III) valence state having the deficiency of positive charge compensated by oxygen vacancies[27]. The relative amount of cerium ions Ce^{3+} and Ce^{4+} is a function of particle size[28]. In general, the fraction of Ce^{3+} ions in the particles increases with decreasing particle size. For this reason, cerium oxide nanoparticles can have a dual role as an oxidation and reduction catalyst, depending on the reaction conditions. The quick change of the oxidation state between Ce^{4+} and Ce^{3+} is due to the cerium ability to change its electronic configuration depending on the immediate environment[29].

Furthermore, cerium oxide also exhibits oxygen vacancies or defects in the lattice structure that arise through loss of oxygen and/or its electrons, alternating between CeO_2 and CeO_{2-x} during redox reactions. Moreover, the addition or removal of oxygen atoms in the oxidizing or reducing process involves a minimal reorganization of the skeleton arrangement of the cerium atoms and the retention of the fluorite structure[30]. This structural property facilitates the regenerative ability of cerium oxide nanoparticles to the initial state.

3. Nanoparticles Synthesis

The synthetic process of cerium(IV) oxide nanoparticles has been developed and deeply studied during this research work in order to obtain optimum nanocrystals for application in superconductivity and biomedical fields. For this reason, the primary requirements to use them in future applications are small size (less than 15 nm), narrow size dispersion, high concentration up to 90 mM, high crystallinity, highly dispersive and stables in polar media such as alcohols and water.

In order to achieve the desired features, two different synthetic routs were used, polyol[31] and benzyl alcohol[32] process. Both mechanism presented similar properties and advantages as for example, the nanocrystals are obtained in one step directly without the need for any template or assembly agent, the solvent can act at the same

time as a stabilizing agent and no subproducts difficult to eliminate are performed.

On one hand, polyol process using triethylene glycol as a solvent was previously studied and described previously in chapter 2. TREG proved to be a good solvent to obtain high concentrations, crystallinity and stabilization in the nanoparticles synthesis.

On the other hand, benzyl alcohol route was also used in the synthesis of CeO_2 nanoparticles in order to investigate the effect of another high boiling point solvent during the formation of the nanocrystals. Benzyl alcohol route is a powerful alternative for the synthesis of oxide nanoparticles especially offering similar advantages as TREG solvent such as high crystallinity, high reproducibility and the ability to control the crystal growth.

In polyol and in benzyl alcohol processes, the nature of the reagents and the thermodynamic factors, in particular the temperature, are important to obtain the desired nanocrystals. Among the different available precursors metal halides were avoided because, although they produced the desired metal oxide nanoparticles, in some cases halide impurities are difficult to eliminate. Furthermore, the use of metal nitrates as precursors produce bigger nanoparticles, > 15 nm, and aggregates as shown in figure 3.2, where $Ce(NO_3)_3$ is used as a precursor in TREG to synthetize of CeO_2 nanoparticles[33]. In order to avoid these undesired effects, our synthetic route is based on the reaction of metal acetates and acetylacetonates with alcohols providing as an optimum alternative.

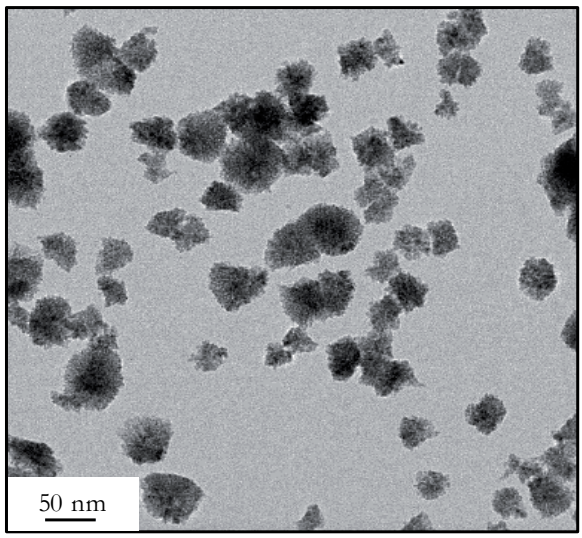

Figure 3.2: TEM image of CeO_2 NPs from $Ce(NO_3)_3$ precursor in TREG

The conversion of the chemical precursors to metal oxide nanoparticles is performed in the simplest case with the exposure of the precursor solution to the air during the reaction, which is enough to oxidize the meta from Ce(III) to Ce(IV)l. This approach takes advantages of the good size and shape control without alterations in the particles during the transformation into the oxide.

In order to understand their impact on the final nanoparticles, the effect of the different variables was evaluated performing an exhaustive analysis of the synthetic and characterization processes.

3.1. Chemical Precursors

Cerium precursors used to produce CeO_2 nanoparticles were cerium(III) and cerium(IV) acetylacetonate ($Ce(acac)_3$, $Ce(acac)_4$) and cerium(III) acetate ($Ce(OAc)_3$), as shown in figure 3.3.

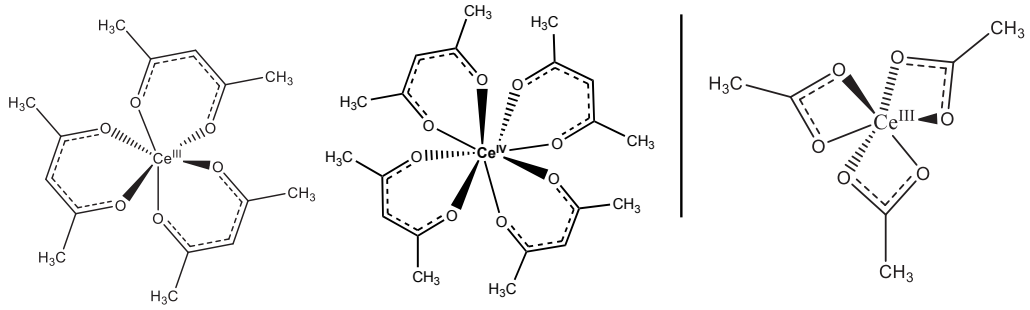

Figure 3.3: ***(left)*** *$Ce(acac)_3$ &* *$Ce(acac)_4$* ***(right)*** *$Ce(OAc)_3$*

Commercial $Ce(acac)_3$ and $Ce(OAc)_3$ precursors were used whereas $Ce(acac)_4$ was prepared in the laboratory following the methodology described by *Behrsing et al*[34].

In order to confirm that $Ce(acac)_4$ was obtained, the two different infrared spectra[35] of Ce^{3+} and Ce^{4+} acetylacetonate were analysed. Table 3.1 shows energies of the principal bands corresponding to C-C-C-O stretching.

	Wavenumber (cm^{-1})		
$Ce(acac)_3$	1576	1507	1366
$Ce(acac)_4$	1560	1502	1350

Table 3.1. C-C-C-O badns of cerium (III) and (IV) acetylacetonates

In cerium(III) and cerium(IV) acetylacetonates, the very strong bands around 1560, 1500 cm^{-1} correspond to stretching vibrations of C-C=C-O and C=C-C=O from the diketonate part and the band around 1360 cm^{-1} to $-CH_3$ symmetric deformation. Ce(IV) acetylacetonate displays these stretching bands at lower energy than the corresponding Ce(III) compound revealing that Ce-O bond is stronger in the more oxidised cerium compound[34].

3.2. Synthesis of Nanoparticles

The synthetic methodologies, which is based on the previously described polyol and benzyl alcohol route, were performed via thermal and microwave process in order to compare the effect of the different activations in the obtained CeO_2 nanoparticles. As was explained in chapter 2, the fast nucleation process produced by microwave route can afford different morphologies, sizes and changes on the stability of the final nanoparticles.

Furthermore, the microwave process is of particular interest reducing the synthesis time, obtaining the nanoparticles faster than in the thermal process (1 hour instead 7 hours).

- **Thermal process:** $Ce(acac)_3$, $Ce(acac)_4$ or $Ce(OAc)_3$ (2.25 mmol) was suspended in benzyl alcohol (BnOH) or triethylene glycol (TREG) (25 mL) using ultrasounds bath. The mixture was poured into a round bottomed flask equipped with a condenser, a magnetic stirrer, a thermograph and a heater. The system was heated at 220ºC (1ºC/min) for the case of BnOH and at 280ºC (1ºC/min) if TREG is used as a solvent. After 2.5h the mixture was cooled to room temperature (ambient rate) and stirred during 2 days. The CeO_2 nanocrystals were separated, and washed thoroughly by repeated centrifugation using diethyl ether to precipitate the

nanoparticles and ethanol to remove the BnOH. Ethyl acetate and ethanol were used to eliminate the excess of TREG. Finally, the nanocrystals were dispersed in ethanol (90 mM) yielding a stable dispersion.

Similar thermal methodology was also studied under argon media. The solvents were purged by bubbling nitrogen gas and generating vacuum to eliminate the oxygen present on them, in order to study the reaction mechanism and the influence of the oxygen from the atmosphere on the composition of the final nanoparticles, as it will be discussed in the following section *5.5. X-Ray Photoelectron Spectroscopy*.

- **Microwave procedure**: $Ce(acac)_3$, $Ce(acac)_4$ or $Ce(OAc)_3$ (2.25 mmol) was suspended in a BnOH or TREG (25 mL) and transferred to a microwave vial. After ultrasonification, the solution was heated under magnetic stirring by microwave radiation (300 W) to 210 ºC in BnOH or 220ºC in TREG. When PVP is mixed to the precursor solution, the final temperature is 260ºC or 275ºC in BnOH depending on the mass fraction of PVP added. After 1 hour at final temperature, the mixture was cooled under nitrogen atmosphere inside of the microwave and was stirred during 2 days at room temperature. Then, CeO_2 nanocrystals were separated and washed thoroughly by repeated centrifugation and dispersed in ethanol (90 mM).

The dispersion of CeO_2 nanoparticles in polar solvents, such as water and alcohols, was highly stable for several months at room temperature for concentrations up to 90 mM. Furthermore, after the synthesis we can conclude that the two different methodologies, thermal and microwave process produce the same nanoparticles without differences in size or in shape as will be shown in following sections.

4. Results and Discussions

CeO_2 nanoparticles were fully studied and characterised using a variety of techniques that helped us in the understanding of their chemical composition and capping ligand which were decisive in their stability in solvents and in their applications.

The results with both solvents TREG and BnOH allowed to obtain the same size, shape and composition in the final nanoparticles. However, the use of the precursor, Ce(III) acetylacetonate or Ce(III) acetate, caused variations on the final morphology and size. For this reason, the nanoparticles results will be discussed in two different sections depending on the precursor used.

4.1. CeO_2 Nanoparticles from Cerium(III) Acetylacetonate Precursor

Cerium(IV) oxide nanoparticles synthetized by Ce(III) acetylacetonate in TREG or BnOH gave similar round shaped nanoparticles with a final size around of 2,5 nm using either hermal or microwave process (figure 3.4).

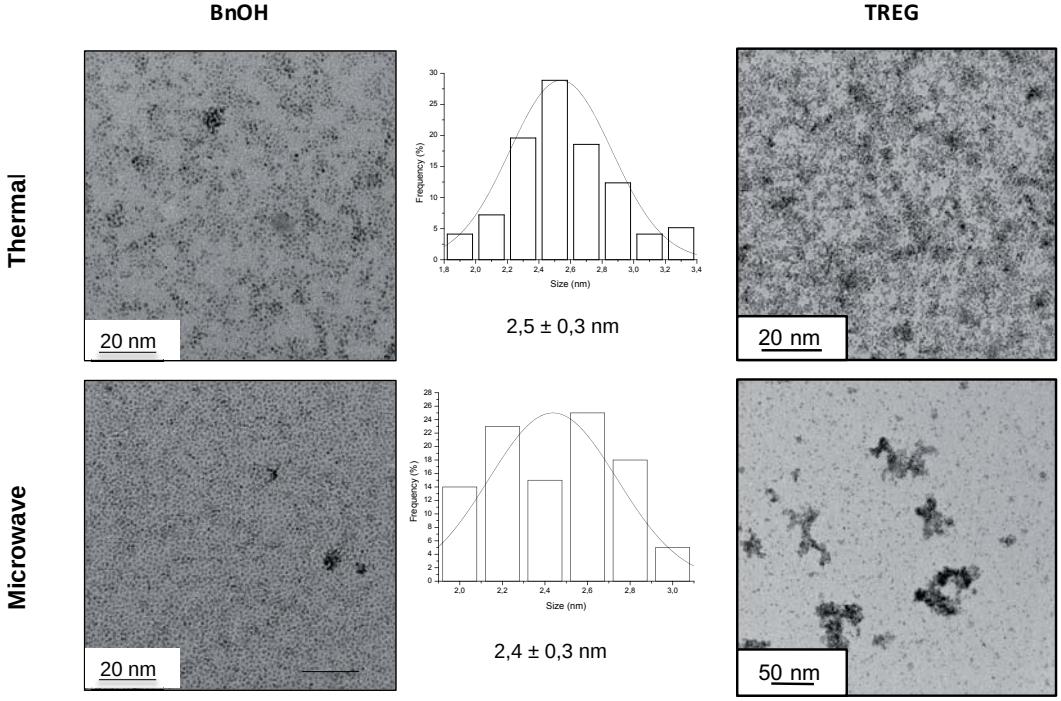

Figure 3.4: BF-TEM image showing size and shape of the CeO_2 nanoparticles starting from $Ce(acac)_3$ using a) BnOH/thermal activation, b) BnOH/MW, c) TREG/thermal activation and d) TREG/MW

As is observed in the TEM images the thermal produced nanoparticles showed lower tendency to aggregation than the microwave activated.

The HRTEM image, as is shown in figure 3.5, confirms the morphology, and the high crystallinity of the final CeO_2 nanoparticles.

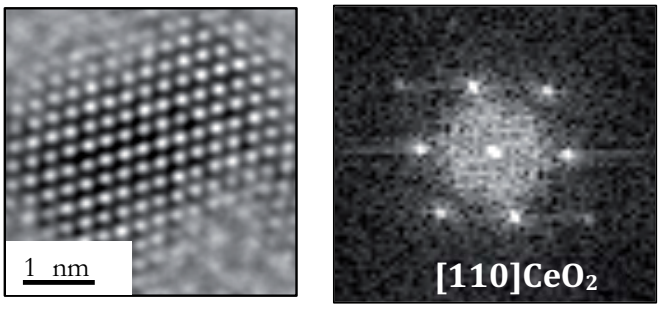

Figure 3.5: HRTEM image of the crystalline structure of one nanoparticle from $Ce(acac)_3$ in TREG within its FFT, showing structural agreement with CeO_2 phase

BF-TEM images from CeO_2 synthetized using Ce(IV) acetylacetonate were also analysed (figure 3.6) to compare the effect on the final nanocrystals.

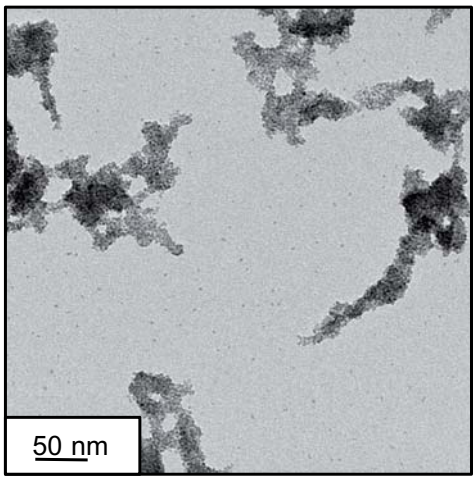

Figure 3.6: BF-TEM image of CeO_2 NPs by $Ce(acac)_4$ in TREG

As it is observed in the TEM images $Ce(acac)_4$ precursor afforded similar size and shape nanoparticles. However, the nanoparticles tend to form aggregates in solution. These results together with the fact that $Ce(acac)_4$ was not commercial prompted us to focus our studies in CeO_2 nanoparticles obtained from the Ce(III) precursor.

In order to know the effect of the temperature conditions during the microwave process in size, shape, stability and composition of the nanoparticles produced by $Ce(acac)_3$ precursor another experiment was designed. The BnOH route was used in this case. The final temperature was increased with the addition of *polyvinylpyrrolidone* (PVP) in the precursor solution in different mass fractions: 0%, 5% and 10%. The T_f arrives to 210ºC, 260ºC and 275ºC respectively (figure 3.7).

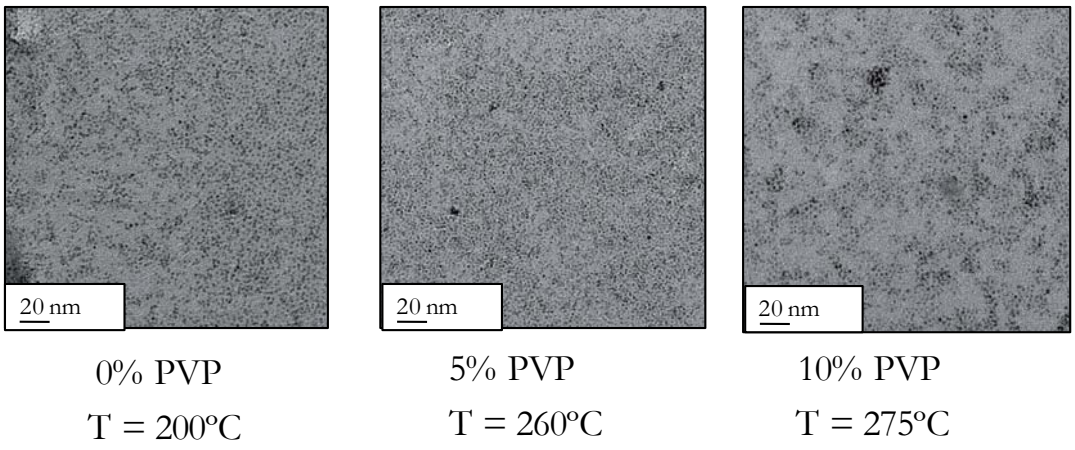

Figure 3.7: Effect of different PVP mass fractions on the CeO_2 nanoparticles synthesized by $Ce(acac)_3$ in BnOH

After the nanoparticles synthesis, TEM images show that the use of PVP to increase the final reaction temperature had not influence in the final nanocrystals. Furthermore, the cleaning process was more complicated due to the difficulty of PVP separation. For all these reasons, the synthesis of CeO_2 nanoparticles were finally performed without the addition of PVP.

Dynamic Light Scattering (DLS) experiments (figure 3.8), were performed for all the synthetized nanoparticles. Is necessary to study their aggregation behaviour for their final applications mainly in superconductivity and biomedical fields. Figure 3.8 is an example of DLS analysis of the CeO_2 nanoparticles synthetized in BnOH.

NPs by $Ce(acac)_3$

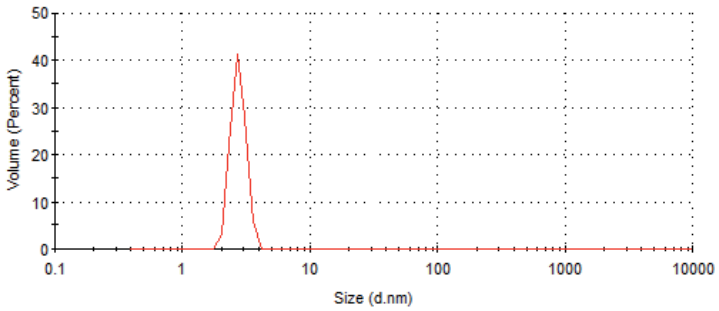

Figure 3.8: DLS experiment of CeO_2 nanoparticles synthetized by $Ce(acac)_3$ in BnOH

After the nanoparticles synthesis, all the colloidal solutions remain stable for a month in polar solvent without the formation of aggregates as was confirmed by DLS experiment, where only one pick around 3 nm is observed.

Furthermore, X-ray powder diffraction patterns (XRPD) of samples obtained from Ce(III) acetylacetonate proved that the obtained nanoparticles were always pure cubic CeO_2 phase independently of the applied synthetic route. As an example, figure 3.9 shows the XRDP from thermal process using BnOH.

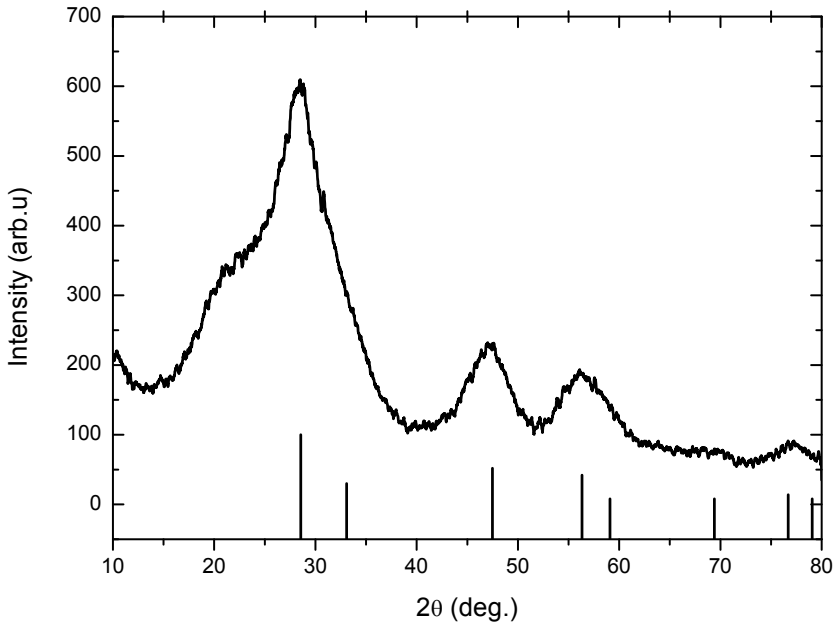

Figure 3.9: XRDP measurement for CeO_2 nanoparticles obtained by $Ce(acac)_3$ in BnOH

In order to use the nanoparticles for the further applications is also important to know the yield and the organic material that remains after the nanoparticles synthesis. For this reason, thermogravimetric analysis (TGA) were performed after the standard washing of the nanocrystals (3 times with ethanol and ethyl acetate or diethyl ether depends) (figure 3.10).

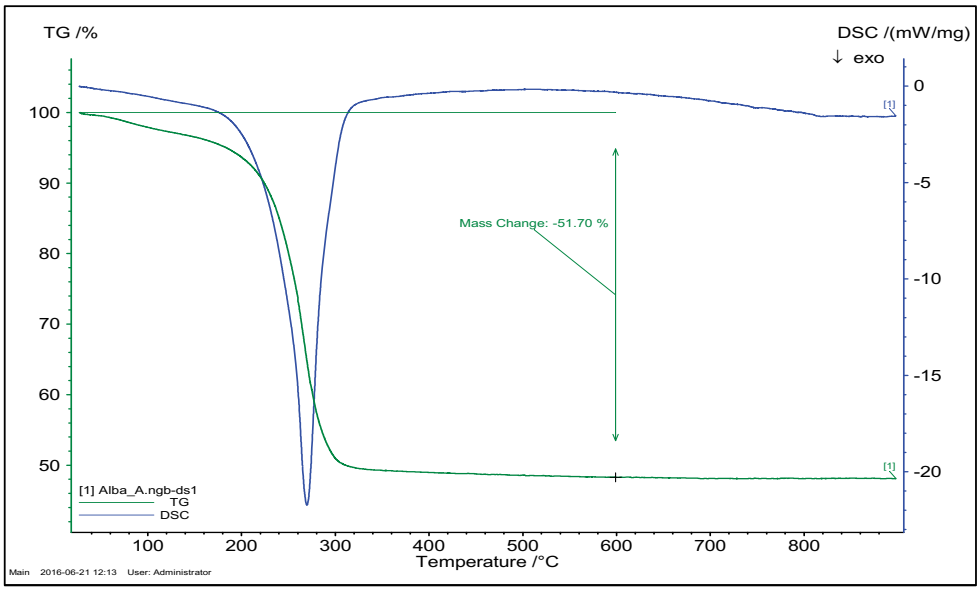

Figure 3.10: TGA measurement for CeO_2 nanoparticles obtained by $Ce(acac)_3$ in BnOH

The quantity of organic material that remains on the solution after the cleaning process is always almost the same (around 50-52%). This is an indication of the reproducibility of the process.

The knowledge of the amount of organics present in the final product gives us the necessary information, for the preparation of the solutions of the CeO_2 nanoparticles at different concentrations.

4.2. CeO_2 Nanoparticles from Cerium(III) Acetate Precursor

Taking into account the very small size (around 2-3nm) of the CeO_2 nanoparticles and the lack of changes in the size when using different solvents and temperatures we decided to move to another starting precursor.

In this case, $Ce(OAc)_3$ precursor in TREG or BnOH using microwave and thermal synthetic routes gave cubic shaped nanoparticles with an average diameter of 4 nm, and a definite size distribution in case of thermal process (figure 3.11).

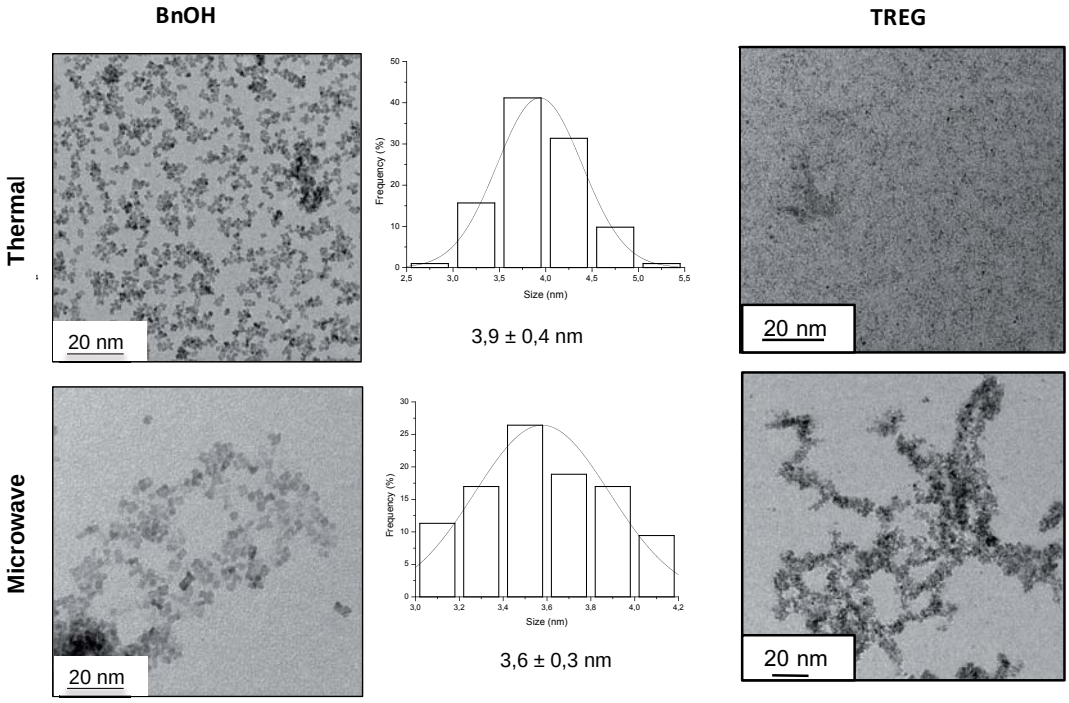

Figure 3.11: BF-TEM image showing size and shape of the CeO_2 starting from $Ce(OAc)_3$

The CeO_2 nanoparticles obtained from $Ce(OAc)_3$ precursor in TREG or in BnOH solvents had also a high stability during more than one month. DLS experiments confirmed no changes in size and aggregation effects (peak around 5-6 nm) (figure 3.12).

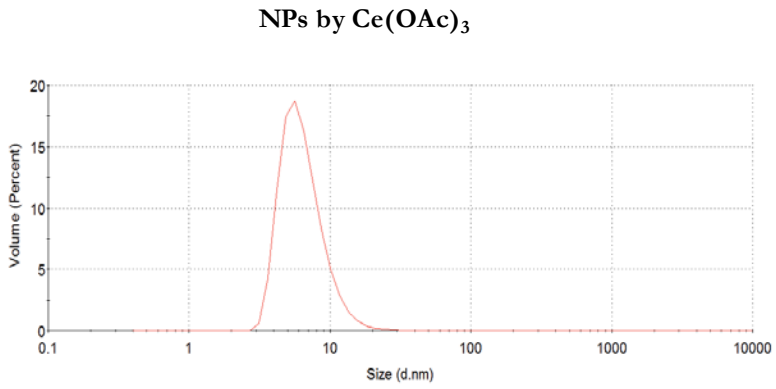

Figure 3.12: DLS experiment of CeO_2 nanoparticles synthetized by $Ce(OAc)_3$ in BnOH

Furthermore, the X-ray powder diffraction patterns of the different samples demonstrated that the nanoparticles obtained were also always pure cubic CeO_2 phase independently of solvent or the synthetic route used as shown in figure 3.13.

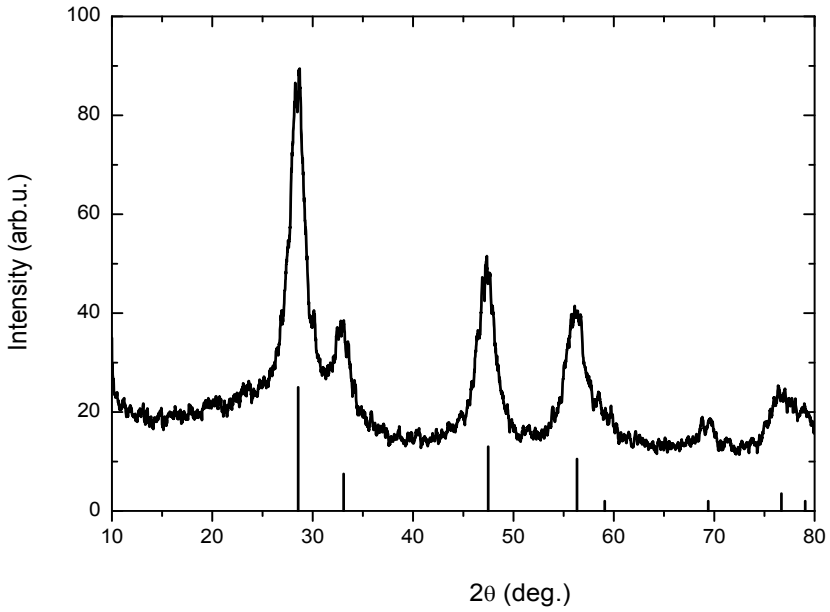

Figure 3.13: XRDP measurement for CeO_2 nanoparticles obtained by $Ce(OAc)_3$ in BnOH

Thermogravimetric analysis (TGA) was also performed to verify the yield and the final concentration. Figure 3.14 shows an example of the TGA obtained after the synthesis of $Ce(OAc)_3$ in BnOH.

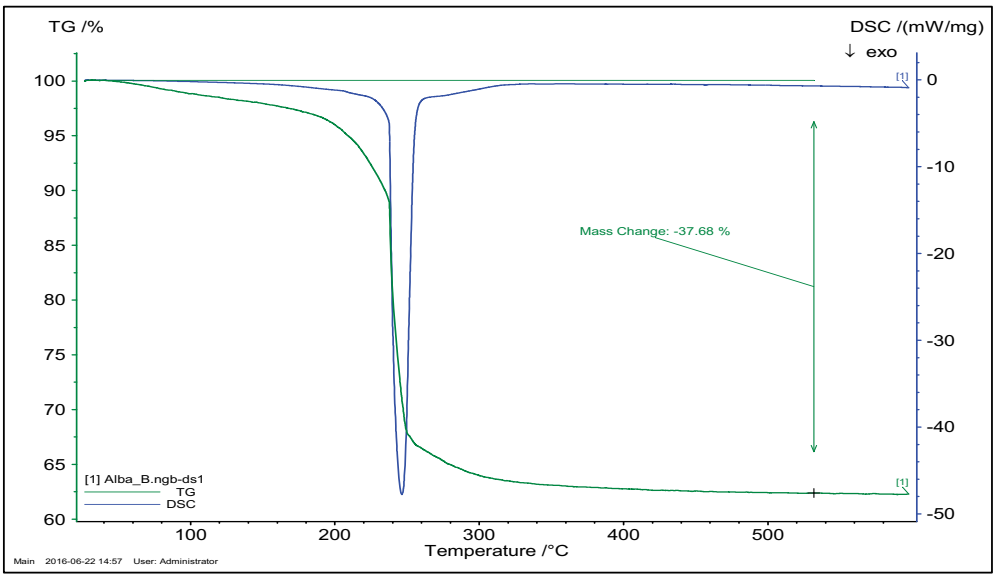

Figure 3.14: TGA measurement for CeO_2 nanoparticles obtained by $Ce(OAc)_3$ in BnOH

TGA analysis shows that the quantity of organic material is lower than for the case of CeO_2 nanoparticles synthetized from $Ce(acac)_3$ (38%) a plausible reason can by the bigger size of the nanocrystals obtained (around 4 nm instead 2 nm).

4.3. CeO_2 Nanoparticles Synthesis Conclusions

CeO_2 nanoparticles have been synthetized using two different precursors, solvents and processes. The nanoparticles obtained using $Ce(acac)_3$ as precursor present a smaller size and different shape than for the case of $Ce(OAc)_3$. This fact proves and confirms, as was explained in chapter 2, the influence of the precursor in the final characteristics of the nanoparticles.

The use of thermal process produces in the cases studied less aggregation on the final nanoparticles than microwave process. This phenomenon can be explained for the case of TREG due to during the thermal process the solvent remains at higher temperatures during more time producing a higher polymerization which, can stabilize more the final nanoparticles increasing their stability in polar solvents during the time. For the case of BnOH the fast increment of the temperature in microwave process can affect to the precursor decomposition and as consequence to the growth pathway decreasing the stabilization of the final nanoparticles.

Finally, CeO_2 nanoparticles in two different size 2-3 nm and 4-5 nm, with a high crystallization and stable for months in polar solvents were obtained achieving all the proposed requirements in order to apply them in superconductivity and biomedicine fields.

5. Surface Nanoparticle

A deeply study of the capping ligand and the surface of the final CeO_2 nanoparticles using different techniques such as infrared spectroscopy, nuclear magnetic resonance and Gas Chromatography-Mass Spectrometry were performed to understand better the behaviour and the stability of the synthetized nanocrystals.

5.1. Spectroscopic Characterization

CeO_2 nanoparticles synthetized starting from $Ce(acac)_3$ or $Ce(OAc)_3$ precursors using triethylene glycol or benzyalcohol showed always the same infrared spectrum pattern, which was similar to the spectrum of $Ce(OAc)_3$ (figure 3.15) after removing all the residual synthetic solvent.

The infrared spectrum patterns for both cases shows the characteristic stretching bands of acetate with absorptions around 1530 cm^{-1} (antisymmetric) and 1400 cm^{-1} (symmetric) (table 3.2) instead of the three typical bands of acetylacetonate due to C-C-C-O stretching around 1560 and 1500 cm^{-1}.

Wavenumber (cm^{-1}) ν(OCO)					
CeO_2 in BnOH from $Ce(OAc)_3$		**Difference $\Delta(\nu_{as}-\nu_{sym})$**	**CeO_2 in TREG from $Ce(OAc)_3$**		**Difference $\Delta(\nu_{as}-\nu_{sym})$**
ν_{as} 1525	ν_{sym} 1403	122	ν_{as} 1537	ν_{sym} 1409	128
CeO_2 in BnOH from $Ce(acac)_3$		**Difference**	**CeO_2 in TREG from $Ce(acac)_3$**		**Difference**
ν_{as} 1532	ν_{sym} 1398	134	ν_{as} 1528	ν_{sym} 1402	126

Table 3.2: IR comparation of CeO_2 NPs by different precursors and solvents

This evidence suggests that acetate could be present in those CeO_2 nanoparticles surface. Assuming this phenomenon, it can be due to the fact that acetylacetonate under oxygen atmosphere and high temperatures can decompose producing acetate on the media[36].

The origin of acetate as capping ligand with $Ce(acac)_3$ precursor has been previously described in the literature[37]. Studies of the thermal decomposition of $Ce(acac)_3$ have also proved that acetate group is present in different decomposition products: $Ce(C_5H_7O_2)_2(CH_3COO)$, $Ce(C_5H_7O_2)_2(CH_3COO)_2$, $Ce(OH)(CH_3COO)_3$, $CeO(CH_3COO)$ and $Ce(CH_3COO)_3$

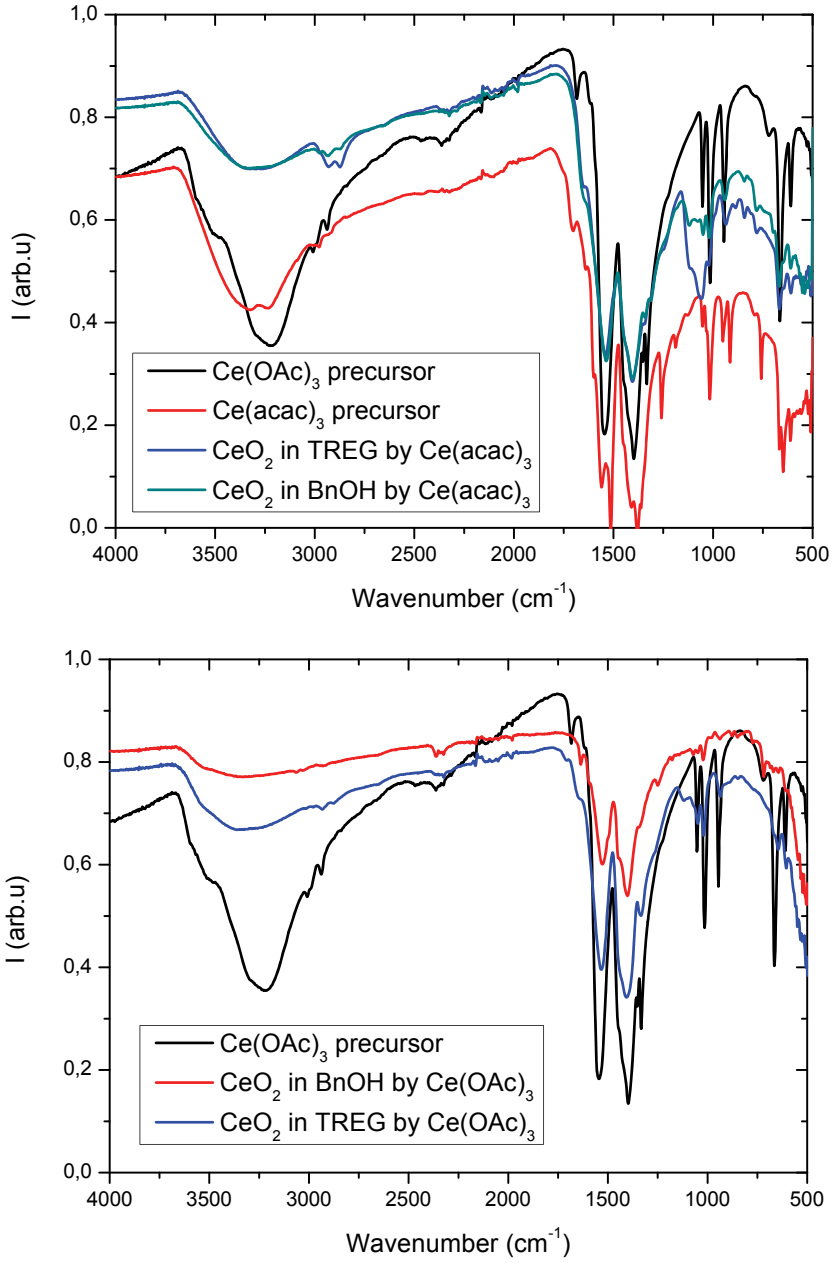

Figure 3.15: IR of CeO_2 nanoparticles by $Ce(acac)_3$ and $Ce(OAc)_3$ using TREG and BnOH compared with the IR obtained by acetate precursor

After recording the infrared spectra for all the samples, it was observed the presence of the acetate ligand onto the surface of the cerium oxide nanoparticles. Thus, both, the asymmetric ν_{as} and the symmetric ν_{sym} energies[38] for the carboxylic group are present with a difference of ca. 120-130 cm^{-1} suggesting the coordination of the acetates as bridging bidentate mode. However, in order to support this

hypothesis, a Gas Chromatography-Mass Spectrometry and NMR studies of nanoparticles solutions were performed.

5.2. Gas Chromatography-Mass Spectrometry Characterization

The solutions obtained after the application of the thermal treatment for the synthesis of the desired nanoparticles were analysed by Gas Chromatography-Mass Spectrometry (GC-MS) in order to detect the organic subproducts after the synthesis of CeO_2 nanoparticles. The specifications of the GC-MS experiments are shown in *section IV Annexes*.

The different solutions analysed after the CeO_2 synthesis were the thermal decompositions of a) $Ce(OAc)_3$ and $Ce(acac)_3$ in TREG and b) $Ce(OAc)_3$ and $Ce(acac)_3$ in BnOH.

a) CeO_2 by $Ce(OAc)_3$ and $Ce(acac)_3$ in TREG

In both cases after the nanoparticles reaction synthesis, the same subproducts were found regardless of the precursor. In these decompositions TREG was identified as the most abundant product. Some polyglycols formed by the coupling of TREG molecules were also found. It is interesting to note that for both precursors the esterification product 2(2-(2-(2-hydroxyethoxy)ethoxy)ethyl acetate was observed in very small quantity.

b) GC-MS of CeO_2 by $Ce(OAc)_3$ and $Ce(acac)_3$ in BnOH

For the case of the nanoparticles synthesis from $Ce(OAc)_3$ or $Ce(acac)_3$ precursors in BnOH, the most abundant product of this decomposition corresponds to the solvent employed in the reaction. The oxidation product benzylaldehyde was identified and the esterification product benzyl acetate was also found in both cases.

During the thermal process to produce CeO_2 nanoparticles benzaldehyde was also obtained. A possible explication of this fact can be due to the oxidation of benzyalcohol to benzaldehyde thanks to the quick change of the oxidation state between Ce^{4+} and Ce^{3+}. Finally, as the reaction is performed in air atmosphere, the oxygen can oxidize again Ce^{+3} to Ce^{+4} in order to obtain CeO_2 nanocrystals.

After the GC-MS analysis we could conclude that indeed acetate is on the reaction media independently of the precursor due to the reaction between the acetate and the alcohols in both cases. These results were in accordance with the analysis performed in the previous Spectroscopic Characterization.

5.3. Nuclear Magnetic Resonance Spectroscopy

Proton Nuclear Magnetic Resonance (^{1}H-NMR 400Hz) analysis of CeO_2 nanoparticles, synthetized by $Ce(OAc)_3$ or $Ce(acac)_3$ as metallic precursors in benzyl alcohol or triethylene glycol as solvent, were performed.

In the NMR study of nanoparticles solutions it is fundamental to ensure that there were no solvent molecules on the nanoparticle surface so, after precipitation, nanoparticles should be washed until the intensity of solvent signals remain constant.

In order to eliminate all the solvent present on nanoparticles surface was necessary to wash three times more with water (in total 6 times) the previously precipitated CeO_2 nanoparticles.

After the cleaning process, when the nanoparticles were dispersed in water using an ultrasonic bath the pH of the solution decrease until 4.65. This fact can be explained by the hypothesis that the acetate on the nanoparticles is ripped from the surface to produce acetic acid reacting with the protons from the hydroxyl groups presents also on the surface. For this reason, in order to better understand the behaviour of the nanoparticles when were dispersed in water, ^{1}H-NMR spectra was registered in D_2O.

Figure 3.16 shows the proton NMR spectra from the CeO_2 nanoparticles synthetized by $Ce(acac)_3$ in BnOH after the cleaning process and their dispersion in D_2O.

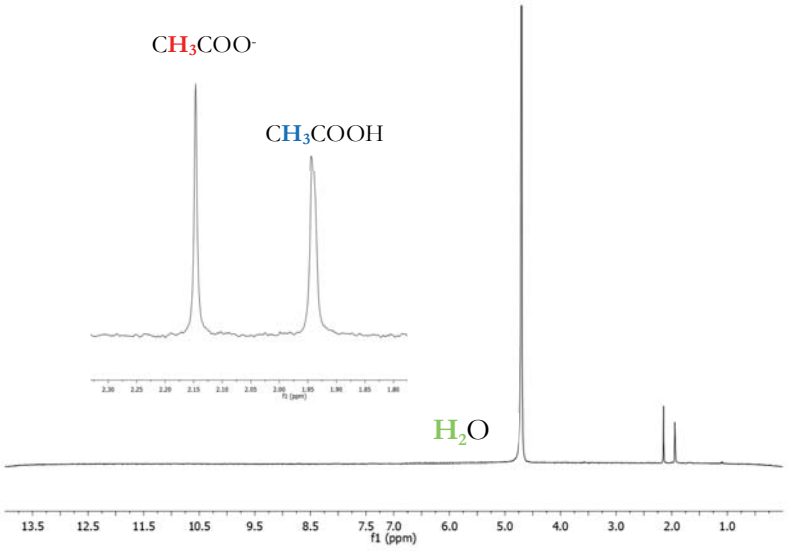

3.16: ^{1}H-NMR in D_2O of CeO_2 nanoparticles by $Ce(acac)_3$ in BnOH

^{1}H-NMR spectrum of CeO_2 nanoparticles in D_2O shows effectively two singlets in the region of acetate protons (2.15 and 1.95 ppm) that suggest the presence of two types of acetate groups; probably one is bonded to the nanoparticle surface and the other is in the solvent as acetic acid confirming our hypothesis. This phenomenon is supported by the fact that when nanoparticles are dispersed in water the pH of the solution decreases until 4.7.

The more deshielded singlet at 2.15 ppm can be assigned to the acetate group that acts as capping ligand and the singlet at 1.95 ppm to free acetic molecules. As shown in figure 3.17 (left) ^{1}H-NMR of acetic acid commercial in D_2O with the corresponding signal at 1.95 ppm in order to support our conjecture. Furthermore, the addition of acetic acid to the dispersion of CeO_2 in D_2O causes a significant increasing of the singlet al 1.95 ppm that confirms the proposed hypothesis.

Figure 3.17 (right) shows this phenomenon in CeO_2 nanoparticles synthetized by $Ce(acac)_3$ in BnOH.

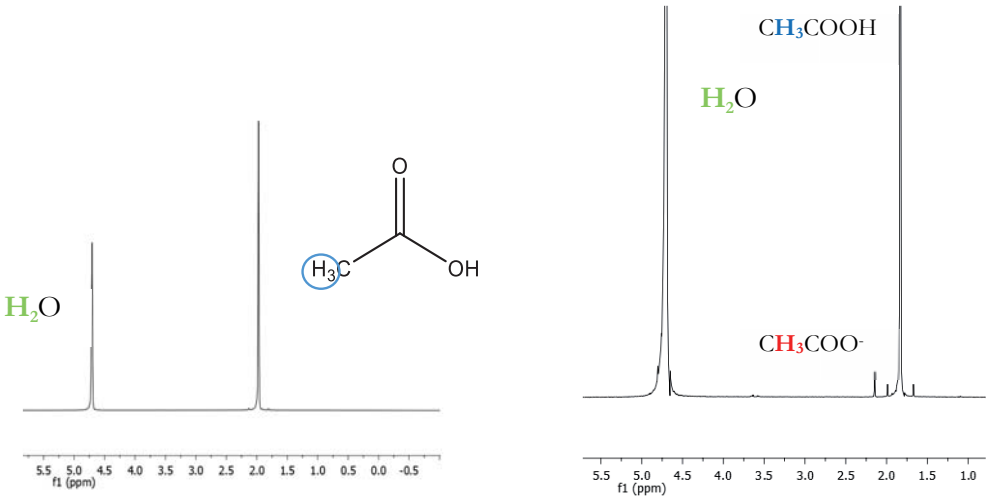

3.17: ***(left)*** *^{1}H-NMR in D_2O of acetic acid* ***(right)*** *commercial ^{1}H-NMR in D_2O of acetic acid with CeO_2 nanoparticles by $Ce(acac)_3$ with BnOH*

In order to certify that the acetic acid in solution comes from the acetate molecules bonded to the nanoparticle, two different experiments were performed. On the one hand, after the cleaning process, the nanoparticles were dispersed in D_2O at room temperature without ultrasonic bath. In this case, the ^{1}H-NMR in D_2O shows only one singlet at 2.15 ppm (figure 3.18 (right)). In a second experiment, the nanoparticles were washed several times more with water in order to remove as much as possible the capping ligand molecules on the surface. The ^{1}H-NMR of this solution does not show any acetate group signal (figure 3.18 (left)) proving that it is possible the elimination of capping molecules by extensive washing of nanoparticles.

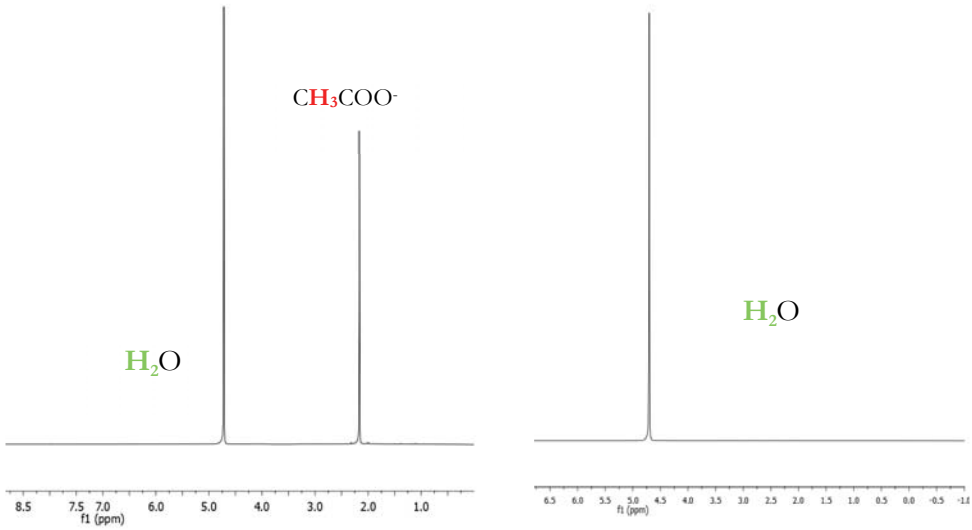

3.18: ^{1}H-NMR in D_2O of CeO_2 by $Ce(acac)_3$ with BnOH ***(left)*** *dispersion without ultrasonic bath* ***(right)*** *after washing the nanoparticles several times more*

As a summary, ^{1}H-NMR experiments have proved that acetic/acetate are present on the nanoparticles surface regardless of the precursor or the solvent used during the synthesis of CeO_2 nanoparticles. For this reason, proton NMR analysis were also agree with the results obtained previously by IR and GC-MS techniques.

In order to understand the presence of acetic acid, *Zeta Potential* measurements were performed. Zeta Potential (ZP) give us an estimation of the net electrical charge contained in the slipping plane, and also depends on the location of that plane. Thus, it is widely used for quantification of the magnitude of the charge of the nanoparticles's surface as shown in picture 3.19.

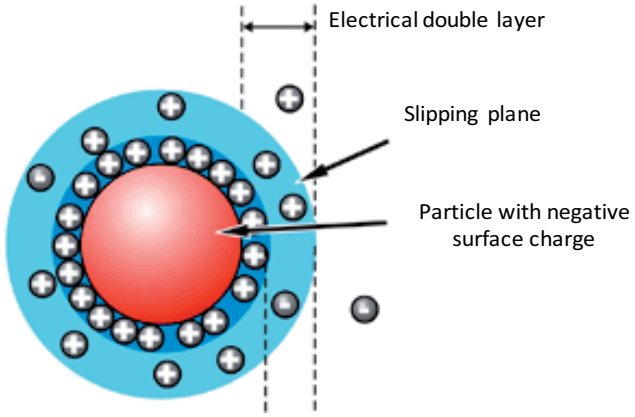

3.19: Zeta Potential scheme

ZP analysis shown in figure 3.20, are the results obtained by **(I)** CeO_2 nanoparticles dispersed in water, where the acetate acts as a capping ligand and **(II)** CeO_2 nanoparticles dispersed in water after removing all the acetate, in for both cases have a positive Z-Potential.

(I) *CeO_2 nanoparticles from $Ce(acac)_3$ in BnOH dispersed in water with acetate as capping ligand*

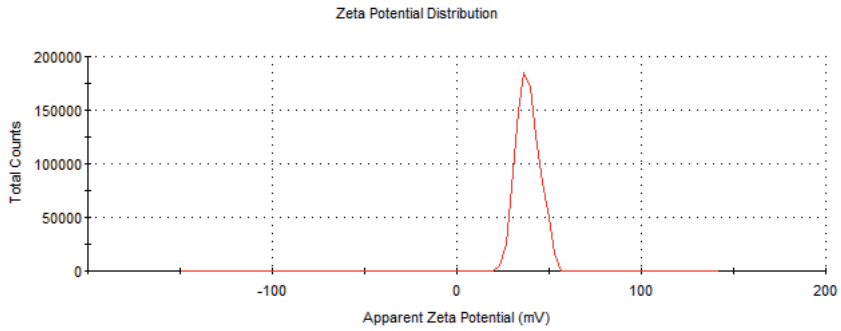

(II) *CeO_2 nanoparticles from $Ce(acac)_3$ in BnOH dispersed in water after removing the acetate*

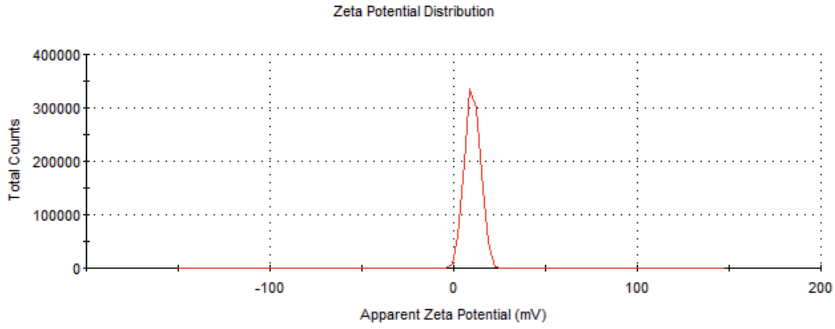

3.20: Positive Zeta Potential of CeO_2 NPs from $Ce(acac)_3$ in BnOH ***(I)*** *acetate acts as a capping ligand* ***(II)*** *after removing the acetate*

The positive value of 35 mV **(I)** can be due to the protons from the hydroxyl group that when they are removed from the surface to generate acetic acid with the acetate, the zeta potential decrease until 16 mV **(II)**.

For this reason, after the NMR and Zeta potential analysis we could confirm our hypothesis performing a surface simulation, where the acetate present on the surface has bridging bidentate coordination as indicate IR technique (figure 3.21).

3.21: Surface nanoparticle coordination with the acetate

The negative surface charge and the difference between ν_{as} and ν_{sym} energies obtained by IR indeed, it can be link by one oxygen with a hydroxyl group and the other with a cerium generating this characteristic coordination as is showing in last figure 3.21.

A possible reaction mechanism is shown in figure 3.22 to explain this phenomenon obtained thanks to NMR and Zeta Potential analysis.

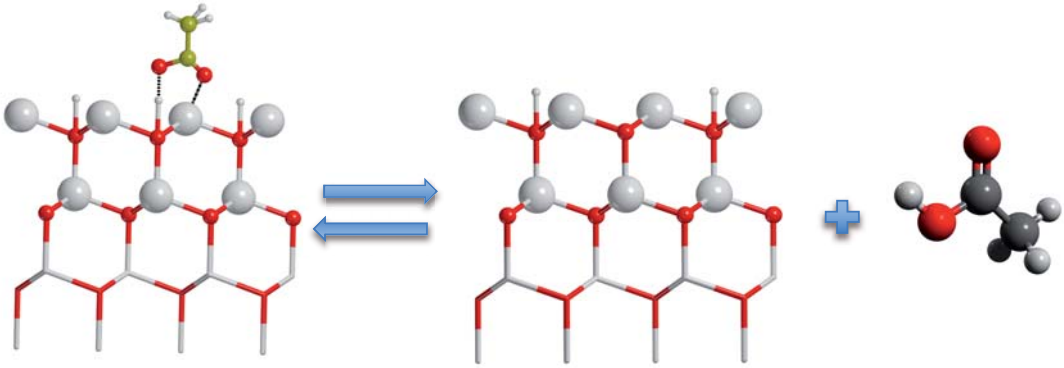

3.22: Reaction mechanism for the acetic acid formation

The proposed mechanism is based on the acetate present on the surface can react with a proton from the hydroxyl group to produce acetic acid generating an equilibrium between the two different species.

As a conclusion, the obtained results show that for all the CeO_2 nanoparticles, acetate is a part of the capping ligand forming a bidentate coordination with hydroxyls groups on the nanoparticle surface.

Furthermore, when the nanoparticles are dispersed in water the acetate is ripped forming acetic acid producing and equilibrium between the two different species. This phenomenon is also confirmed for zeta potential techniques, which shows a negative charge nanoparticles surface due to their coordination.

5.4. Capping Ligand Exchange

In order to solve the problems caused by TREG due to its high viscosity in the fabrication of superconducting nanocomposites thin films, as will be explained in

chapter 4: *Nanostructuring $YBa_2Cu_3O_{7-\delta}$ Layers*, a capping ligand exchange is performed.

The capping ligand exchange was performed after the nanoparticles synthesis by $Ce(acac)_3$ in TREG, where nanocrystals were washed 6 times and dispersed in 10 ml of ethanol to obtain concentrations up to 90 mM. After that, decanoic acid was mixed with tetramethylammonium hydroxide (1:1) in order to deprotonate the acid and added on the nanoparticles dispersed in ethanol, with a concentration of 10% molar respect the nanoparticles solution. Finally, the mixture was stirring during 24 hours to perform the ligand exchange. After that, the nanoparticles were cleaned several times more with ethanol and dispersed in methanol.

Infrared spectroscopy pattern shows in figure 3.23 that decanoic was indeed present on the surface of the nanoparticles and the capping ligand exchange was confirmed.

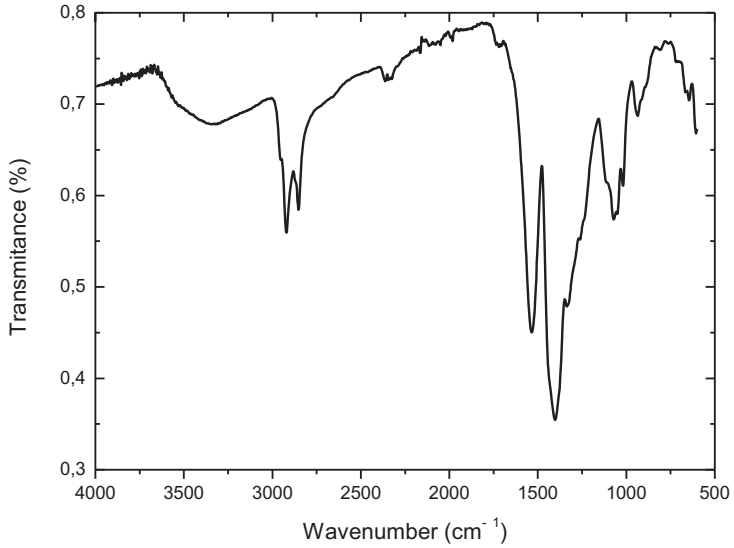

3.23: IR of CeO_2 NPs with $CH_3(CH_2)_8COO^-$ as a capping ligand

The principal bands[39] are at 2895 cm^{-1} and 2835 cm^{-1} due to Csp3 C–H stretching and C–H bending, at 1547 cm^{-1} and 1418 cm^{-1} as a result of carboxylate CO_2^- group[40] and at 1073 cm^{-1} by cause of C-O stretching.

The nanoparticles, after the capping ligand exchange, were analysed also by TEM technique as is shown in figure 3.24.

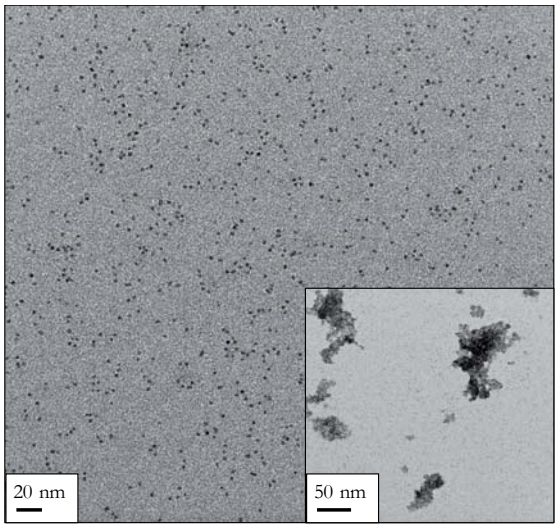

3.24: TEM image of CeO_2 NPs with $CH_3(CH_2)_8COO^-$ as a capping ligand

The capping ligand exchange gave the same shape of the nanoparticles than in TREG as was shown in TEM image, but in this case the aggregation is higher and the colloidal solution only was stable during a day. *Dynamic Light Scattering* (DLS) technique was used to check the aggregation of the nanoparticles (figure 3.25).

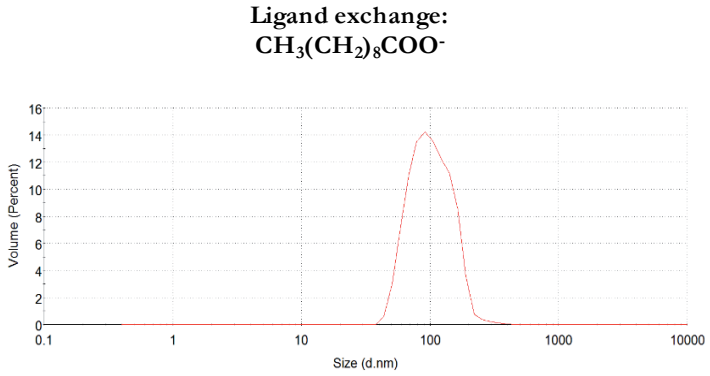

3.25: DLS analysis of CeO_2 nanoparticles after capping ligand exchange with $CH_3(CH_2)_8COO^-$

DLS analysis shows effectively, that the nanoparticles were forming aggregates inside of the solution around 100 nm, when CeO_2 were dispersed again in methanol.

5.5. X-Ray Photoelectron Spectroscopy

The X-Ray Photoelectron Spectroscopy (XPS) technique, also called as Electron Spectroscopy for Chemical Analysis (ESCA) was used in order to investigate why Ce(IV) is obtained in the final nanoparticles composition if Ce(III) precursor was used to produce them. The study was performed with the BnOH prepared nanoparticles.

The main hypothesis is that benzyl alcohol was oxidized to benzaldehyde thanks to the change of the oxidation state from Ce^{4+} to Ce^{3+}. XPS analysis could give elemental and chemical state information regardless of the natural of material sample which wants to be analysed and for this reason, if Ce(III) was formed on the nanocrystal during the reaction, it will be able to detect with this technique.

Figure 3.26 shows an example of XPS analysis after the nanoparticles synthesis where for all the cases only Ce^{4+} is obtained.

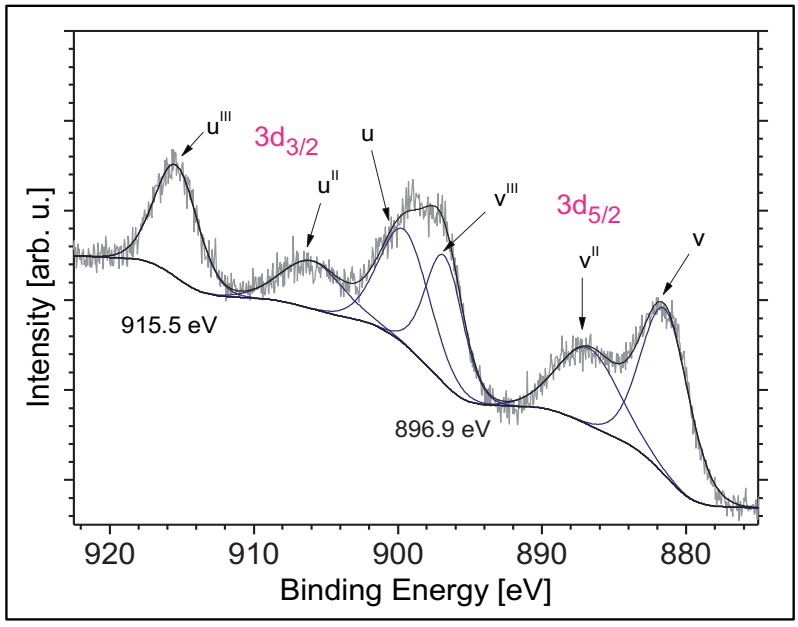

Figure 3.26: XPS analysis from CeO_2 by $Ce(OAc)_3$ in BnOH

Results show signals for Ce 3d at 882 eV with an atomic concentration around 5% depends on the used precursor. Other signals for O 1s and C 1s were detected at 530 and 284 eV respectively, with an atomic concentration between 42 % for O

1s and 57 % for C 1s. All atomic concentrations were calculated from the photoelectron peak areas.

Two sets of multiplets (u and v) were obtained, corresponding to the spin-orbit split $3d_{5/2}$ and $3d_{3/2}$, with a value around 18 eV. For Ce(IV) samples, each spin-orbit component ($3d_{5/2}$, $3d_{3/2}$) was dominated by three features, opposite to Ce(III), which present only two. These three were presents in last figure 3.23 as six peaks corresponding to the pair of spin-orbit doublets.

The highest binding energy peaks u^{III} and v^{III} appear around 915.5 and 896.9 eV. These are the result of a Ce $3d^9$ $4f^0$ O $2p^6$ state, where the u^{III} associated to the Ce $3d_{3/2}$ is characteristic of the presence in the sample of tetravalent Ce.

After the analysis and the confirmation that the nanoparticles were composed only by Ce (IV), the reaction was preformed with the same precursor and solvents conditions but under argon, as was explained in previous section *3.2. Synthesis of Nanoparticles*, in order to try to obtain Ce_2O_3 instead of CeO_2 nanoparticles.

The main difference in the XPS pattern between Ce(III) and Ce(IV) oxide is that they have different multiplet splitting and for the case of Ce(IV), it has a peak around 917 eV which is absent in Ce(III) spectrum. Figure 3.27 shows a theoretical XPS of Ce(3d) core level spectra in CeO_2 and Ce_2O_3.

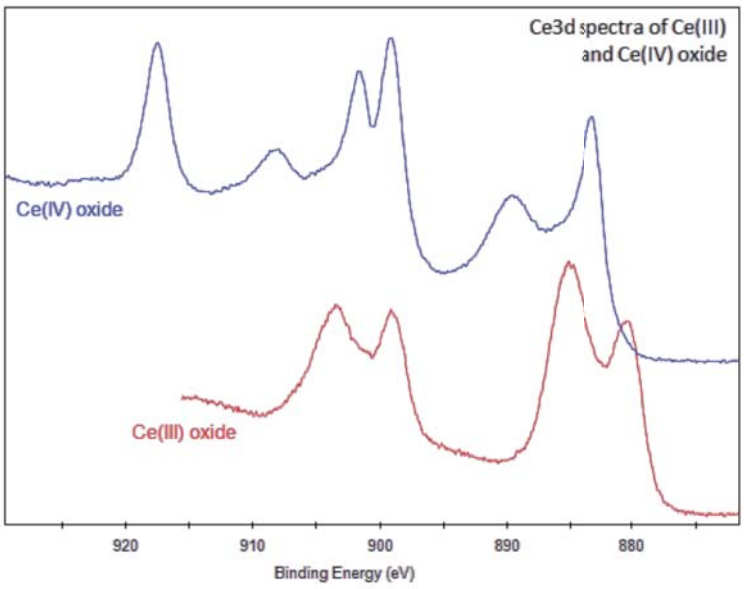

Figure 3.27: Theoretical XPS analysis of Ce(III) and Ce(IV) oxide

After the nanoparticles synthesis under argon media, the XPS obtained shows that Ce(IV) was mainly present on the sample (figure 3.28).

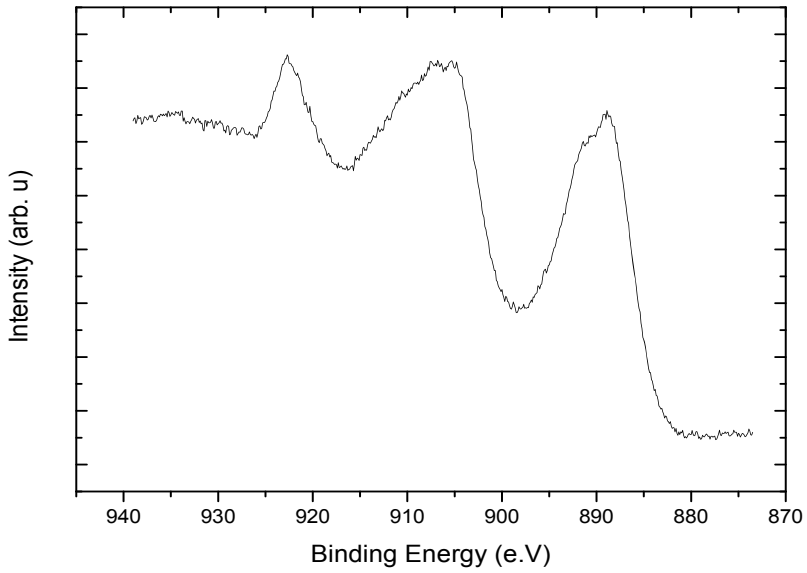

Figure 3.28: XPS of CeO_2 by $Ce(OAc)_3$ in BnOH under argon condition

CeO_2 nanoparticles were the most abundant product because the shape of the curve compared with the theoretical XPS present a similar behaviour. However, the curve allows us to confirm that also a few quantity of Ce(III) was also present on the compound.

The main advantage to find part of Ce(III) on the sample is that this fact allows us to explain the formation of benzaldehyde found by GC-MS technique after the nanoparticles synthesis in BnOH which, it can be due to Ce(IV) could oxidize part of benzyl alcohol forming Ce_2O_3 and benzaldehyde and after that, the Ce(III) could be oxidize again to CeO_2 with the presence of the atmospheric oxygen.

This phenomenon was also reported on CeO_2 applications, as a typically process used in pharmaceutical industries or pharmacy to produce benzaldehyde from benzyl alcohol[41].

6. Conclusions

CeO_2 nanoparticles were produced via thermal and microwave process using $Ce(acac)_3$, $Ce(acac)_4$ and $Ce(OAc)_3$ precursors in high boiling point solvents, triethylene glycol or benzyl alcohol.

The main advantage of this methodology is due to is a one-pot and fast process without undesired subproducts, which allows to control the size, shape and composition of the nanoparticles with high reproducibility.

For the case of acetylacetonate precursors round shape nanoparticles of 2.5 nm were obtained. If acetate precursor was employed, the obtained nanocrystals were with square shape and size around 4 nm.

All the CeO_2 nanoparticles prepared proved to be stable in polar solvents in high concentration (90 mM) as is shown in DLS studies. These high concentrate solutions remain stable for more than one month in the case of TREG and BnOH synthesis.

The structure, composition and capping ligand were deeply studied by different techniques. The final results show that acetate ligand was on the surface of the nanoparticles acting as a capping ligand and generating a bridging bidentate coordination independently of the nature of the precursor. Moreover, when the nanoparticles were dispersed in water, this acetate can form acetic acid deceasing the pH. This characteristic can be used in order to perform a capping ligand exchange because was an easy mechanism to modify the physical properties of the nanoparticles such as the stabilization in different solvents (polar or nonpolar).

It has been demonstrated by XPS measurements that CeO_2 is the major component of the nanoparticles when the synthesis was performed in air. However, XPS results show that if the reaction is performed under argon a small amount of Ce_2O_3 is also found.

As a summary, CeO_2 nanoparticles with a high controllability of the size, shape, composition and stability in different polar solvents were obtained useful for further applications like nanocomposite YBCO preparation.

7. Bibliography

1) Xu, C., & Qu, X. (2014). Cerium oxide nanoparticle: a remarkably versatile rare earth nanomaterial for biological applications. *NPG Asia Materials*, *6*(3), e90. doi: 10.1038/ am.2013.88.

2) Bouzigues, C., Gacoin, T., & Alexandrou, A. (2011). Biological applications of rare-earth based nanoparticles. *ACS Nano*, *5*(11), 8488–505. doi:10.1021/nn202378b.

3) Harthoj, A., & Moller, P. (2014). Oxidation behaviour and electrical properties of cobalt/cerium oxide composite coatings for Solid Oxide Fuel Cell Interconnects. *In Preparation*, *281*, 227–237. doi: 10.1016/j.jpowsour.2015.01.128.

4) Walkey, C., Das, S., Seal, S., Erlichman, J., Heckman, K., Ghibelli, L., & Self, W. T. (2015). Catalytic properties and biomedical applications of cerium oxide nanoparticles. *Environmental Science: Nano*, *2*(1), 33–53. doi:10.1039/C4EN00138A.

5) Corma, A., Atienzar, P., García, H., & Chane-Ching, J.-Y. (2004). Hierarchically mesostructured doped CeO2 with potential for solar-cell use. *Nature Materials*, *3*(6), 394–397. doi:10.1038/nmat1129.

6) Celardo, I., Pedersen, J. Z., Traversa, E., & Ghibelli, L. (2011). Pharmacological potential of cerium oxide nanoparticles. *Nanoscale*, *3*(4), 1411–20. doi:10.1039/c0nr00875c.

7) Haneda, M., Kaneko, T., Kamiuchi, N., & Ozawa, M. (2015). Improved three-way catalytic activity of bimetallic Ir–Rh catalysts supported on CeO_2–ZrO_2. *Catal. Sci. Technol.*, *5*, 1792–1800. doi:10.1039/C4CY01502A.

8) Yu, S. H., Cölfen, H., & Fischer, A. (2004). High quality CeO2 nanocrystals stabilized by a double hydrophilic block copolymer. *Colloids and Surfaces A: Physicochemical and Engineering Aspects*, *243*(1-3), 49–52. doi:10.1016/j.colsurfa.2004.05.006.

9) Gu, H., & Soucek, M. D. (2007). Preparation and Characterization of Monodsiperse Cerium Oxide Nanoparticles in Hydrocarbon Solvents. *Chem. Mater.*, *19*(22), 1103–1110.

10) Sreeremya, T. S., Thulasi, K. M., Krishnan, A., & Ghosh, S. (2012). A novel aqueous route to fabricate ultrasmall monodisperse lipophilic cerium oxide nanoparticles. *Industrial and Engineering Chemistry Research*, *51*(1), 318–326. doi:10.1021/ie2019646.

11) Sathyamurthy, S., Leonard, K. J., Dabestani, R. T., & Paranthaman, M. P. (2005). Reverse micellar synthesis of cerium oxide nanoparticles. *Nanotechnology*, *16*(9), 1960–1964. doi:10.1088/0957-4484/16/9/089.

12) Miyazaki, H., Kato, J. I., Sakamoto, N., Wakiya, N., Ota, T., & Suzuki, H. (2010). Synthesis of CeO_2 nanoparticles by rapid thermal decomposition using microwave heating. *Advances in Applied Ceramics*, *109*(2), 123–127. doi:10.1179/174367509X12503626841631.

13) Mädler, L., Kammler, H., Mueller, R., & Pratsinis, S.E. (2002). Flame-made ceria nanoparticles. *Journal of Materials Research, 17*(6), 1356-1362. doi:10.1557/JMR.2002.020258.

14) Hirst, S. M., Karakoti, A. S., Tyler, R. D., Sriranganathan, N., Seal, S., & Reilly, C. M. (2009). Anti-inflammatory properties of cerium oxide nanoparticles. *Small*, *5*(24), 2848–2856. doi:10.1002/smll.200901048.

15) Karakoti, A. S., Singh, S., Kumar, A., Malinska, M., Kuchibhatla, S. V. N. T., Wozniak, K., Self, W. T. & Seal, S. (2009). PEGylated nanoceria as radical scavenger with tunable redox chemistry. *Journal of the American Chemical Society*, *131*(40), 14144–14145. doi:10.1021/ja9051087.

16) Li, M., Shi, P., Xu, C., Ren, J., & Qu, X. (2013). Cerium oxide caged metal chelator: anti-aggregation and anti-oxidation integrated H_2O_2-responsive controlled drug release for potential Alzheimer's disease treatment. *Chemical Science*, *4*(6), 2536. doi:10.1039/c3sc50697e.

17) Kaittanis, C., Santra, S., Asati, A., & Perez, J. M. (2012). A cerium oxide nanoparticle-based device for the detection of chronic inflammation via optical and magnetic resonance imaging. *Nanoscale*, *4*(6), 2117–23. doi:10.1039/c2nr11956k.

18) Pulido-Reyes, G., Rodea-Palomares, I., Das, S., Sakthivel, T. S., Leganes, F., Rosal, R., & Fernández-Piñas, F. (2015). Untangling the biological effects of cerium oxide nanoparticles: the role of surface valence states. *Scientific Reports*, *5*, 15613. doi:10.1038/srep15613.

19) Li, M., Shi, P., Xu, C., Ren, J., & Qu, X. (2013). Cerium oxide caged metal chelator: anti-aggregation and anti-oxidation integrated H_2O_2-responsive controlled drug release for potential Alzheimer's disease treatment. *Chemical Science*, *4*(6), 2536. doi:10.1039/c3sc50697e.

20) Mandoli, C., Pagliari, F., Pagliari, S., Forte, G., Nardo, P. Di, Licoccia, S., & Traversa, E. (2010). Stem cell aligned growth induced by CeO2 nanoparticles in PLGA scaffolds with improved bioactivity for regenerative medicine. *Advanced Functional Materials*, *20*(10), 1617–1624. doi:10.1002/adfm.200902363.

21) Cayado, P., De Keukeleere, K., Garzón, A., Perez-Mirabet, L., Meledin, A, De Roo, J., Valles, F., Mundet, B., Rijckaert, H., Pollefeyt, G., Coll, M., Ricart, S., Palau, A., Gázquez, J., Ros, J., Van Tendelco, GObradors, X. (2015). Epitaxial $YBa_2Cu_3O_{7-x}$ nanocomposite thin films from colloidal solutions. *Superconductor Science and Technology*, *28*(12), 124007. doi:10.1088/0953-2048/28/12/124007.

22) Vilé, G., Colussi, S., Krumeich, F., Trovarelli, A., & Pérez-Ramírez, J. (2014). Opposite face sensitivity of CeO_2 in hydrogenation and oxidation catalysis. *Angewandte Chemie - International Edition*, *53*(45), 12069–12072. doi:10.1002/ anie.201406637

23) Zhou, W., Liu, J., Pan, J., Sun, F., He, M., & Chen, Q. (2015). Effect of Mg2+ on the catalytic activities of CoMgAl hydrotalcites in the selective oxidation of benzyl alcohol to benzaldehyde. *Catalysis Communications*, *69*, 1–4. doi:10.1016/ j.catcom.2015.05.012.

24) M. Hudlucky, *Oxidations in Organic Chemistry*, ACS Monograph Series, American Chemical Society, Washington, DC, 1990.

25) Suzuki, T., Kosacki, I:, & Anderson, Harlan. (2001). Electrical Conductivity and Lattice Defects in Nanocrystalline Cerium Oxide Thin Films. *Journal of the American Ceramic Society, 84*(9), 2007-14. doi:10.1111/j.1151-2916.2001.

26) Conductivity, E., Oxide, C., & Films, T. (2001). Electrical Conductivity and Lattice Defects in Nanocrystalline Cerium Oxide Thin Films, *84*(9), 2007–2014. doi: 10.1111/ j.1151-2916.2001.

27) Conesa, J. C. (1995). Computer Modeling of Surfaces and Defects on Cerium Dioxide. *Surface Science*, *339*(3), 337–352. doi:doi:10.1016/0039-6028(95)00595-1.

28) Zhang, F., Chen, C. H., Raitano, J. M., Hanson, J. C., Caliebe, W. A., Khalid, S., & Chan, S. W. (2006). Phase stability in ceria-zirconia binary oxide nanoparticles: The effect of the Ce3+ concentration and the redox environment. *Journal of Applied Physics*, *99*(8). doi:10.1063/1.2190712.

29) Kuchma, M. H., Komanski, C. B., Colon, J., Teblum, A., Masunov, A. E., Alvarado, B., & Baker, C. H. (2010). Phosphate ester hydrolysis of biologically relevant molecules by cerium oxide nanoparticles. *Nanomedicine: Nanotechnology, Biology, and Medicine*, *6*(6), 738–744. doi:10.1016/j.nano.2010.05.004.

30) Skorodumova, N. V, Simak, S. I., Lundqvist, B. I., Abrikosov, I. A., & Johansson, B. (2002). Quantum Origin of the Oxygen Storage Capability of Ceria. *Physical Review Letters*, *89*(16), 166601. doi:10.1103/PhysRevLett.89.166601.

31) Viau, G., Fievet-Vincent, F., & Fievet, F. (1996). Monodisperse iron-based particles: precipitation in liquid polyols. *Journal of Materials Chemistry*, *6*(6), 1047. doi: 10.1039/jm9960601047.

32) Niederberger, M. (2007). Nonaqueous sol-gel routes to metal oxide nanoparticles. *Accounts of Chemical Research*, *40*(9), 793–800. doi:10.1021/ar600035e.

33) B. Melara Benítez, *Synthesis and Characterization of CeO_2 Nanoparticles*. Master thesis, UAB, 2015.

34) Behrsing, T., Bond, A. M., Deacon, G. B., Forsyth, C. M., Forsyth, M., Kamble, K. J., & White, A. H. (2003). Cerium acetylacetonates - New aspects, including the lamellar clathrate [Ce(acac)4]·10H2O. *Inorganica Chimica Acta*, *352*, 229–237. doi:10.1016/S0020-1693(03)00147-6.

35) Nakamoto, K., Morimoto, Y., & Martell, A. E. (1961). Infrared Spectra of Metal Chelate Compounds.\nIV. Infrared Spectra of Addition Compunds of Metallic Acetylacetonates. *Journal of the American Chemical Society*, *83*(8), 4533–4536. doi:10.1021/ja01466a014.

36) Straganz, G. D., Glieder, A., Brecker, L., Ribbons, D. W., & Steiner, W. (2003). Acetylacetone-cleaving enzyme Dke1: a novel C–C-bond-cleaving enzyme from Acinetobacter johnsonii. *Biochemical Journal*, *369*, 573–581. doi:10.1042/BJ20021047.

37) Ristoiu, T., Ciontea, L., Suciu, R. C., Petrisor, T., Gabor, M. S., Thalmayer, G., & Petrisor, T. (2008). Thermal decomposition study by DTA-TG-MS of cerium [III] acetylacetonate used as ceria thin film precursor. *Journal of Optoelectronics and Advanced Materials*, *10*(9), 2223–2227.

38) Dobson, K., & McQuillan, A. (1999). In situ infrared spectroscopic analysis of the adsorption of aliphatic carboxylic acids to TiO2, ZrO2 ,Al2 O3 , and Ta2 O5 from aqueous solutions. *Spectrochimica Acta Part A*, *55*, 1395–1405. doi:10.1016/S1386-1425(98)00303-5.

39) West, D. B. (1984). Analysis of a Phase Transition at 134 K in Decanoic Acid by Infrared Spectroscopy,. *The Journal of Physical* Chemistry, 7(6), 6644–6648.

40) Dong, T.-Y., Chen, W.-T., Wang, C.-W., Chen, C.-P., Chen, C.-N., Lin, M.-C., & Kao, T.-H. (2009). One-step synthesis of uniform silver nanoparticles capped by saturated decanoate: direct spray printing ink to form metallic silver films. *Physical Chemistry Chemical Physics : PCCP*, *11*(29), 6269–75. doi:10.1039/b900691e.

41) Wang, T., Yuan, X., Li, S., Zeng, L., & Gong, J. (2015). CeO_2 -modified Au@SBA-15 nanocatalysts for liquid-phase selective oxidation of benzyl alcohol. *Nanoscale*, *7*(17), 7593–7602. doi:10.1039/C5NR00246J.